



UNIVERSITAT
POLITÈCNICA
DE VALÈNCIA



INSTITUTO DE
TECNOLOGÍA
QUÍMICA



UNIVERSITAT POLITÈCNICA DE VALÈNCIA
INSTITUTO DE TECNOLOGIA QUIMICA (ITQ, UPV-CSIC)

Doctoral Thesis:

*Novel mechanistic insights on the photoredox
degradation of CECs using organic photocatalysts.*

Alice Pavanello

Directors:

Prof. M. Luisa Marin Garcia

Prof. Miguel A. Miranda Alonso

Valencia, June 2022

Summary

Water request and water pollution are two bonded problems not only of the last years but also for the future. A lot has been done in the past in order to eliminate contaminants of emerging concerned (CECs) from the aquatic systems, using different kind of techniques; among them, those mediated by light have obtained great attention in the last years, due to their high efficiency and their low costs. Among all these techniques, Advanced Oxidation and Reduction Processes (AOPs and ARPs, respectively) have been developed in order to efficiently remove CECs. In detail, in this thesis the use of organic molecules as photocatalysts has been investigated in combination with solar and visible light; riboflavin and eosin Y have been selected as photocatalysts for their different chemical properties: the first is a natural molecule, well-known for its oxidative properties, while the second one is a synthetic dye.

The main aim of this doctoral thesis was to investigate the degradation of various classes of CECs through the use of organic photocatalysts and visible light. In detail, degradation trends of each CEC was monitored vs time under different working conditions, in order to find the best photodegradation system. Moreover, the operating mechanism was investigated through the determination of the main photoproducts and through the study of the generated reactive species, involved in the processes. Additional toxicity tests were performed in order to have an overall view of all the participants of the system. At the end, all the information was combined to postulate an hypothetical degradation mechanism for all the CECs. More specifically, the thesis could be divided in two main parts: in chapters 3 and 4 oxidation of CECs was carried out, while in chapters 5 and 6 reductive conditions were evaluated.

In detail, in chapters 3 and 4, three pharmaceutical compounds were oxidized in the presence of acetylated riboflavin (RFTA) and visible light. Specifically, carbamazepine, atenolol and noscapine were investigated under oxidative conditions. Photodegradation studies of the initial compounds and of their photoproducts were important in order to understand their natural oxidation in the natural aqueous systems. All the oxidative pathways were considered in a final hypothetical degradation mechanism.

Moreover, in chapters 5 and 6, the photodegradation of a few examples of the benzotriazole UV-stabilizers (BUVSs) was investigated. BUVSs are very recalcitrant compounds, not affected under oxidative conditions. Consequentially, multiple photocatalytic systems were tested and finally, various BUVSs were degraded under reductive conditions in the presence of RFTA or eosin Y (EOY) as photocatalysts, a sacrificial donor as DABCO and visible light. As in the previous chapters, photochemical measurements were necessary to determine the main degradation pathway and the reactive chemical species involved in the process. Additional experiments in the presence of other sacrificial donors and marine water have been performed in order to recreate a real natural environment for future studies.

Resumen

La demanda de agua y la contaminación del agua son dos problemas ligados no solo de los últimos años sino también para el futuro. Mucho se ha hecho en el pasado para eliminar los contaminantes emergentes (CEC) de los sistemas acuáticos, utilizando diferentes tipos de técnicas; entre ellos, los mediados por luz han obtenido gran atención en los últimos años, debido a su alta eficiencia y sus bajos costos. Entre todas estas técnicas, se han desarrollado Procesos Avanzados de Oxidación y Reducción (AOPs y ARPs, respectivamente) para eliminar eficientemente las CECs. En detalle, en esta tesis se ha investigado el uso de moléculas orgánicas como fotocatalizadores en combinación con luz solar y visible; La riboflavina y la eosina Y han sido seleccionadas como fotocatalizadores por sus diferentes propiedades químicas: la primera es una molécula natural, conocida por sus propiedades oxidativas, mientras que la segunda es un colorante sintético.

El objetivo principal de esta tesis doctoral fue investigar la degradación de varias clases de CEC mediante el uso de fotocatalizadores orgánicos y luz visible. En detalle, se monitorearon las tendencias de degradación de cada CEC frente al tiempo en diferentes condiciones de trabajo, con el fin de encontrar el mejor sistema de fotodegradación. Además, se investigó el mecanismo de funcionamiento mediante la determinación de los principales fotoproductos y mediante el estudio de las especies reactivas generadas, involucradas en los procesos. Se realizaron pruebas de toxicidad adicionales para tener una visión general de todos los participantes del sistema. Al final, toda la información se combinó para postular un mecanismo de degradación hipotético para todos los CEC. Más concretamente, la tesis se podría dividir en dos partes principales: en los capítulos 3 y 4 se llevó a cabo la oxidación de CECs, mientras que en los capítulos 5 y 6 se evaluaron las condiciones reductoras.

En detalle, en los capítulos 3 y 4, se oxidaron tres compuestos farmacéuticos en presencia de riboflavina acetilada (RFTA) y luz visible. Específicamente, se investigaron carbamazepina, atenolol y nospapina en condiciones oxidativas. Los estudios de fotodegradación de los compuestos iniciales y de sus fotoproductos fueron importantes para comprender su oxidación natural en los sistemas acuosos naturales. Todas las vías oxidativas se consideraron en un mecanismo de degradación hipotético final.

Además, en los capítulos 5 y 6, se investigó la fotodegradación de algunos ejemplos de estabilizadores UV de benzotriazol (BUVS). Los BUVS son compuestos muy recalcitrantes, que no se ven afectados en condiciones oxidativas. En consecuencia, se probaron múltiples sistemas fotocatalíticos y, finalmente, varios BUVS se degradaron en condiciones reductoras en presencia de RFTA o eosina Y (EOY) como fotocatalizadores, un donante de sacrificio como DABCO y luz visible. Al igual que en los capítulos anteriores, las mediciones fotoquímicas fueron necesarias para determinar la principal ruta de degradación y las especies químicas reactivas involucradas en el proceso. Se han realizado experimentos adicionales en presencia de otros donantes de sacrificio y agua marina para recrear un entorno natural real para estudios futuros.

Resum

La demanda d'aigua i la contaminació de l'aigua són dos problemes lligats no sols dels últims anys sinó també per al futur. Molt s'ha fet en el passat per a eliminar els contaminants emergents (CECs) dels sistemes aquàtics, utilitzant diferents tipus de tècniques; entre ells, els mediats per llum han obtingut gran atenció en els últims anys, a causa de la seua alta eficiència i els seus baixos costos. Entre totes aquestes tècniques, s'han desenvolupat Processos Avançats d'Oxidació i Reducció (AOPs i ARPs, respectivament) per a eliminar eficientment les CECs. Detalladament, en aquesta tesi s'ha investigat l'ús de molècules orgàniques com fotocatalitzadores en combinació amb llum solar i visible; la riboflavina i l'eosina I han sigut seleccionades com fotocatalitzadores per les seues diferents propietats químiques: la primera és una molècula natural, coneguda per les seues propietats oxidatives, mentre que la segona és un colorant sintètic.

Detalladament, es van monitorar les tendències de degradació de cada CEC enfront del temps en diferents condicions de treball, amb la finalitat de trobar el millor sistema de fotodegradació. A més, es va investigar el mecanisme de funcionament mitjançant la determinació dels principals *fotoproductos i mitjançant l'estudi de les espècies reactives generades, involucrades en els processos. Es van realitzar proves de toxicitat addicionals per a tindre una visió general de tots els participants del sistema. Al final, tota la informació es va combinar per a postular un mecanisme de degradació hipotètic per a tots els *CEC. Més concretament, la tesi es podria dividir en dues parts principals: en els capítols 3 i 4 es va dur a terme l'oxidació de CECs, mentre que en els capítols 5 i 6 es van avaluar les condicions reductores.

Detalladament, en els capítols 3 i 4, es van oxidar tres compostos farmacèutics en presència de *riboflavina *acetilada (*RFTA) i llum visible. Específicament, es van investigar *carbamazepina, atenolol i *noscipina en condicions oxidatives. Els

estudis de *fotodegradación dels compostos inicials i dels seus *fotoproductos van ser importants per a comprendre la seua oxidació natural en els sistemes aquosos naturals. Totes les vies oxidatives es van considerar en un mecanisme de degradació hipotètic final.

A més, en els capítols 5 i 6, es va investigar la fotodegradación d'alguns exemples d'estabilitzadors UV de benzotriazol (BUVS). Els BUVS són compostos molt recalcitrants, que no es veuen afectats en condicions oxidatives. En conseqüència, es van provar múltiples sistemes *fotocatalític i, finalment, diversos *BUVS es van degradar en condicions reductores en presència de RFTA o eosina I (EOY) com fotocatalitzadores, un donant de sacrifici com DABCO i llum visible. Igual que en els capítols anteriors, els mesuraments fotoquímics van ser necessàries per a determinar la principal ruta de degradació i les espècies químiques reactives involucrades en el procés. S'han realitzat experiments addicionals en presència d'altres donants de sacrifici i aigua marina per a recrear un entorn natural real per a estudis futurs.

Outline

| | |
|---|-----------|
| 1. Introduction | 15 |
| 1.1. Water pollution | 15 |
| 1.2. AQUAlity project | 18 |
| 1.3. Traditional degradation methods | 19 |
| 1.4. New water treatments: Advanced oxidation processes (AOPs) and Advanced reduction processes (ARPs) | 21 |
| 1.4.1. Acetylated riboflavin (RFTA) | 26 |
| 1.4.2. Eosin Y (EOY) | 31 |
| 1.5. Photochemistry | 33 |
| 1.6. Photochemistry in the degradation of pollutants | 36 |
| 2. Objectives | 41 |
| 3. Photocatalytic degradation of drugs in water mediated by acetylated riboflavin and visible light: a mechanistic study | 43 |
| 3.1. Introduction | 43 |
| 3.2. Results and discussion | 44 |
| 3.2.1. Photodegradation of RFTA | 44 |
| 3.2.2. Photodegradation of CBZ and ATN | 47 |
| 3.2.3. Singlet and triplet excited state and singlet oxygen involvement | 53 |
| 3.2.4. Overall discussion | 60 |
| 3.3. Conclusions | 63 |
| 4. Biomimetic photooxidation of noscapine sensitized by a riboflavin derivative in water: the combined role of natural dyes and solar light in environmental remediation | 65 |
| 4.1. Introduction | 65 |
| 4.2. Results and discussion | 67 |
| 4.2.1. Photodegradation of NSC and its photoproducts | 67 |

| | |
|--|------------|
| 4.2.2. Involvement of the excited state of RFTA in the degradation..... | 72 |
| 4.2.3. Overall discussion..... | 77 |
| 4.3. Conclusions | 79 |
| 5. Degradation of benzotriazole UV filters with acetylated riboflavin | |
| 5.1. Introduction | 81 |
| 5.2. Results and discussion..... | 82 |
| 5.3. Conclusions | 97 |
| 6. Photodegradation of benzotriazole UV filters by Eosin Y | 99 |
| 6.1. Results and discussion..... | 99 |
| 6.1.1. Photodegradation of BUVSs | 99 |
| 6.1.2. Photochemical experiments..... | 103 |
| 6.1.3. Overall discussion..... | 109 |
| 6.2. Conclusions | 110 |
| 7. Experimental..... | 113 |
| 7.1. Chemicals | 113 |
| 7.2. Photodegradation experiments and analytical procedures..... | 113 |
| 7.3. Toxicity tests..... | 115 |
| 7.4. Photophysical experiments | 116 |
| 7.5. Synthesis of cotarnine and opianic acid..... | 117 |
| 8. Conclusions | 125 |
| 9. Reference | 127 |

ABREVIATIONS AND SYMBOLS

| | |
|-------------------|-------------------------------------|
| A | Acceptor |
| ACN | Acetonitrile |
| AOP | Advanced Oxidation Processes |
| ARP | Advanced Reduction Processes |
| ATN | Atenolol |
| BUVVs | Benzotriazoles UV-Stabilizers |
| CECs | Contaminants of Emerging Concern |
| CBZ | Carbamazepine |
| D | Donor |
| DABCO | 1,4-Diazabicyclo[2.2.2]octane |
| DMF | N,N'-Dimethylformamide |
| DMSO | Dimethyl sulfoxide |
| E* | Energy of the excited state |
| E_{red}° | Redox potential |
| E _S | Energy of the singlet excited state |
| E _T | Energy of the triplet excited state |
| EOY | Eosin Y |
| I | Intensity |

| | |
|----------|---|
| IC | Internal conversion |
| ISC | Intersystem crossing |
| LPF | Laser Flash Photolysis |
| k_q | Kinetic constant |
| K_{sv} | Stationary Stern Volmer constant |
| O_2^- | Superoxide radical anion |
| NSC | Noscapine |
| RB | Rose Bengal |
| RF | Riboflavin |
| RFTA | Acetylated Riboflavin |
| ROS | Reactive Oxygen Species |
| SCE | Saturated calomel electrode |
| S_0 | Ground state |
| S_1 | First singlet excited state |
| T_1 | Triplet excited state |
| UV | Ultraviolet |
| UV-vis | Ultraviolet – Visible |
| UV-326 | 2-(2'-Hydroxy-3'-tert-butyl-5'-methylphenyl)- -5-chlorobenzotriazole |
| UV-327 | 2,4-Di-tert-butyl-6-(5-chloro-2H-benzotriazol-2- |

| | |
|--------------|---|
| | yl) phenol |
| UV-328 | 2-(2H-Benzotriazol-2-yl)-4,6-di-tert-pentylphenol |
| ΔG^0 | Gibbs Free energy |
| 1O_2 | Singlet oxygen |
| Φ_F | Fluorescence quantum yield |
| Φ_{ISC} | Intersystem crossing quantum yield |
| τ | Lifetime |
| WHO | World Health Organization |

1. Introduction

1.1. Water pollution

Water is a primary source, necessary for the survival of human beings and all the natural species on Earth. The 71% of the Earth's surface is water; this amount of water is distributed as: 97% is ocean, while only the 3% is freshwater. Moreover, most of this 3% is locked up in ice and in the ground, and only 1% is accessible (Figure 1.1). So, only a small percentage of the water present on Earth is available for human purposes.[1]

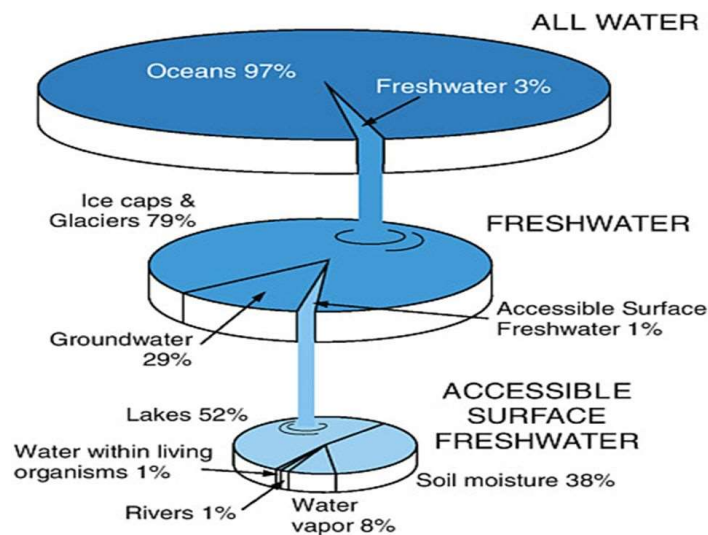


Figure 1.1. Distribution of water on Earth.

Water is used for many purposes; for instance, regarding the anthropogenic activities, water is mainly used for agriculture, not only to produce food, but also to grow biota, for maintaining temperature balances within plants or for leaching salts and other minerals away from the root zone. In urban and residential settings, it is used for drinking, cooking, cleaning, bathing, in small-scale for irrigation of gardens or municipal landscapes, waste disposal, and commercial and industrial activities.

As a matter of fact, almost all forms of production of goods and services require water. Sometimes water is embodied in the production of a good, such as water used to can fruits and vegetables or to make beverages. Other times, water is simply used to clean, cool, or operate machinery. Finally, a substantial fraction of water is used for the production of energy, either directly in hydroelectric plants or indirectly for power plant cooling.[2]

The increasing number of inhabitants increases the demand of food, and consequentially of water to grow it, and it comes along with an increase in drinking water's demand.

About 15% of the world's population lives in areas of water stress. Many people struggle to obtain access to enough water to drink, keep clean, and meet their other needs to live. According to the 2021's water report of World Health Organization (WHO), 3.4 billion people, 45% of the global population, lack access to safely managed sanitation facilities. According to independent assessments, the world will face a global water deficit of 40% by 2030. This situation will be worsened by global challenges such as COVID-19 and climate change.[3,4] In rural areas, particularly in Africa, the same water that is essential to life may be the cause of infections that lead to suffering, chronic disabilities, and death.[5,6]

In addition to bacteria and biological contamination, most of the time water is polluted by anthropogenic factors. A water pollutant is defined as a physical, chemical or biological factor causing aesthetic or detrimental effects on aquatic life. Generally, water pollution relates with industrialisation, civilisation and living standards, which are directly related to the economical level of people.[7]

The principal classes of pollutants in water are:[8]

- Heavy metals and organometallic compounds

- Radioactive molecules
- Inorganic pollutants
- Biological pathogens
- Carcenogenic chemical compounds
- Sediments
- Organic pollutants as polychlorinated biphenyls (PCB), polycyclic aromatic hydrocarbons (PAHs), pesticides, chlorinated aliphatic molecules,... also known as Contaminant of Emerging Concern (CECs).

In particular, contaminants of emerging concern (CECs) belong to a class of pollutants, which includes not only new compounds or molecules that recently appeared in the scientific literature, but also already known molecules never before detected in the environment or whose toxic effects are recently discovered.[9] As a matter of fact, the implementation of modern analytical techniques provides new data and promotes the detection of new pollutants at low concentrations, that are classified as CECs.

Along the years, European Community (EU) is trying to protect and maintain the health of aqueous systems in Europe, establishing limits for some chemical pollutants that have been labelled as priority substances. The European environmental quality standards (EQSs) for these priority substances were set in the Directive 2008/105/EC and later in the Directive 2013/39/EU. Directive 2013/39/EU also led to the creation of a watch list of CECs, which still are not routinely monitored but may pose a significant risk due to potential toxicological effects when present in waterbodies. Most of the time their environmental and human effects are unknown, but constant and long-term exposure may cause chronic effects. These substances have been listed in a Watch List in the Decision 2015/495/EU.[10,11] For example, in this group, industrial products, some pharmaceutical compounds and biocides are included.[12]

1.2. AQUAlity project

AQUAlity is a European consortium of eighteen partners, founded in 2017 as a multidisciplinary and interdisciplinary, as well as, cross – sectorial European Training Network, aiming to generate and promote 15 highly skilled scientists in the field of the removal of pollutants present in very small amount in aqueous systems. The consortium comprises 7 universities, 3 research institutes and 8 companies with a balanced participation of beneficiaries and partner organizations, academic and non-academic. Regarding the scientific point of view, the project is divided in three main Work Packages (WP) with the purpose of investigating different topics on water pollution (Figure 1.2):

- WP2 – High resolution analytical methods for the determination of CECs in aqueous systems and investigation of their environmental fate,
- WP3 – Enhanced photochemical methods for the removal of CECs and pathogens in water and wastewater,
- WP4 – Removal of CECs by hybrid membranes/Advanced Oxidation Processes (AOP) systems.

This thesis, entitled “Novel mechanistic insights on the photoredox degradation of CECs using organic photocatalysts”, belongs to WP3 and it was mainly developed at Instituto de Tecnología Química (ITQ), a joint research center, that belongs to the “Consejo Superior de Investigacion Cientificas” (CSIC) and the Universitat Politècnica de València (UPV) under the supervision of Prof. M. L. Marin Garcia and Prof M. A. Miranda Alonso. In addition to the main part of this experimental work carried out at ITQ, three secondments have been performed abroad, in particular at:

- Università degli studi di Torino, Torino, Italy; Tutor Prof. D.Fabbri

- Université Clermont-Auvergne, Clermont-Ferrand, France; Tutor Prof. M. Sleiman
- Norwegian Institute for Water Research (NIVA), Oslo, Norway; Tutor Dr. C. Escudero-Oñate.

In addition to the scientific work, AQUALity's members are also involved in training courses, dissemination & outreach activities and networking activities in order to widen the knowledge on water field, to spread and raise audience's awareness about water pollution and water treatments and to collaborate with other research projects.

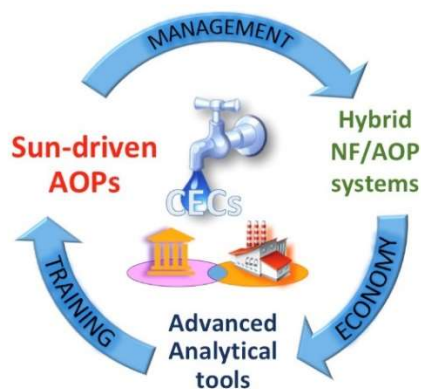


Figure 1.2. Main AQUALity's divisions.

This project has received funding from the European Union's Horizon 2020 research and innovation programme under the Marie Skłodowska-Curie grant agreement N. 765860.

1.3. Traditional water degradation methods

Considering the big problem of pollution, water is generally treated in wastewater treatment plants (WWTP). The process is divided in four different and consecutive

treatments as shown in Figure 1.3: the pre-treatment, the primary treatment, the secondary treatment, and the tertiary treatment; separately, sludges are also treated to remove all the possible pollutants and recover the most amount of water.[13]

| Level | Removal |
|-------------|---|
| Preliminary | <ul style="list-style-type: none"> • Coarse suspended solids (larger material and sand) |
| Primary | <ul style="list-style-type: none"> • Settleable suspended solids • Particulate (suspended) BOD (associated to the organic matter component of the settleable suspended solids) |
| Secondary | <ul style="list-style-type: none"> • Particulate (suspended) BOD (associated to the particulate organic matter present in the raw sewage, or to the non settleable particulate organic matter, not removed in the possibly existing primary treatment) • Soluble BOD (associated to the organic matter in the form of dissolved solids) |
| Tertiary | <ul style="list-style-type: none"> • Nutrients • Pathogenic organisms • Non-biodegradable compounds • Metals • Inorganic dissolved solids • Remaining suspended solids |

Note: depending on the treatment process adopted, the removal of nutrients (by biological processes) and pathogens can be considered an integral part of secondary treatment.

Figure 1.3. Wastewater treatments in a wastewater treatment plant (WWTP).[13]

In the pre-treatment, all the constituents of residual water, which could damage the system and create maintenance problems, are eliminated (for example big materials, sand, rocks and coarse solids). In the primary treatment, the aim is to remove all the sedimentable solids, the suspended solids, the natural organic matter and the heavy metals. Because of the nature of the removed materials, physical mechanisms are applied in these two treatments of the WWTP: decantation, coagulation, flocculation, chemical precipitation are several of the applied techniques, which, at the end, gives rise to a big number of materials in the form of sludge.

The main objective of the secondary treatment is to remove the organic matter, that was not removed in the previous physical techniques: in this step, the main treatment

is biological. Bacteria, protozoa, fungi, algae and worms use the organic matter as nutrients, that is finally converted into CO₂, water and cell tissues, which can be easily separated by decantation. Biological treatment is delicate, because microorganisms need O₂ and the maintenance of some physical environmental parameters as temperature, pH, contact time, etc.[14] Moreover, the presence of some toxic metals or pollutants could kill all the microorganisms.

The tertiary treatment depends on the required quality of water. It includes processes like chlorination, ozonation and UV treatments, which can remove the bacteria, that are still in the water and oxidized organic pollutants, impossible to remove in the previous steps. Today's pollutants, such as heavy metals, chemical compounds, and toxic substances, are more difficult to remove from water with the traditional treatments: so, new techniques have been implemented not only for the last steps of the WWTP but also for the initial one. Generally, these new implemented techniques could not be used alone, but combined with the traditional treatments. Filtration, advanced oxidation processes (AOPs), carbon absorption, membranes, reverse osmosis are some of the new alternatives.[15]

1.4. New water treatments: Advanced oxidation processes (AOPs) and Advanced reduction processes (ARPs)

Advanced Oxidation Processes (AOPs) consist of several innovative techniques to eliminate pollutants from the environment. In particular, these technologies have been implemented and used with high efficiency in the treatment of water and wastewater in recent decades. They are based on the *in situ* generation of oxidative radicals, which are very reactive towards pollutants. Hydroxyl radical (OH•) is the most common one and the most performant one because of its high oxidation potential ($E^\circ=2.8$ V vs SCE): the reaction rate constants between OH• radicals and organic species are in the range of 10^8 – 10^{10} M⁻¹s⁻¹. [16,17] It is also a non-selective

oxidant thus, it reacts with a high variety of organic substances. In addition to $\text{OH}\cdot$ radicals, other oxidant species can be produced such as superoxide radical anions ($\text{O}_2^{\bullet-}$), hydroperoxyl radical ($\text{HO}_2\cdot$), hydrogen peroxide (H_2O_2), solvated electrons (e^-) or hydrogen radicals ($\text{H}\cdot$), amongst others. [18–21]

Some examples of AOPs (Figure 1.4) are:

- I. Ozone-based: $\text{O}_3/\text{H}_2\text{O}_2$, O_3/UV , $\text{O}_3/\text{UV}/\text{H}_2\text{O}_2$
- II. UV-based: UV , $\text{UV}/\text{H}_2\text{O}_2$
- III. Fenton-related: $\text{Fe}/\text{H}_2\text{O}_2$, including photo-Fenton, electro-Fenton, etc.
- IV. Heterogeneous photocatalysis: $\text{TiO}_2/h\nu$
- V. Radiolysis
- VI. Ultrasound-based: sonolysis, ultrasound-supported Fenton, etc [22]

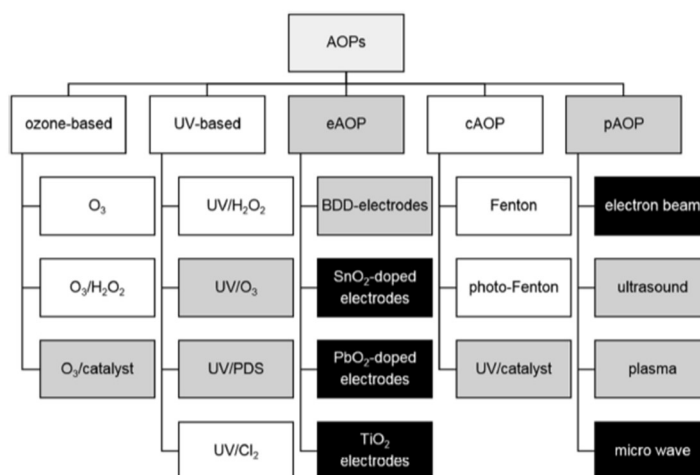
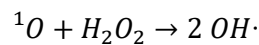
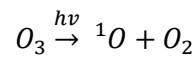


Figure 1.4. Scheme of the AOP's techniques.[23]

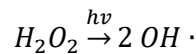
The first group of techniques is the ozone-based one. Ozone (O_3) is a powerful oxidant ($E^\circ = 2.07 \text{ V vs SCE}$) [17] capable of reacting with a lot of chemical groups, for example double bonds. Moreover, if coupled with UV irradiation (under 330 nm) or H_2O_2 , it can be used as a good source of hydroxyl radicals, and consequently as a

technique for water treatment.[24–26] The ozone molar absorption coefficient at 254 nm is $3600 \text{ M}^{-1}\text{cm}^{-1}$. [26]

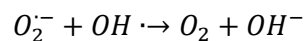
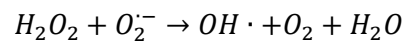
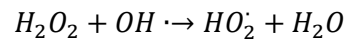
I.



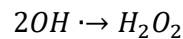
II. Hydroxyl radicals could also be formed by the photolysis of hydrogen peroxide under UV light ($\lambda < 280\text{nm}$). As a matter of fact, the maximum of absorption of hydrogen peroxide is 254 nm with a molar absorption coefficient around $43.6 \text{ M}^{-1}\text{cm}^{-1}$. The reaction is:



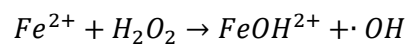
This reaction could also be followed by others, for example:



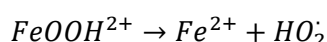
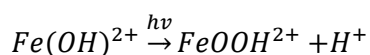
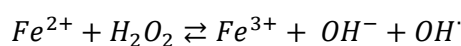
At the same time, reactive species could also recombine, as for example:



III. The Fenton reaction is based on decomposition of hydrogen peroxide in the presence of iron (II) at $\text{pH} < 3$ ($\text{pH} < 3$ is necessary to avoid the precipitation of Iron (II)):

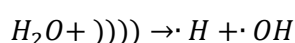


A more efficient reaction is the photo-Fenton reaction, in which UV-Vis light is used to regenerate Fe^{2+} : [27]



IV. Ionizing radiations (X rays) in water may produce a lot of reactive species like OH^\cdot , $e^-(aq)$, H^\cdot , and others less stable. This is one of the most efficient techniques of production of hydroxyl radicals, but it is very expensive and very risky, so it is not well developed. More efficient and soft is the use of UV light (<200nm) because its quantum yield for the production of OH^\cdot is around 30-40% at 185 nm.[28]

V. Cavitation or radiation could be an alternative technique: cavitation is the formation, growth, and subsequent collapse of the bubbles in water by using ultrasonic irradiation (i.e., ultrasound). Because of the cavitation, a huge amount of energy is released into the liquid. The cavity collapse results in the creation of local hot spots at a very high temperature and pressure up to 10,000 K and 1000 atm, respectively. The cavitation bubbles containing dissolved gases and water vapor could split water, according to the following reaction:



Unfortunately, the yield is very low because of the radical–radical recombination that occurs in the gas phase or at the air–water interface of collapsing bubbles and constitutes a considerable limit to the energy efficiency for degradation of pollutants. Indeed, most of the energy required to form reactive radicals is lost during recombination.[26]

VI. For these reasons, heterogeneous photocatalysis is still one of the most applied AOPs techniques; generally, a semiconductor photocatalyst is used,

combined with UV light. TiO_2 is one of most famous photocatalysts and it is considered as a model in the photocatalytic reactions.[29–31] Unfortunately TiO_2 has the big disadvantage that it is able to absorb only UV light, and UV light represents less than 5 % of the solar light. Therefore, with the aim of making a better use of the solar spectrum (Figure 1.5), the most recent contributions in this field are focusing more on a better use of solar light. [32–34]

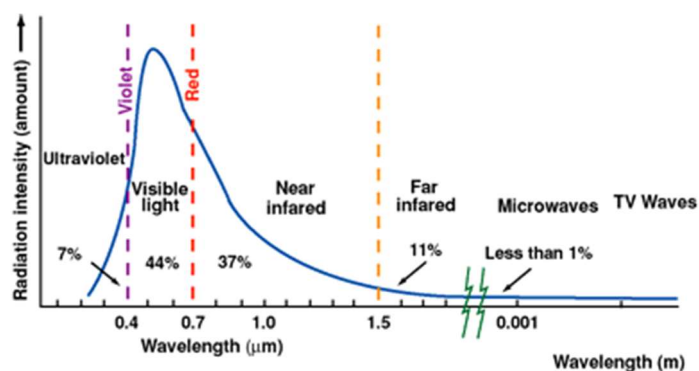


Figure 1.5. Solar light spectrum.

Alternatively, the synthesis of new visible-light absorbing organic complexes could be a feasible alternative to TiO_2 . For example, several tris(bipyridine) ruthenium and iridium complexes have been used as visible light photoredox catalysts; however, the high costs, the possible toxicity and the limited availability of these metals could be a problem for their use in large scale. Moreover, these photocatalysts are soluble in water, so they couldn't be reused.[35]

On the other hand, the implementation of organic molecules as organic photocatalysts is a less explored approach to some of these problems: as a matter of fact, these molecules can absorb in the visible region and promote electron transfer processes, which could degrade recalcitrant pollutants. Moreover, as organic, they are metal free and in most cases, they are natural and non-toxic compounds (as for

example riboflavin, which is a natural vitamin). Indeed, organic dyes have been considered as an attractive alternative to transition metal complexes as Ruthenium and Iridium, because they are less expensive and less toxic, easy to handle and sometimes even better performing.[36–38] Even if organic photocatalysts are mostly soluble in water as the previously mentioned metal complexes, they could be easily supported into materials to be reused: for example synthetic materials, based on riboflavin supported on SiO₂, revealed a high photodegradation efficiency even after multiple reuses.[39]

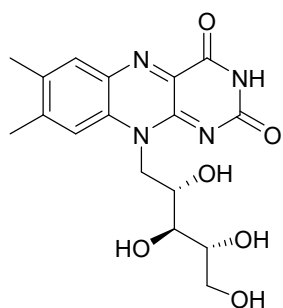
Even if AOPs are the best known advanced techniques, in the last years reductive techniques have started to be explored; the Advanced Reduction Processes (ARPs) are a new class of techniques which degrades oxidized contaminants by producing highly reactive reducing radicals by combining reagents and activation methods.[40] The involved reducing radicals typically include e_{aq}⁻ and H[•], in addition to others such as sulfite radical anions (SO₃^{•-}) and sulfur dioxide radical anions (SO₂^{•-}), depending on the used activation methods and chemical solutes.[41] Even if the term ARP was introduced a decade ago, the use of ARPs for environmental purposes and in particular for water treatment is quite recent. Some studies revealed that ARPs were effective for various organic oxidized contaminants, as vinyl chlorides, perchlorate, bromate, nitrate and per- and polyfluoroalkyl substances (PFAS).[41–46] Moreover, ARP could be associated with AOP, forming AO/RPs: combined techniques where both oxidizing and reducing species are formed. These could represent an advantage because they allow the simultaneous degradation of multiple classes of contaminants.[47]

1.4.1. Acetylated riboflavin (RFTA)

Riboflavin (RF) is the natural soluble vitamin B₂, which widely exists in fruits, vegetables, and microorganisms. Its chemical structure is composed of an

isoalloxazine ring bound to a ribitol side chain (Figure 1.6A). It is well established that riboflavin participates in a diversity of redox reactions central to human metabolism, through the cofactors flavin mononucleotide (FMN) and flavin adenine dinucleotide (FAD), which act as electron carriers, so it is an important human nutrient.[48,49]

A



B

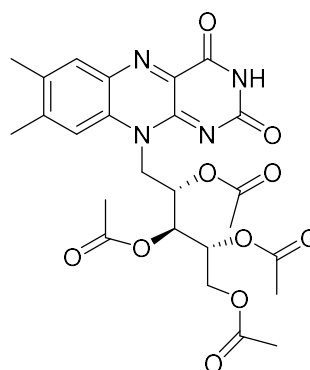


Figure 1.6. (A) Riboflavin (RF) and (B) acetylated riboflavin (RFTA).

RF exhibits a characteristic UV-visible spectrum with two absorption bands centred at around 450 and 350 nm with high molar absorption coefficients. In particular, the spectra and the main photophysical parameters for RF and RFTA are reported in Figure 1.7 and Table 1.1.

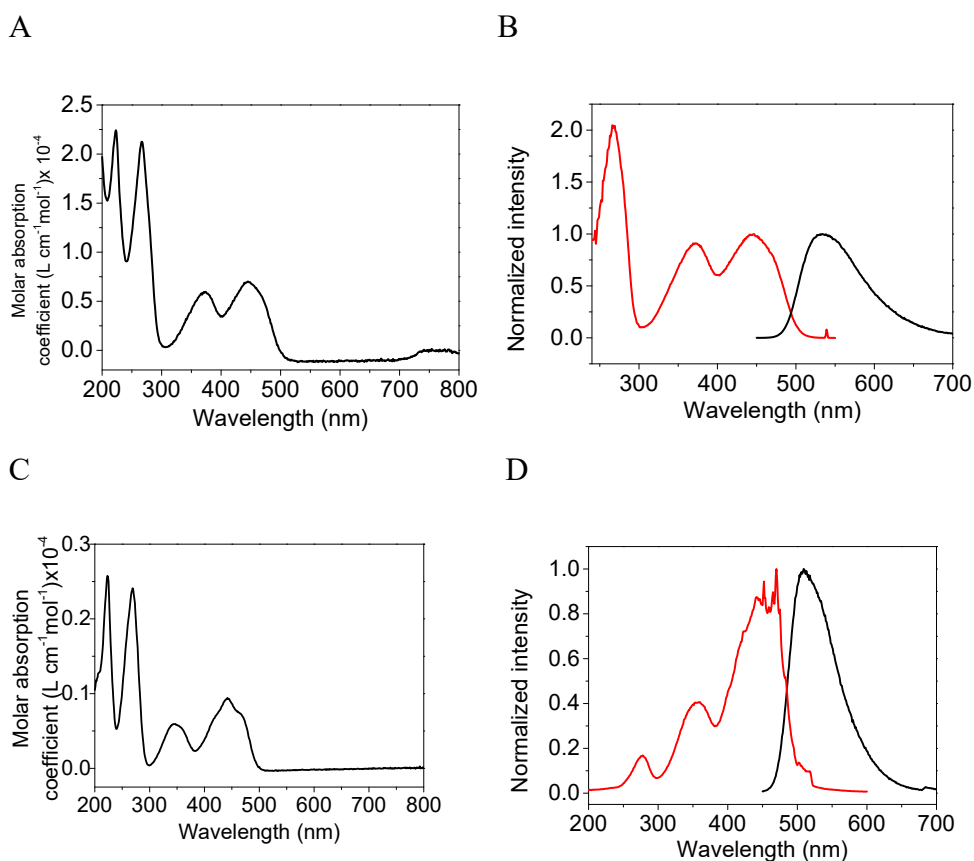


Figure 1.7. UV-visible spectrum of RF(A) and RFTA (C). Excitation (—) and emission (—) spectra of RF (B) and RFTA (D)

| Thermodynamic parameters | Thermodynamic data |
|--------------------------------|--------------------|
| ${}^1\text{RF}^*$ | 2.48 eV |
| ${}^3\text{RF}^*$ | 2.17 eV |
| $\text{RF}/\text{RF}^{\cdot-}$ | -0.8 V |
| Φ_{F} | 0.53 |
| Φ_{ISC} | 0.47 |

Table 1.1 Photophysical and redox properties of RF.[50]

In particular, the first band, at 450 nm, could be used for visible light technologies: RF could be supported on SiO₂ particles in order to degrade contaminants under visible light.[39] More generally, RF is used to study the natural photodegradation of organic pollutants in the aqueous environment: as a matter of fact, it is one of the components of natural organic matter (NOM) and being in the aqueous systems, it could be responsible for the natural degradation of CECs. In fact, this hypothesis has been deeply mentioned in literature.[51–53] Oxidation of contaminants in water using RF as possible photocatalyst may occur through two main pathways, called Type I and Type II (Figure 1.8).

The two pathways start when RF absorbs light with the subsequent formation of its singlet excited state (¹RF*), which is then converted into the triplet excited state (³RF*) by intersystem crossing (ISC). In the Type-I mechanism, the triplet excited state (and also the singlet excited state) is reduced by taking an electron or by hydrogen abstraction from another molecule (Q) (in our specific case it could be a contaminant) to form riboflavin radical anion (RF^{•-}). The catalytic cycle is closed upon interaction between RF^{•-} and oxygen with the consequent formation of ground state riboflavin and superoxide anion. In Type-II mechanism, ³RF* reacts with oxygen forming singlet oxygen (¹O₂), a well-known reactive oxygen species (ROS). Moreover, singlet oxygen and/or superoxide anion could not only oxidize contaminants in water, but they are also responsible for the degradation of RF itself.[54–56]

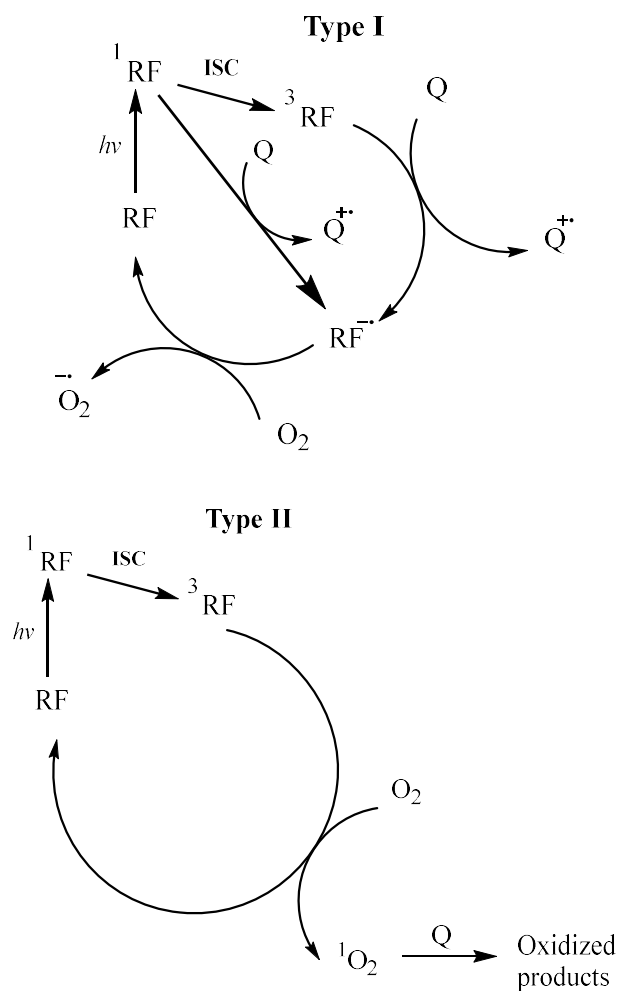


Figure 1.8. Degradation of CECs in water photocatalyzed by RF through Type I and Type II mechanisms.

As it can be degraded itself under light irradiation, improving photochemical stability is an important issue for using RF as photocatalyst: as a matter of fact, the modification of the ribose chain may change the yield, the lifetime of the excited state and make riboflavin a more photostable molecule.[39] For example, upon esterification, RF can be converted to 2',3',4',5'-tetraacetylriboflavin (RFTA) (Figure

1.7B) which is reported to be more stable; therefore, it would be more efficient in the degradation of contaminants in water. [57]

1.4.2. Eosin Y (EOY)

Eosin Y (EOY) is a xanthene dye, synthesised for the first time at the end of the XIX century in Germany. It was mainly commercialized as a dye because of its red-pink colour (Figure 1.9).[58,59] As a classic dye, it finds application in cell staining, as a pH indicator, as an indicator in the analytical halide determination and as a dye pigment.[60]

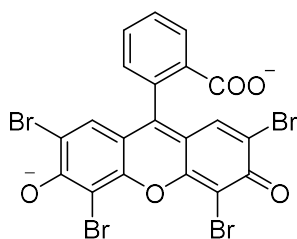


Figure 1.9. Chemical structure of Eosin Y dianion (EOY).

EOY has a characteristic absorption band at 530 nm, responsible for the pink colour; from the intersection between the excitation and the emission spectra, a value of 527 nm ($E = 54.27$ kcal/mol) for the singlet excited state can be estimated (Figure 1.10). It has been reported that the excitation of the dye by green light is followed by a rapid intersystem crossing from the singlet to the lowest energy triplet state, which has a lifetime of ca. 24 μ s.[61,62] Then, an electron transfer from the triplet excited state of the molecule could occur with the consequent formation of reactive radical species. The reported excited state oxidation and reduction potentials, together with the involved species, are represent in Figure 1.11. Hence, Eosin Y has been widely used as an organo-photocatalyst in synthetic transformations using both photooxidation and photoreduction possibilities.[63–65]

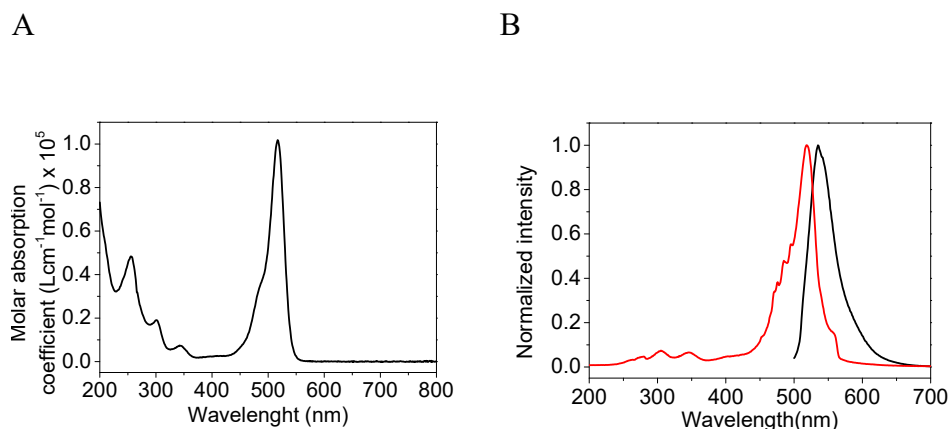


Figure 1.10. UV-vis spectrum of EOY (A) and excitation (—) and emission (—) spectra of EOY (B).

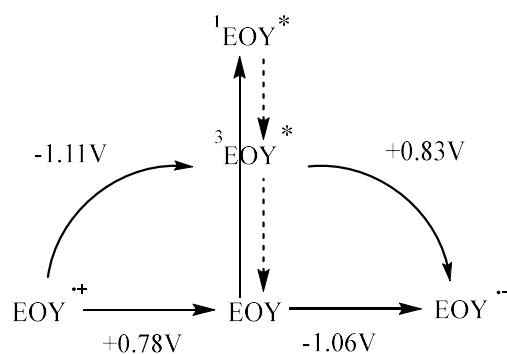


Figure 1.11. Redox potential of EOY.[63]

The main disadvantage of EOY as a photocatalyst is that it is easily degraded under irradiation. On the other hand, as a dye, it is considered as a contaminant for the aqueous system because it can absorb visible solar light and interfere with the biochemical aqueous photoreactions. In addition, some studies revealed that EOY could

be carcinogenic and toxic for humans and physical contact can cause redness, swelling and pain.[59,66] For this reason, in literature a lot of studies focus their attention on the degradation of EOY and dyes in general.[66,67] In this thesis, we used EOY as a photocatalyst, combined with green light: this is an innovating technique, which wants to prove the possibility of degrading two or more contaminants at the same time under the same working condition.

1.5. Photochemistry

The use of Acetylated Riboflavin and Eosin Y combined with visible light for the degradation of organic contaminants implies a deep understanding of the major principles of photochemistry. Photochemistry is the branch of chemistry concerned with the chemical effects of light on matter. So light is always considered “a reactant” in a photochemical reaction (Figure 1.12).

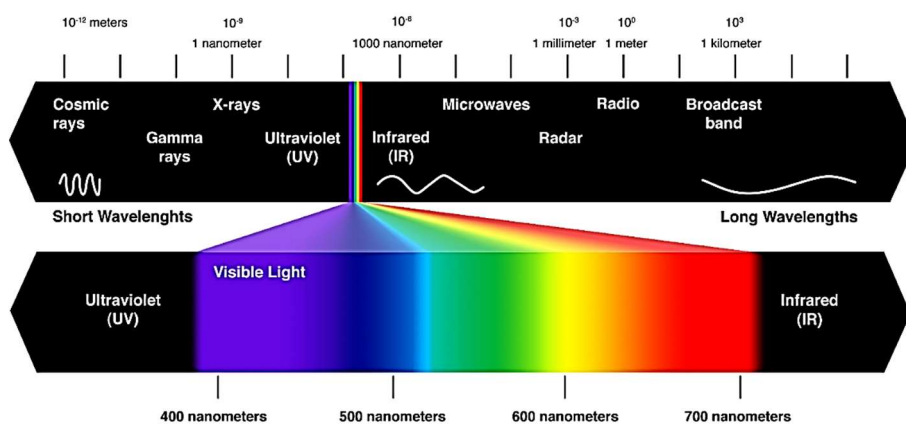


Figure 1.12. Solar electromagnetic spectrum with a focus on Visible light region (400-700 nm).

In general, the portion of the spectrum between 150 nm (far UV) and 800 nm (near-infrared) is the most frequently used in photochemical reactions. The first law of

photochemistry states that only the light absorbed by a molecule can produce a photochemical modification in the matter (Grotthuss–Draper law).

The Jablonski diagram is an energy scheme of the different states of each molecule and it pretends to present all the possible pathways a molecule can follow after the interaction with light (Figure 1.13).[68]

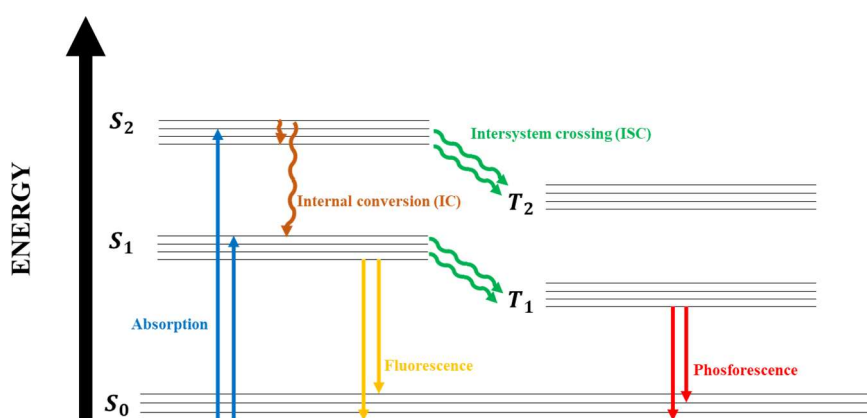


Figure 1.13. Jablonski diagram. The horizontal lines represent the electronic singlet (S_n) and triplet (T_n) levels while the thin horizontal lines represent vibrational levels. The acronyms are vibrational relaxation (VR), internal conversion (IC) and intersystem crossing (ISC). [69]

All these possible pathways that a molecule can pursue after the absorption of light are not exclusive but competitive among them.[70]

When a molecule absorbs light, one electron can be promoted from the lower energetic state, the HOMO, to an excited state, usually the LUMO (Figure 1.14).

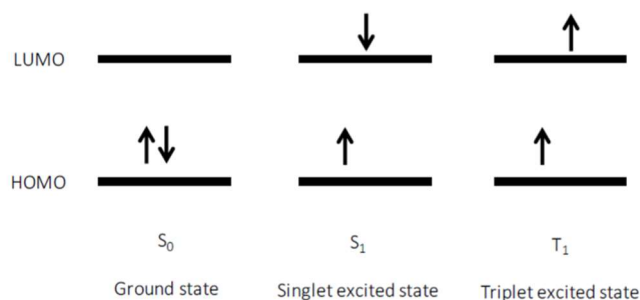


Figure 1.14. Spin electron configuration in the HOMO and LUMO.

Generally excited states are very unstable and short-lived, so they tend to lose their energy following radiative or non-radiative mechanisms. Radiative mechanisms are for example fluorescence (F) and phosphorescence (P) and they imply the loss of energy through the emission of light. Fluorescence generally happens from the lower energetic singlet excited state to the ground state, while phosphorescence happens from the triplet excited state to the ground state. As triplet excited states are less energetic than the corresponding singlet excited states, phosphorescence imply longer emission wavelengths than fluorescence. On the other hand, non-radiative mechanisms include internal conversion (IC) and intersystem crossing (ISC) and consist of the loss of thermal energy.

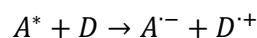
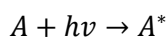
In detail, after absorption of light, an electron in the HOMO of a molecule reaches a singlet-excited state, S_1 or higher. Rapidly it relaxes, passing from the upper vibrational levels of S_n to S_1 by internal conversion (IC). From the S_1 , the electron can reach the ground state again by IC or fluorescence (F). On the other hand, from S_1 its spin could be converted into a triplet. This mechanism is called intersystem crossing (ISC) and it is a forbidden transition, because it implies a change in multiplicity. Through ISC, the molecule in a singlet excited state is converted into a triplet excited state (T_1). From T_1 , electron can lose its energy again thermally by

back ISC, followed by IC to reach the ground state or radiatively by phosphorescence (P). The spin conversion associated to the processes needed to relax the triplet excited states makes lifetimes of triplets longer, in the order of microseconds, compared to those of the singlets, in the order of nanoseconds.

In addition, if the light-sensitive molecule is in the same media of other molecules, singlet or triplet excited states (or even both) of the light-sensitive molecule could react with the other molecules, through electron or energy transfer processes. Generally, in the field of water treatment and photocatalysis, the majority of the processes occurs through electron transfer. Consequently, one molecule will become an acceptor of electrons (A), while the other will be the donor (D). In particular, the capability of the excited molecules to act as electron donors and acceptors is the key factor for the photoredox catalysis and, in the specific case of this thesis, for the photodegradation of pollutants in water.

1.6. Photochemistry in the degradation of pollutants

Considering the importance of electron transfer in this thesis, it is crucial to revise the thermodynamic equations that describe their processes. In a photoredox reaction, one of the species, in general the acceptor (A) acts from an excited state (singlet or triplet), so the process could be written as:



The Gibbs free energy of this process is calculated according to the following equation:[71]

$$\Delta G_{et}^{\circ} = E_{red}^{\circ}(D^+/D) - E_{red}^{\circ}(A/A^-) - E^*(A \text{ or } D) + \Delta E_{coulombic}$$

where $E_{red}^{\circ}(D^{+}/D)$ and $E_{red}^{\circ}(A/A^{-})$ are the redox potential of the donor and the acceptor, $E^{*}(A \text{ or } D)$ is the energy of the involved excited state and $\Delta E_{Coulombic}$ represents the interaction between the radical ions in the employed solvent. This term could be omitted in the case of polar solvents because the high dielectric constants reduce the Coulombic attraction between the ions.[72]

According to this thermodynamic equation, redox potentials are an important tool in deciding whether a given reaction is plausible, as the redox potentials relate directly to the thermodynamic viability of a reaction. Thus, a reaction that faces a significant free energy barrier is unlikely to occur.

While thermodynamics determines whether a reaction can take place, it is kinetics that determines whether it does take place: through the use of steady-state and time-resolved fluorescence, as well, as laser flash photolysis (LFP) techniques, we can determine the kinetic constants and then evaluate the contribution of both the singlet and triplet excited states of the photocatalyst in the photodegradation.

First, the quenching of the singlet state and its intrinsic decay are regulated by the following equations:

$$\text{Quenching of singlet excited state (\%)} = \frac{k_{qs}[Q]}{\frac{\Phi_F + \Phi_{ISC}}{\tau_s} + k_{qs}[Q]} \times 100$$

$$\text{Singlet excited state intrinsic decay (\%)} = \frac{\frac{\Phi_F}{\tau_s}}{\frac{\Phi_F + \Phi_{ISC}}{\tau_s} + k_{qs}[Q]} \times 100$$

where: k_{qs} is the quenching constant of the singlet excited state of the photocatalyst by Q, $[Q]$ is the concentration of the pollutant, Φ_F is the fluorescence quantum yield, Φ_{ISC} is the intersystem crossing quantum yield and τ_s is the lifetime of the singlet excited state of the photocatalyst.

Next, the quenching of the triplet excited state by the pollutants and by oxygen and the intrinsic decay depend on the following equations:

Quenching of triplet excited state (%) =

$$\frac{\frac{\Phi_{ISC}}{\tau_s}}{\frac{\Phi_F + \Phi_{ISC}}{\tau_s} + k_{qs}[Q]} \times \frac{k_{qT}[Q]}{\frac{1}{\tau_T} + k_{qT}[Q] + k_{O_2T}[O_2]} \times 100$$

Quenching of triplet excited state by O₂ (%) =

$$\frac{\frac{\Phi_{ISC}}{\tau_s}}{\frac{\Phi_F + \Phi_{ISC}}{\tau_s} + k_{qs}[Q]} \times \frac{k_{O_2T}[O_2]}{\frac{1}{\tau_T} + k_{qT}[Q] + k_{O_2T}[O_2]} \times 100$$

Triplet excited state intrinsic decay (%) =

$$\frac{\frac{\Phi_{ISC}}{\tau_s}}{\frac{\Phi_F + \Phi_{ISC}}{\tau_s} + k_{qs}[Q]} \times \frac{\frac{1}{\tau_T}}{\frac{1}{\tau_T} + k_{qT}[Q] + k_{O_2T}[O_2]} \times 100$$

where k_{qS} and k_{qT} are the quenching constants of the singlet and triplet excited state by Q, [Q] the concentration of the pollutant, Φ_F the fluorescence quantum yield, Φ_{ISC} the intersystem crossing quantum yield, τ_s and τ_T are the lifetime of the singlet and triplet excited states of the photocatalyst, k_{O_2T} is the quenching constant of triplet by oxygen and $[O_2]$ is the concentration of oxygen.

Furthermore, even assuming that 100% of the quenching of the triplet excited state of the catalyst by O₂ gives rise to singlet oxygen (¹O₂), the quenching of ¹O₂ by pollutants and ¹O₂ intrinsic decay could be calculated according to the following equations:

$$\text{Quenching of } ^1O_2 \text{ by the pollutants (\%)} = \frac{\frac{\Phi_{ISC}}{\tau_s}}{\frac{\Phi_F + \Phi_{ISC}}{\tau_s} + k_{qs}[Q]} \times \frac{k_{qTO_2}[O_2]}{\frac{1}{\tau_T} + k_{qT}[Q] + k_{qTO_2}[O_2]} \times \frac{k_{q1O_2}[Q]}{\frac{1}{\tau_{1O_2}} + k_{q1O_2}[Q]} \times 100$$

Intrinsic decay of 1O_2 (%) =

$$\frac{\frac{\Phi_{ISC}}{\tau_s}}{\frac{\Phi_F + \Phi_{ISC}}{\tau_s} + k_{qs}[Q]} \times \frac{k_{qTO_2}[O_2]}{\frac{1}{\tau_T} + k_{qT}[Q] + k_{qTO_2}[O_2]} \times \frac{\frac{1}{\tau_{1O_2}}}{\frac{1}{\tau_{1O_2}} + k_{q1O_2}[Q]} \times 100$$

Where k_{qO_2} is the quenching constant of oxygen by Q, k_{q1O_2} is the quenching constant of singlet oxygen by Q, [Q] the concentration of the pollutant, Φ_F is the fluorescence quantum yield, Φ_{ISC} is the intersystem crossing quantum yield, τ_s , τ_T and τ_{1O_2} are the lifetimes of the singlet and triplet excited states of the photocatalyst and of singlet oxygen.

2. Objectives

This Doctoral Thesis is part of the AQUALity project and in particular it is associated to WP3: it mainly involves the degradation of CECs in water using organic photocatalysts with special focus on the degradation mechanisms. Specifically, according to the soul of this project, this doctoral thesis sets the following goals:

- To find out and characterize different organic molecules as organic photocatalysts in the degradation of contaminants of emerging concern (CECs);
- To degrade different classes of CECs using different organic photocatalysts;
- To investigate the mechanisms of degradation, detecting and assigning the reaction intermediates. A particular effort will be devoted to the kinetics of the intermediates;
- To study degradation of CECs not only in an ideal chemical system (in milliQ water without other chemical species) but also in a real natural system (as for example marine water).

All these objectives will be developed in 3 years basically at Instituto de Tecnología Química (ITQ) at the Universitat Politècnica de València (UPV) under the supervision of Prof. M. L. Marin Garcia and M. A. Miranda Alonso.

3. Photocatalytic degradation of drugs in water mediated by acetylated riboflavin and visible light: a mechanistic study

3.1. Introduction

Pharmaceutical and personal care products (PPCPs) constitute one of the many classes of contaminants of emerging concern (CECs): this family is very wide, and it includes a variety of molecules with different chemical, biological and toxicological properties. As a matter of fact, PPCPs comprise all drugs and molecules used in personal care products: antibiotics, analgesics, plasticizers, antiseptics, antiepileptics, hormones, sunscreens, stimulants, organic/inorganic pollutants, and heavy metal are only some examples.[73–75] Their concentrations in the sewage water range from ng/L to µg/L.[73,76] Even if their concentration is far from the therapeutic one, if presented in water, they could show negative effects both on humans and the aquatic system and in mixtures, they could react and participate into unknown reactions with additional toxicological effects.[77,78]

In this chapter, the selected PPCPs are carbamazepine (CBZ) and atenolol (ATN) (Figure 3.1.).

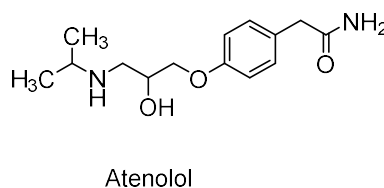
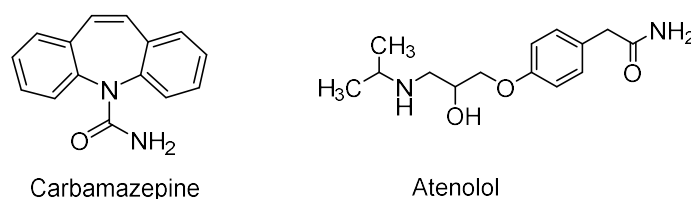


Figure 3.1. Structure of Carbamazepine (CBZ) and Atenolol (ATL)

Carbamazepine (CBZ) (Figure 3.1) is an anticonvulsant dibenzoazepine, mainly used for epilepsy, seizure disorders and neuropathic pain. Because of its wide use

and its conversion in the human liver, CBZ and its metabolites are easily detected in the aqueous environment. It is considered one of the most persistent pharmaceuticals: as a matter of fact, it is resistant to the bio and photochemical natural degradation and to the most used wastewater treatment techniques.[79,80]

Atenolol (ATN) is a β -blocker drug, used for cardiovascular diseases, hypertension, coronary heart diseases, arrhythmias, sinus tachycardia and myocardial infarction.[81] Although recent reports have shown that ATN is unlikely to cause acute toxicity at low concentrations, as CBZ, it is not naturally degraded because of its stability and so it is often detected in the natural aqueous system.[82]

In this chapter, the power of RF as a natural photocatalyst is investigated through the degradation of CBZ and ATN. In particular, RF is replaced with RFTA and a solar simulator is used as source of light. Intermediates have been detected and assigned through MS analysis. Photophysical measurements have been carried out to understand the role of excited states of RFTA and the formation of chemical reactive species. Both intermediates and photophysical data have been used to draw a plausible degradation mechanism.

3.2. Results and discussion

3.2.1. Photodegradation of RFTA

Acetylated riboflavin (RFTA, Figure 1.7), used in this work, is itself able to absorb light (see Figure 1.8), and to be consequently degraded: so preliminary irradiation tests were necessary to determine its ability to maintain its activity in the working conditions; acute toxicity was an extra interesting information for the environment. Experimental obtained data are represented in Figure 3.2.

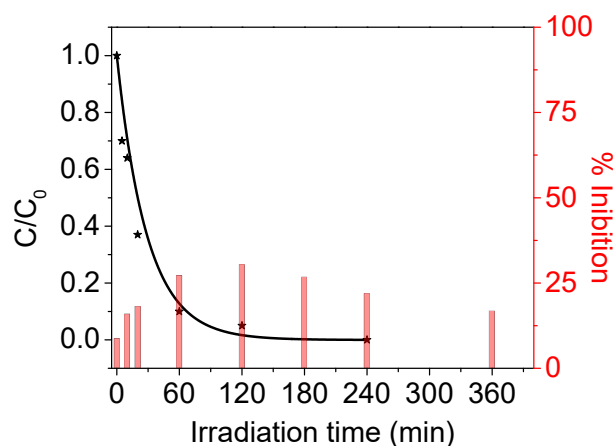
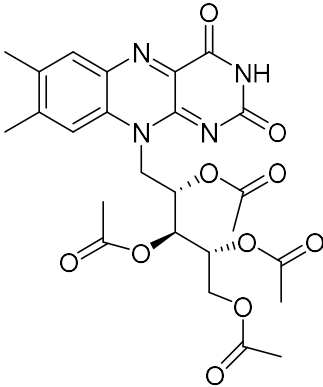
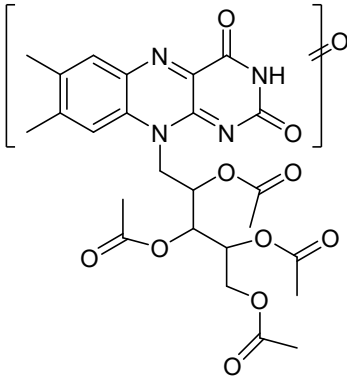
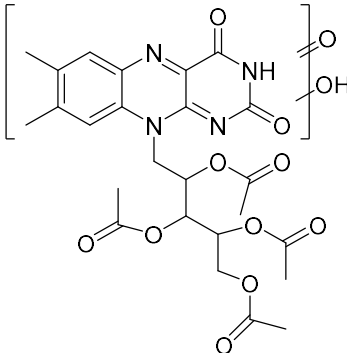


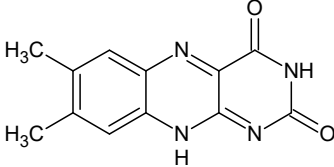
Figure 3.2. Degradation trend for RFTA (in black) and acute toxicity (in red) under visible light working conditions.

Under solar light (with a filter at 420 nm), RFTA was completely degraded in 2 hours, while the toxicity was maintained low throughout the experimental time, as the calculated EC50 for RFTA was 195 mg L⁻¹. These data confirm that neither RFTA nor the photoproducts formed during the photodegradation have a high acute toxicity.

Moreover, during the irradiation, 6 photoproducts were detected by UFLC-MS² and they are reported in Table 3.1 with the proposed chemical structure and the MS² fragmentations.

Table 3.1. Photodegradation products of RFTA.

| | R_t (min) | m/z | Product ions (MS²) | Structure |
|-----------------------|--------------------------------------|------------|--|--|
| RFTA | 6.3 | 545 | 545(100), 503(40), 461(10), 485(70), 443(20), 243(10) |  |
| Photoproduct 1 | 5.9 | 559 | 559(100), 517(50), 499(80), 475(20), 457(30), 433(10), 416(10), 257(10) |  |
| Photoproduct 2 | 5.4 | 575 | 575(100), 533(60), 515(80), 491(50), 473(50), 449(20), 431(30), 273(20) |  |

| | | | | |
|-----------------------|-----|-----|--|--|
| Photoproduct 3 | 4.6 | 243 | 243(100), 216(20), 198(40), 172(50) |  |
| Photoproduct 4 | 3.9 | 462 | 462(40), 420(50), 402(100), 384(20), 360(40), 342(20) | |
| Photoproduct 5 | 4.2 | 414 | 414(50), 353(30), 220(100) | |
| Photoproduct 6 | 4.3 | 416 | 416(30), 374(40), 356(100), 314(100), 296(30), 272(35), 254(30) | |

Initial molecule, RFTA, has a mass of 545 m/z. Photoproduct 1 with m/z of 559 and 2 with m/z of 573 could be related to the oxidation of the initial molecule, in particular of one of the methyl groups of the isoalloxazine structure; this is confirmed by the detection of the allylic groups in the MS² fragmentations. Another degradation pathway of RFTA involves the loss of the N-alkyl chain with the consequential detection of the isoalloxazine structure (Photoproduct 3), which is generally called in literature Lumichrome.[83,84] Finally, photoproducts 4, 5 and 6 seem to be obtained from the rupture of the isoalloxazine ring and the lateral chains. The cleavage of the pyrimidine ring to form quinoxaline derivatives has been previously reported for photodegradation of RF products.[85]

3.2.2. Photodegradation of CBZ and ATN

Once the stability and the toxicity of RFTA has been studied, solutions of ATN and CBZ at 10 ppm in the presence of RFTA (1ppm) were irradiated under a solar box

with a filter at 420 nm to prevent any absorption from the drugs (the UV-Vis spectra of the contaminants are in Figure 3.3A and B). The evolution of the abatement of each pollutant was monitored by HPLC-UV and they are represented vs irradiation time in Figure 3.3C.

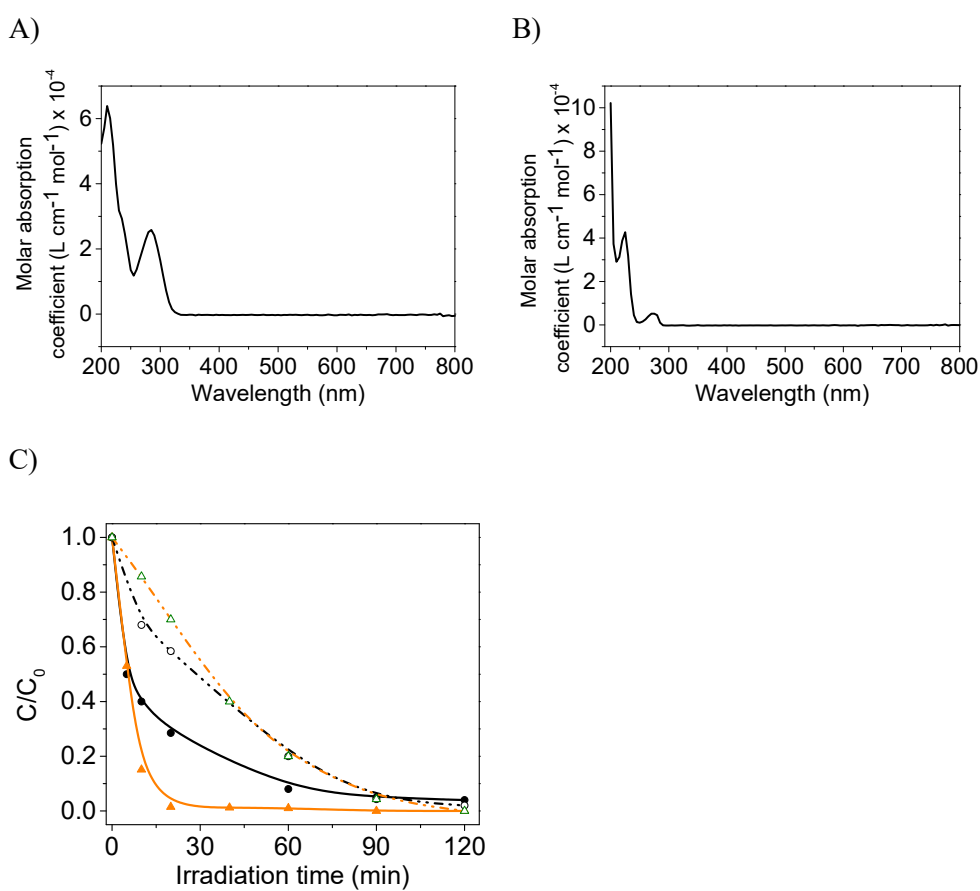


Figure 3.3. UV-Vis spectra of (A) Carbamazepine and (B) Atenolol.

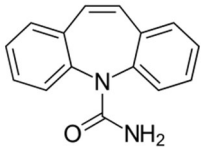
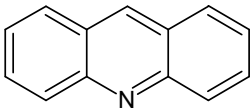
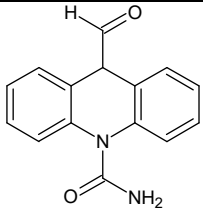
Disappearance of drugs in the presence of RFTA (solid lines and symbols) and concentration of RFTA in each experiment (dashed lines and empty symbols):

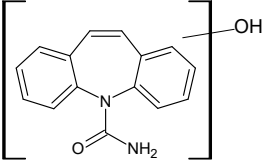
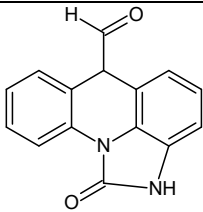
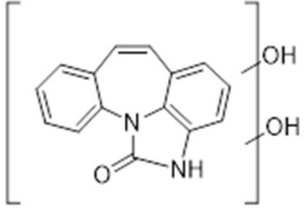
Carbamazepine (orange), Atenolol (black) (C).

As reported in Figure 3.3C, degradation of both pollutants happened in a short time: CBZ is easily degraded in less than 30 minutes, while ATN in less than 90 minutes. These results are impressive compared to the normal trends of wastewater treatment plants, in which both of the considering pollutants are not easily degraded.[80,86,87] At the same time, the stability of RFTA was enhanced in the presence of CBZ and ATN, although it was completely degraded in 120 min, as previously demonstrated in Figure 3.2.

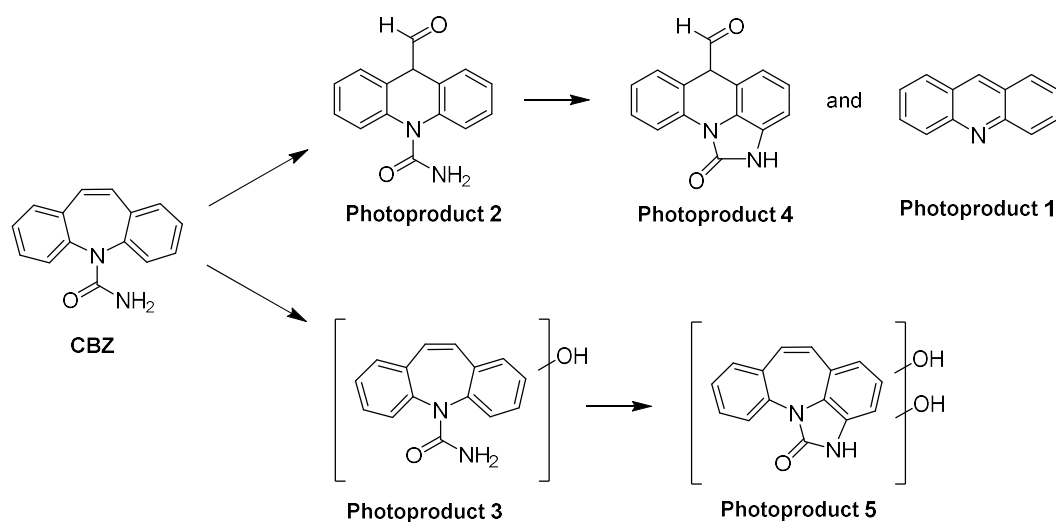
Moreover, the irradiated solutions were also analyzed by UFLC-MS² to determine the photodegradation products: in the case of CBZ, five photodegradation products were detected and their hypothetical structures, determined by the MS² spectra and the literature information,[88,89] were represented in Table 3.2.

Table 3.2. Photodegradation products of CBZ in the presence of RFTA.

| | R_t (min) | m/z | Product ions (MS²) | Structure |
|-----------------------|----------------------------|------------|---|---|
| CBZ | 5.9 | 237 | 237(80), 220(10), 194(100) |  |
| Photoproduct 1 | 3.2 | 180 | 180(100), 152(20) |  |
| Photoproduct 2 | 3.0 | 253 | 253(20), 236(30), 208(20) 210(60), 182 (50), 180(100) |  |

| | | | | |
|-----------------------|-----|-----|--|--|
| Photoproduct 3 | 4.1 | 253 | 253(60), 236(80), 208(30) 210(90), 182(50),180(100), 167(5) |  |
| Photoproduct 4 | 4.4 | 251 | 251(100), 223(20), 208(85), 195(15), 180(100) |  |
| Photoproduct 5 | 4.7 | 267 | 267(50), 249(45), 224(50), 196(100) |  |

The degradation of CBZ in the presence of RFTA could occur following two possible pathways: the first one implies hydroxylation of the molecule with the formation of photoproduct 2. Subsequently, its cyclization could lead to formation of photoproducts 1 and 2. The second route implies the formation of compound 4, the isobaric species of 2, and a second hydroxylation combined with cyclization, giving rise to the compound 5. All these photoproducts have already been described in the literature resulting from different advanced oxidation processes.[88–90] A plausible mechanism is depicted in Scheme 3.1.

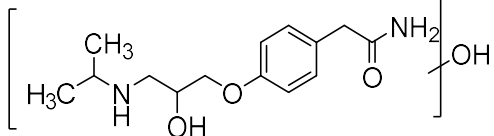
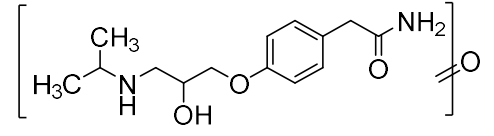
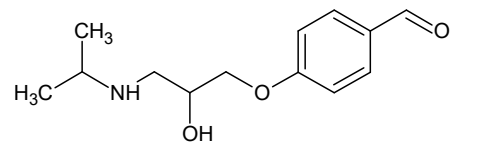


Scheme 3.1. Proposed pathway for the phototransformation of CBZ assisted by RFTA.

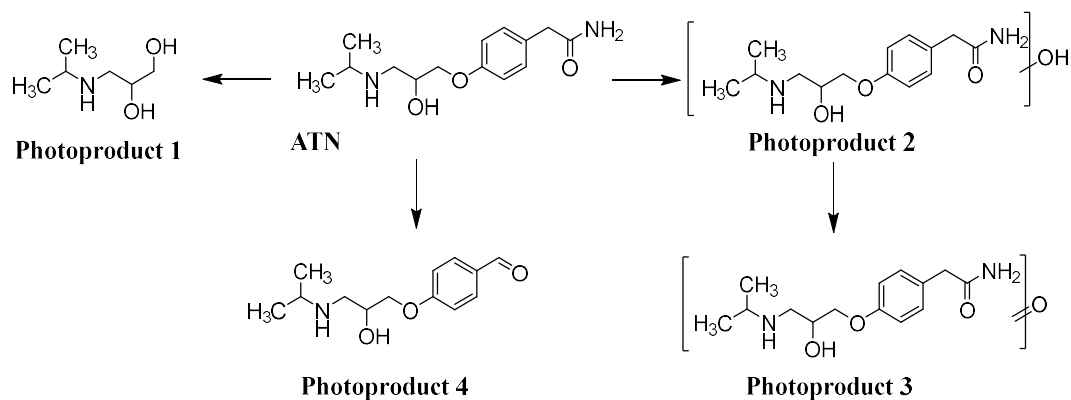
In the case of ATN, four photodegradation products were detected and their hypothetical structures, determined by the MS² spectra and the literature information, are represented in Table 3.3.[91–93]

Table 3.3. Photodegradation products of ATN in the presence of RFTA.

| | R_t (min) | m/z | Product ions (MS²) | Structure |
|-----------------------|--------------------------------------|------------|---|------------------|
| ATL | 7.9 | 267 | 267(100), 250(5), 225(25), 208(20), 190(40), 145(40), 116(20), 98(15), 74(10) | |
| Photoproduct 1 | 5.7 | 134 | 134(100), 116(20), 92(20), 74(10) | |

| | | | | |
|-----------------------|-----|-----|--|--|
| Photoproduct 2 | 7.1 | 283 | 283(100), 265(15), 160(10), 116(100) |  |
| Photoproduct 3 | 8.1 | 281 | 281(100), 263(5), 239(10), 218(15), 194(20), 176(20), 133(10), 121(75), 116(50), 98(10), 74(10) |  |
| Photoproduct 4 | 8.9 | 238 | 238(100), 220(10), 196(35), 178(5), 161(35), 149(10), 133(45), 116(20), 105(40), 98(15), 74(10) |  |

Photodegradation of ATN occurs through three different pathways: firstly, ATN could be hydroxylated, forming photoproducts 2 and 3 after a further oxidation. Secondly, ATN could lose the amide group next to the aromatic ring, forming photoproduct 4 with a characteristic aldehydic group. Thirdly, the C-O bond next to the benzene ring could be broken and the alkyl chain (photoproduct 1) could be easily detected at MS. A plausible mechanism is depicted in Scheme 3.2.



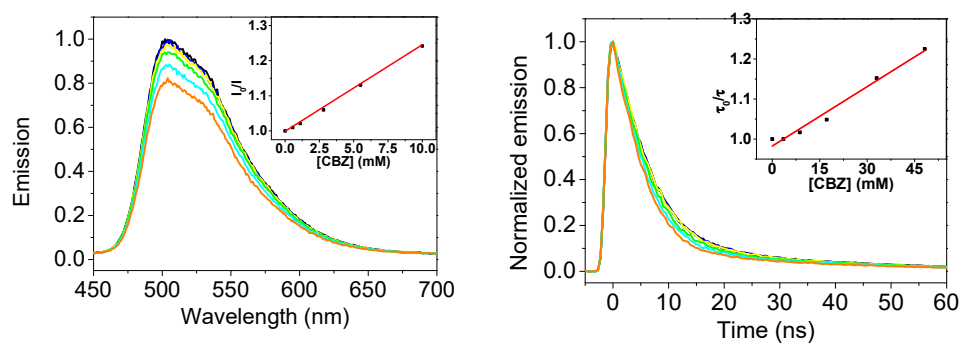
Scheme 3.2. Proposed pathway for the phototransformation of ATN assisted by RFTA.

3.2.3. Singlet and triplet excited states and singlet oxygen involvement

Interaction of singlet and triplet excited states of RFTA with each drug was investigated through fluorescence and laser flash photolysis (LFP) experiments.

In the case of singlet excited state, both steady-state and time-resolved fluorescence measurements were performed with increasing concentration of the drugs and represented in Figure 3.4. The corresponding quenching constants were determined from Stern-Volmer plots and summarized in Table 3.4. High values for the quenching constants k_{qS} were obtained in all the cases. As expected, steady-state experiments led to higher k_{qS} , due to the contribution of static quenching.

A)



B)

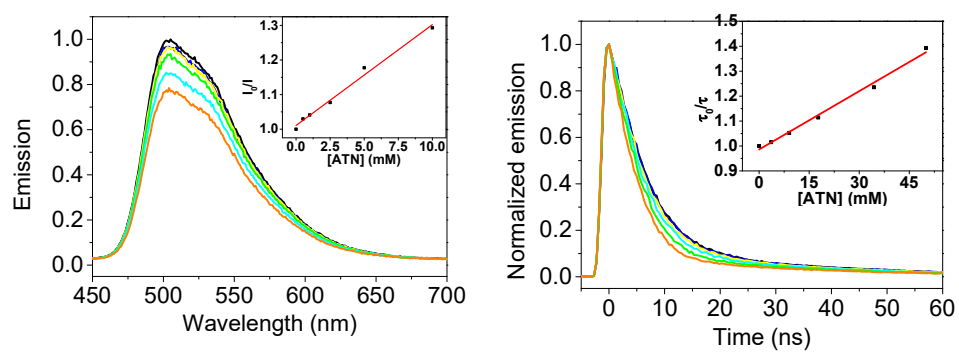


Figure 3.4. Steady-state (left) and time-resolved fluorescence (right) quenching experiments of RFTA in the presence of increasing concentrations of CBZ (A) and ATN (B), in aerated acetonitrile. $\lambda_{exc}=445$ nm for steady-state and $\lambda_{exc}=460$ nm for time-resolved experiments.

Table 3.4. Rate constant values for the reaction between the drugs and $^1\text{RFTA}^*$ obtained from steady-state and time-resolved quenching experiments emission.

| Drugs | k_{qS} ($\text{M}^{-1}\text{s}^{-1}$) from steady-state measurements | k_{qS} ($\text{M}^{-1}\text{s}^{-1}$) from time-resolved experiments |
|---------------------|--|--|
| Carbamazepine (CBZ) | 3.3×10^9 | 6.7×10^8 |
| Atenolol (ATN) | 3.9×10^9 | 1.1×10^9 |

In the case of the triplet excited state investigation, firstly LFP of RFTA alone was performed to determine the typical characteristic bands of $^3\text{RFTA}^*$: as shown in Figure 3.5, triplet excited state of RFTA is characterized by a signal at 380 nm and a broad band between 500 nm and 700 nm.

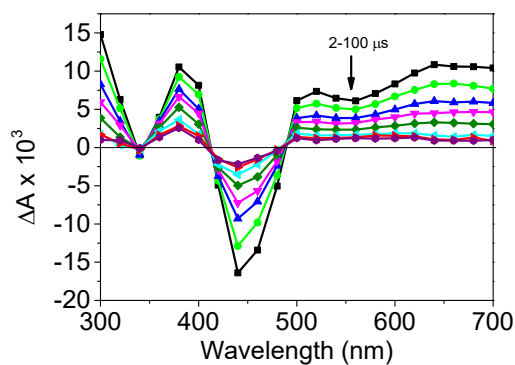
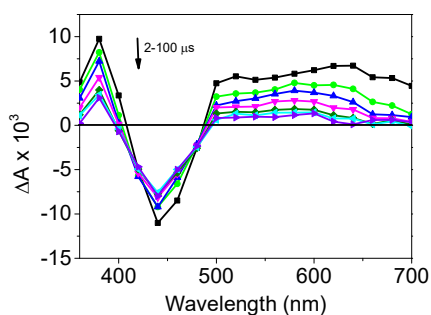


Figure 3.5. Transient absorption spectra of RFTA obtained at different times after the laser pulse (absorbance *ca.* 0.3 at $\lambda_{\text{exc}} = 355$ nm). The experiment was performed in deaerated acetonitrile.

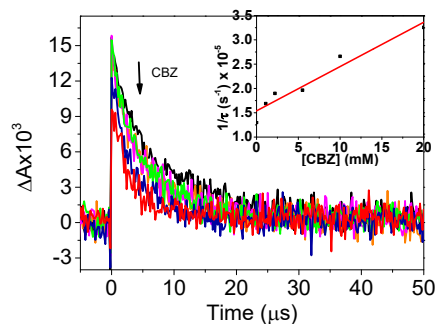
Next, the transient absorption spectrum of RFTA with the highest concentration of CBZ was recorded (Figure 3.6A): triplet excited state seems to be not completely quenched by the pollutant as it still exhibits the broad band between 500 nm and 700 nm. When the triplet excited state quenching was investigated at 680 nm, in the presence of increasing concentration of CBZ, the observed quenching was slow: this is confirmed by the determined rate constant $k_{qT} = 9.1 \times 10^6 \text{ M}^{-1} \text{ s}^{-1}$ (Figure 3.6B).

At 380 nm (Figure 3.6C), the tendency of a slower decay reveals the presence of two different species simultaneously at 380 nm: as a matter of fact, the fast decay could be related to the quenching of the triplet excited state, while the longer-lived signal could be related to the formation of RFTA^{•+}, the protonated radical of RFTA, suggesting an electron transfer oxidation of the drug under these conditions. Unfortunately, the signals of triplet and RFTA^{•+} could not be resolved in the transient absorption spectrum, since they overlap at 380 nm.

A)



B)



C)

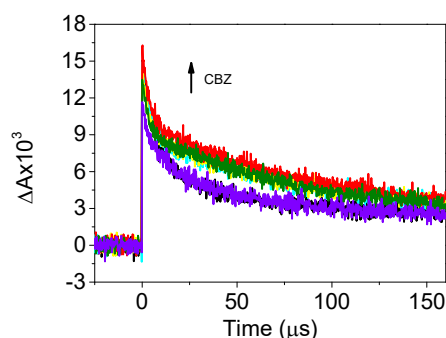


Figure 3.6. Transient absorption spectra of RFTA in the presence of carbamazepine (2×10^{-2} M), recorded at different times after the laser pulse from 300 nm to 700 nm ($\lambda_{\text{exc}} = 355$ nm) (A). Transient absorption decays of $^3\text{RFTA}^*$ with increasing additions of CBZ, recorded at 680 nm (B) and 380 nm (C). $\lambda_{\text{exc}} = 355$ nm, $[\text{CBZ}] = 0-2 \times 10^{-2}$ M. Inset represents Stern-Volmer plot corresponding to data registered at 680 nm. The experiments were performed in deaerated acetonitrile.

Likewise, $^3\text{RFTA}^*$ studies in the presence of ATN are represented in Figure 3.7. As in the case of CBZ, two main signals are centered at 380 nm and between 500 and 700 nm (Figure 3.7A).

Again, as in the previous case, quenching of RFTA triplet excited state was investigated at 680 nm, and the corresponding Stern-Volmer plot was represented in Figure 3.7B: as shown, ATN is able to quench $^3\text{RFTA}^*$ more efficiently than CBZ and for this reason the determined k_{qT} value for ATN ($k_{qT} = 3.7 \times 10^8 \text{ M}^{-1}\text{s}^{-1}$) is higher than the one of CBZ.

Moreover, at 380 nm (Figure 3.7.C), in addition to the decay, assigned to $^3\text{RFTA}^*$, the growth of a new signal was observed: this new signal, which increases with the concentration of ATN and it is more stable in time, could be assigned to RFTA^H, the protonated radical of acetylated riboflavin.

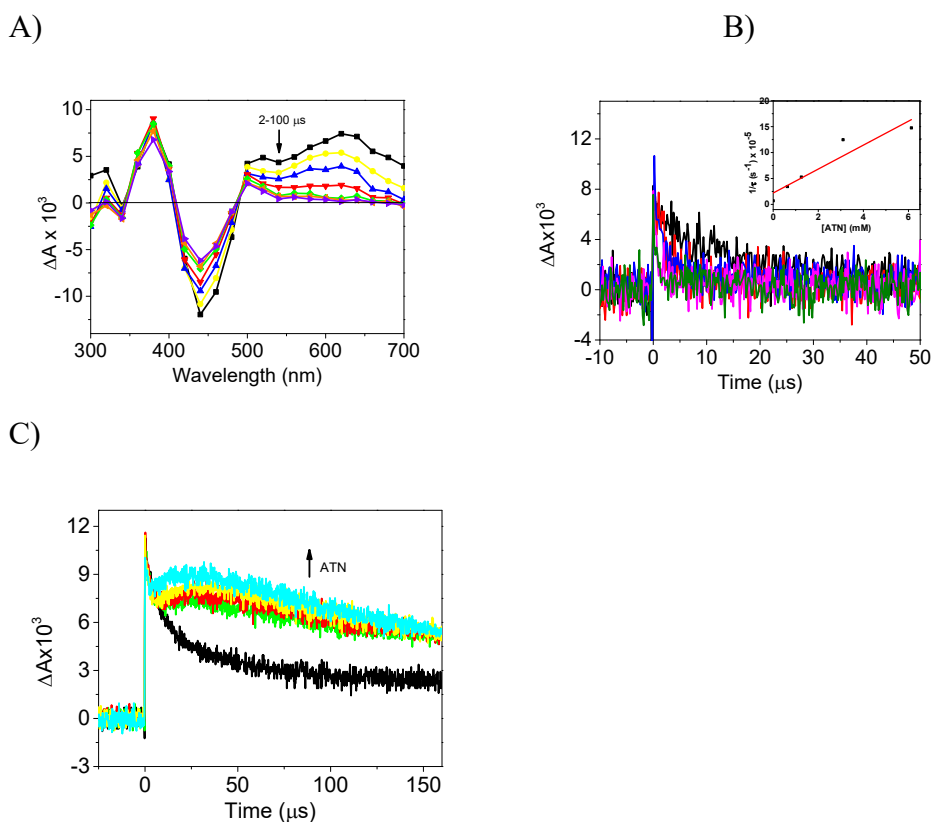


Figure 3.7. Transient absorption spectra of RFTA in the presence of atenolol ($1.9 \times 10^{-3} \text{ M}$), recorded at different time after the laser pulse from 300 nm to 700 nm ($\lambda_{\text{exc}}=355 \text{ nm}$)(A). Transient absorption decays of RFTA with increasing additions of ATN, obtained at different times after the laser pulse, recorded at 680 nm (B) and 380 nm (C). Insert image represents Stern-Volmer plot, corresponding to the quenching experiment recorded at 680 nm.

Laser flash photolysis (LFP) was also used for the study of singlet oxygen, generated in the presence of acetylated riboflavin. First, the rate constant for the quenching of $^3\text{RFTA}^*$ by O_2 was determined (Figure 3.8) and the obtained value was $k_{q\text{TO}_2} = 9.5 \times 10^9 \text{ M}^{-1}\text{s}^{-1}$.

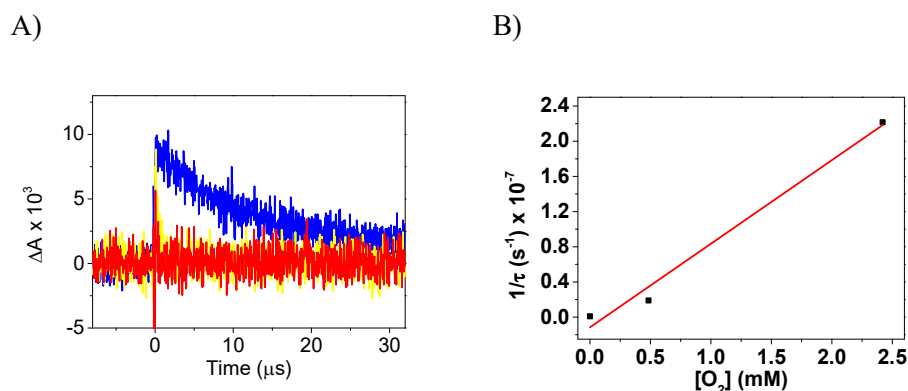


Figure 3.8. (A) RFTA triplet traces recorded at 680 nm in acetonitrile, upon increasing concentration of O_2 ; (B) Stern–Volmer fitting for the corresponding quenching.

Next, the interaction of each drug with $^1\text{O}_2$ was investigated: figure 3.9 represents the emission of $^1\text{O}_2$, registered in aerated acetonitrile upon LFP excitation of RFTA in the presence of increasing concentration of CBZ (Figure 3.9A) and ATN (Figure 3.9B). In addition, the corresponding quenching rate constants ($k_{q1\text{O}_2} = 6.4 \times 10^5 \text{ M}^{-1}\text{s}^{-1}$ for CBZ and $k_{q1\text{O}_2} = 1.4 \times 10^7 \text{ M}^{-1}\text{s}^{-1}$ for ATN) were determined from the corresponding Stern-Volmer plots, represented in the insets.

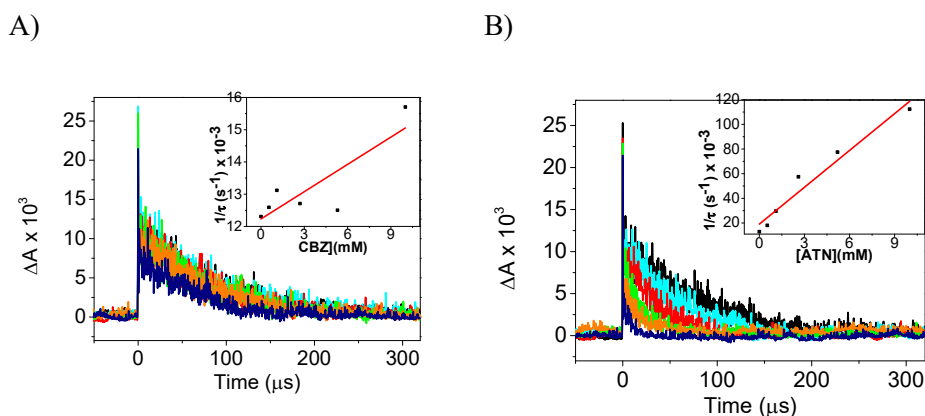


Figure 3.9. Transient emission decays of $^1\text{O}_2$ generated upon laser flash excitation ($\lambda_{\text{exc}} = 355 \text{ nm}$) of RFTA, and monitored at 1270 nm upon increasing concentrations of CBZ (A) and ATN (B). Inset represent the corresponding Stern-Volmer plots.

3.2.4. Overall discussion

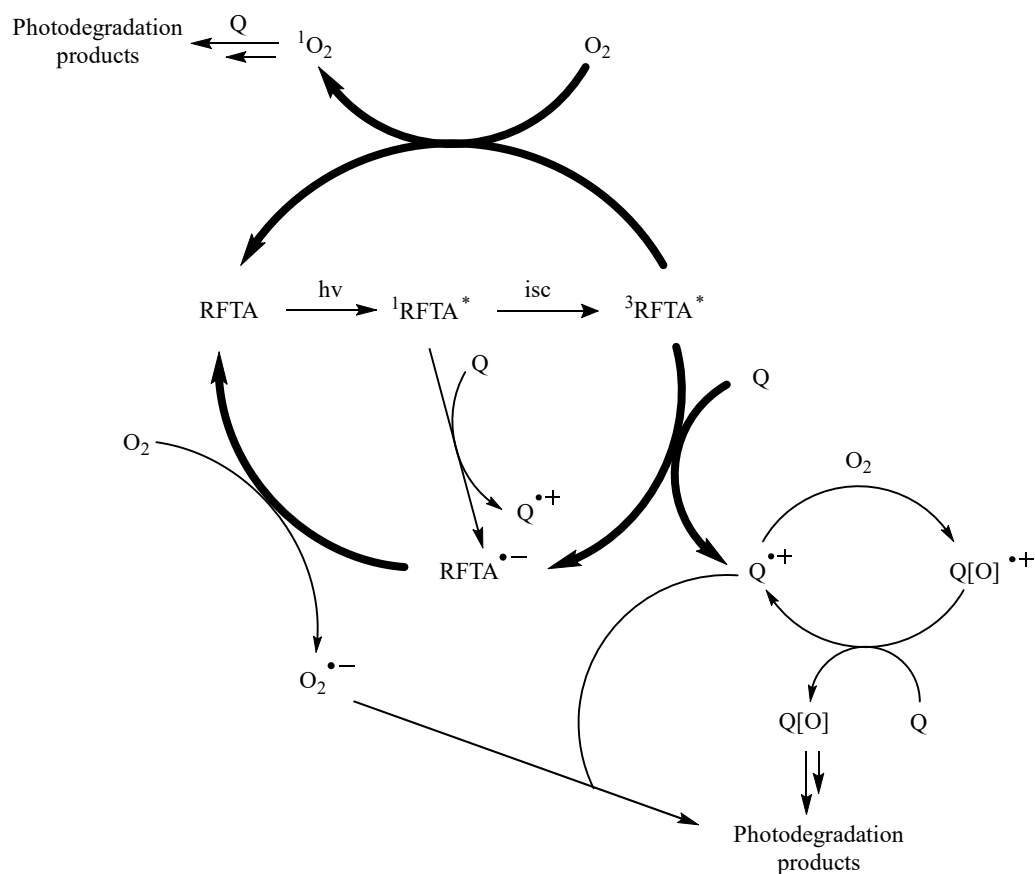
Once the interaction between the excited species of RFTA and $^1\text{O}_2$ with each drug was determined, the relative contribution of each of them was calculated. In the previous paragraph, the formation of RFTA $\cdot\text{H}^\cdot$ resulting from e^- transfer and followed by H^+ transfer has been evidenced. Now, the relative weight of each pathway was calculated taking in account the photophysical data, the concentrations of the species and the lifetime of each excited species. Using the equations already introduced in chapter 1.5, and the quenching constants, obtained from the photophysical experiments, we obtained the data shown in table 3.5.

Table 3.5. Relative contribution of the quenching of singlet and triplet excited states of RFTA and $^1\text{O}_2$ in the photocatalytic degradation of the pollutants, at different concentrations.

| [Q] (M) | Pollutant | Quenching of $^1(\text{RFTA})^*$ (%) | $^1(\text{RFTA})^*$ intrinsic decay (%) | Quenching of $^3(\text{RFTA})^*$ (%) | $^3(\text{RFTA})^*$ intrinsic decay (%) | Quenching of $^3(\text{RFTA})^*$ by O_2 (%) | Quenching of $^1\text{O}_2$ by the pollutants | $^1\text{O}_2$ intrinsic decay |
|-----------|-----------|--------------------------------------|---|--------------------------------------|---|--|---|--------------------------------|
| 10^{-3} | CBZ | 0.5 | 52.7 | 0.0 | 0.1 | 46.6 | 2.3 | 44.3 |
| | ATN | 0.8 | 52.6 | 0.4 | 0.1 | 46.0 | 24.9 | 21.1 |
| 10^{-5} | CBZ | 0.0 | 53.0 | 0.0 | 0.1 | 46.9 | 0.0 | 46.8 |
| | ATN | 0.0 | 53.0 | 0.0 | 0.1 | 46.9 | 0.5 | 46.3 |
| 10^{-8} | CBZ | 0.0 | 53.0 | 0.0 | 0.1 | 46.9 | 0.0 | 46.9 |
| | ATN | 0.0 | 53.0 | 0.0 | 0.1 | 46.9 | 0.0 | 46.9 |

As expected, the quenching is always more efficient with high concentrations of pollutants.

According to all the data obtained and the calculations done, we were able to postulate the degradation mechanism, represented in Scheme 3.3. Upon irradiation, RFTA is able to absorb visible light and reach the singlet excited state, which is slightly affected by the drugs. Consequently, most of the singlet is converted into the triplet excited state upon ISC. Here, triplet could react following two different pathways: on one hand it could be directly quenched by the drugs, with the consequent electron transfer mechanism and the formation of radical ion pairs $^3(\text{RFTA}^{\cdot-}/\text{Q}^{\cdot+})$. On the other hand, $^3\text{RFTA}^*$ could react with the oxygen in the air, forming singlet oxygen. $^1\text{O}_2$ could be quenched by CBZ and in particular by ATN. At the end, oxidative photoproducts were obtained.



Scheme 3.3. Proposed photocatalytic degradation route of CBZ and ATN in the presence of RFTA and visible light.

Considering the kinetics, according to table 3.5, the main degradation pathway seems occurring from the singlet excited state and from singlet oxygen. Nevertheless, the reaction between singlet oxygen and drugs is stoichiometric, while the quenching of $^3RFTA^*$ by CBZ and ATN implies the formation of radicals, able to initiate a chain reaction, which could be more efficient in the degradation of contaminants. Consequently, involving radicals and chain reactions, the direct quenching of

$^3\text{RFTA}^*$ by the drugs could be more effective than what suggested at a first sight by the values of table 3.5.

3.3.Conclusions

Acetylated riboflavin (RFTA) could act as an efficient photocatalyst for the photodegradation of pharmaceutical molecules, as CBZ and ATN. In particular, degradation occurs in less than 2h in the presence of visible light. Photophysical studies shed lights into the two main pathways, able to oxidize the initial pollutants: on one hand CBZ and ATN are oxidized by the singlet oxygen, formed in the presence of RFTA under visible light. On the other hand, $^3\text{RFTA}^*$ is directly quenched by the pollutants with the consequent formation of oxidative radicals, able to start a chain reaction. In both cases, the final oxidative photoproducts, were detected and identified through an UFLC-MS² analysis and are in agreement with the postulated mechanism.

4. Biomimetic photooxidation of noscapine sensitized by a riboflavin derivative in water: the combined role of natural dyes and solar light in environmental remediation

4.1. Introduction

Besides carbamazepine and atenolol, noscapine (NSC) is another interesting pharmaceutical contaminant, detected in water systems. In particular, noscapine (also called narcotine, nectodon, nospen, and anarcotine) is a benzyl-isoquinoline alkaloid, one of the most abundant alkaloids in opium.[94] At the beginning of the XX century, it started to be used as an antitussive drug, probably because it has a depressant effect on citric acid-induced cough.[95–98] It is still used as an antitussive drug, because, differently from the other alkaloids (as codeine and the opium derivatives), noscapine does not cause the typical addictive effect of opiates and the other secondary sedative, hypnotic, or euphoric effects.[99,100] Moreover, in the last decades some studies revealed antitumoral activities both in vivo and in vitro against tumors: as a matter of fact, noscapine is able to bind itself to tubulin and inhibit the microtubule assembly.[101–103] Recent computational studies revealed that NSC is able to attack the protease enzyme of COVID-19, and thus, could be used as antiviral for COVID-19 pandemic.[104–107] Considering its high intake and its promising uses, some pharmacokinetics and toxicity studies were done: NSC has shown negligible toxicity and it is not mutagenic in animals.[108,109] Moreover, it has a relatively low bioavailability (around 30%) due to a substantial first-pass loss, so most of NSC is metabolized by human body, giving rise to the main metabolites (cotarnine, hydrocotarnine, and meconine), coming from the cleavage of the C–C bond between isoquinoline and phthalide groups (Figure 4.1).[110,111]

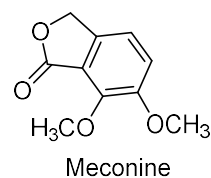
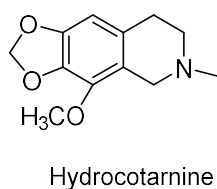
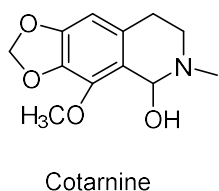
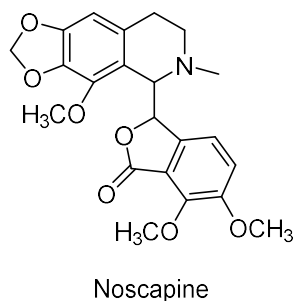


Figure 4.1. Chemical structure of Noscapine (NSC), and its metabolites cotarnine, hydrocotarnine and meconine.[110,111]

Therefore, its widespread use may imply a high release of NSC and its metabolites in the environment that is expected to increase in coming years.

Considering all of this, this part of the thesis intends to investigate the photocatalytic abatement of NSC. A detailed study of the mechanisms involved in the photodegradation reveals the similarities between the biomimetic and the photocatalyzed processes. As a matter of fact, nature is full of organic oxidants as natural organic matter (NOM), which is a mixed entity, whose composition changes seasonally and according to the environment. Among all the possible chemical molecules, riboflavin is also part of NOM. For this reason, once again, we select it not only as an organic photocatalyst as in the previous chapter. As in the previous work, acetylated riboflavin (RFTA) was used instead of natural riboflavin (RF) to take advantage of its higher stability.

4.2. Results and discussion

4.2.1. Photodegradation of NSC and its photoproducts

A solution of Noscapine (10 ppm) was irradiated in the presence of RFTA (1 ppm) and solar light with a filter at 420 nm to eliminate any possible absorption and consequent photolysis of the contaminant due to the UV light. As a matter of fact, NSC is able to absorb mainly between 200 and 250 nm but it has a weaker absorption up to 350 nm (Figure 4.2).

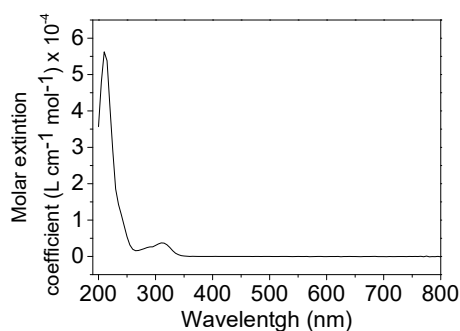


Figure 4.2. UV-Vis spectrum of Noscapine.

Concentration of NSC and RFTA was monitored through an HPLC-UV analysis and it is represented vs time in Figure 4.3A. Under these specific working conditions, NSC was degraded in 1 hour, while RFTA was still present in the solution after 2 hours of irradiation. Moreover, Figure 4.3B represents the toxicity of the treated solution: as expected, the graph has a bell shape with an increase of the total toxicity probably due to the formation of more toxic photoproducts of NSC or RFTA. Fortunately, after 40 min, toxicity decreased again.

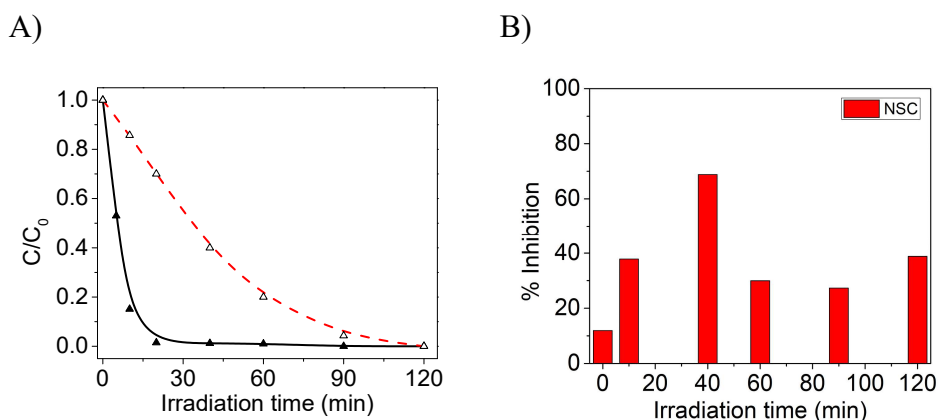
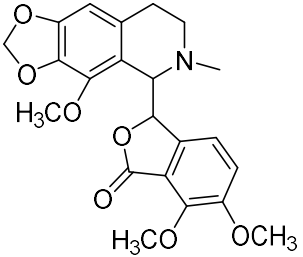
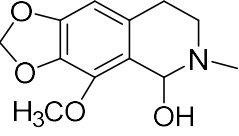
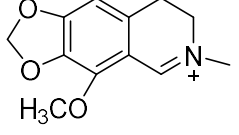
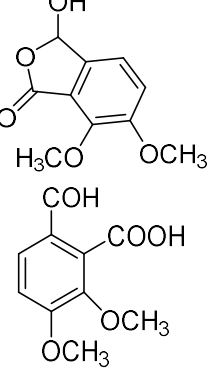


Figure 4.3. Photodegradation of NSC in the presence of RFTA under solar light irradiation with a filter at 420 nm. Evolution of the concentration of NSC (in black) and RFTA (dashed traces in red) (A) and toxicity trend (B).

The same treated solutions were also analyzed by a UPLC with a MS spectrometer to determine the main photoproducts. Results are reported in Table 4.1. In addition to the initial NSC with m/z 414, other four main peaks were detected (respectively m/z of 238, 210, 221 and 193). In particular, products with m/z 238 and 211, respectively, could be associated to cotarnine and opianic acid, the two hydroxylated fragments of the initial NSC, after the C-C bonding cut. On the other hand, photoproducts with m/z of 220 and 193 refer to the same dehydrated compounds. More in detail, the low intensity of the molecular ion of photoproduct with m/z of 238 in the UPLC-MS chromatogram could be associated to the high stability of the dehydrated ion. This hypothesis was confirmed by the same fragmentations at the MS-MS analysis and the same retention time. In addition, cotarnine and opianic acid were synthesised through the chemical oxidation of NSC and used as standards at the UPLC-MS, where both couples with m/z of 238-220 and 211-193 were detected (See section 7.5). Moreover, opianic acid represents a mixture of two tautomers, which are in equilibrium in solution.[111]

Table 4.1. List of main $[M+H]^+$ and spectra product ions obtained for NSC and its phototransformation intermediates observed in the presence RFTA under visible irradiation.

| | R_t (min) | m/z | Product ions (MS^2) | Structure |
|-----------------------------|----------------|-------|---|---|
| NSC | 5.0 | 414 | 414(100), 396(5), 365(20), 353(30), 220(90), 205(10), 179(10) |  |
| Cotarnine | 3.8 | 238 | - |  |
| Dehydrated cotarnine | 3.8 | 220 | 220, 205 |  |
| Opianic acid | 5.8 | 211 | 211, 193 |  |

| | | | | |
|--------------------------------|-----|-----|----------------------------------|--|
| Dehydrated opianic acid | 5.8 | 193 | 193, 163, 149, 135, 122, 107, 77 | |
|--------------------------------|-----|-----|----------------------------------|--|

In conclusion, NSC is mainly broken in two pieces, cotarnine and opianic acid, as reported in Figure 4.4. Cotarnine is also one of the metabolites obtained by the human biotransformation, while opianic acid could be related to meconine, another metabolite, demonstrating the biomimetic degradation of NSC through the oxidative cleavage of the C-C bond linking the two benzylic positions.

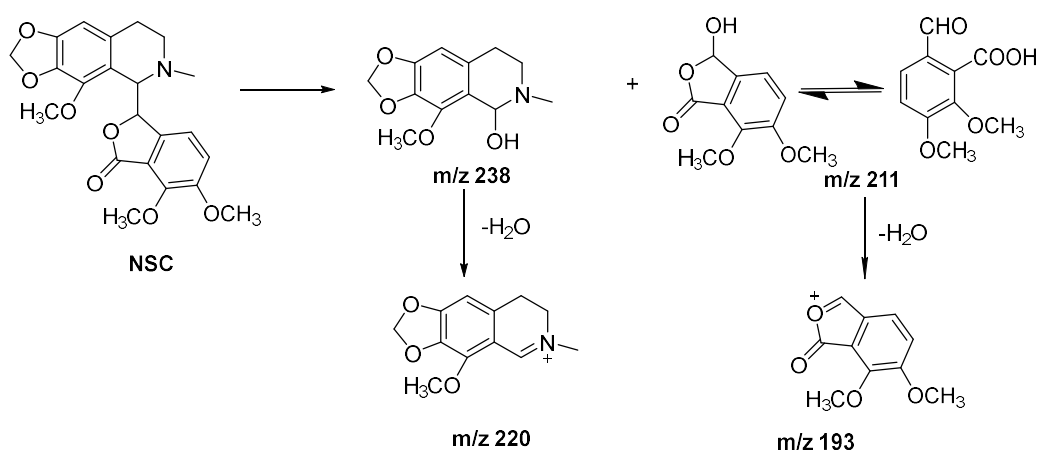


Figure 4.4. Hypothetical pathway for the photo transformation of NSC assisted by RFTA.

Next, the synthesised photoproducts cotarnine and opianic acid were not only used as standards for the UPLC-MS analysis, but also used to study their photodegradation in the aqueous system. UV-Vis spectra, reported in Figure 4.5, show that the two molecules are not able to absorb in the visible range, so they could

be irradiated under the same working conditions of NSC. As a matter of fact, cotarnine has a stronger absorption band at 350 nm and a weaker one at 240 nm, while opianic acid has weak band at 310 nm and a strong one in the UVC.

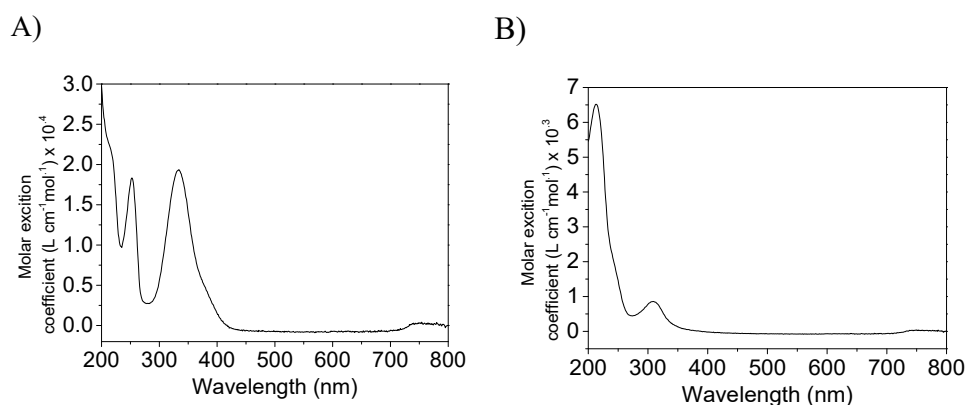


Fig 4.5. UV-Vis spectra of cotarnine (A) and opianic acid (B).

Degradation of the two metabolites was performed in the presence of RFTA and followed at HPLC-UV and their degradation trends are reported in Figure 4.6.

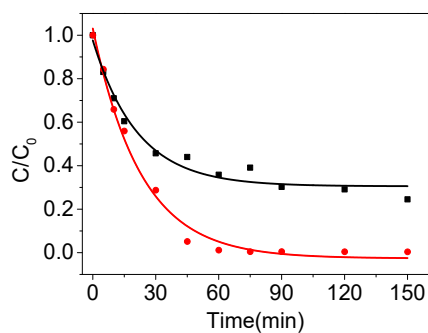


Fig 4.6. Degradation of cotarnine (●) and opianic acid (■) in the presence of RFTA and visible light.

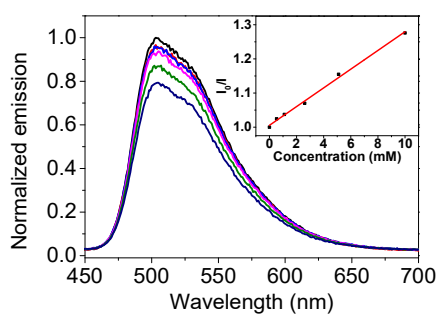
As shown in Figure 4.6, degradation of cotarnine is related to that of the initial noscapine, because both are degraded in 60 minutes. On the other hand, opianic acid is more recalcitrant: in 1 hour only 60% was degraded, while, after 150 minutes, only 30% of the initial concentration is still in solution. So, degradation of opianic acid is not complete under the same working conditions.

4.2.2. Involvement of the excited states of RFTA in the degradation

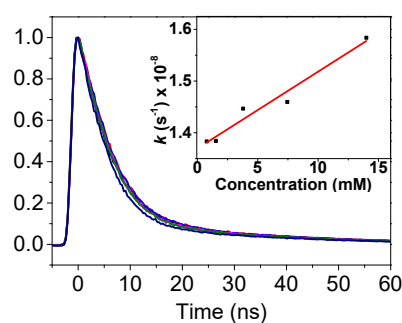
As in the previous chapter, photophysical experiments were performed to understand the role of the excited species in the degradation of NSC and its photoproducts.

First, steady-state and time-resolved fluorescence measurements were carried out to investigate the role of the singlet excited state of RFTA in the degradation. Results are reported in Figure 4.7 and quenching constants are reported in Table 4.2. As expected, steady-state experiments led to higher k_{qS} , due to the contribution of the static quenching. Only cotarnine shows a significant quenching of both the steady-state and time-resolved emission (Figures 4.7C and D), while no reliable quenching could be proven from time-resolved experiments of NSC and opianic acid.

A)



B)



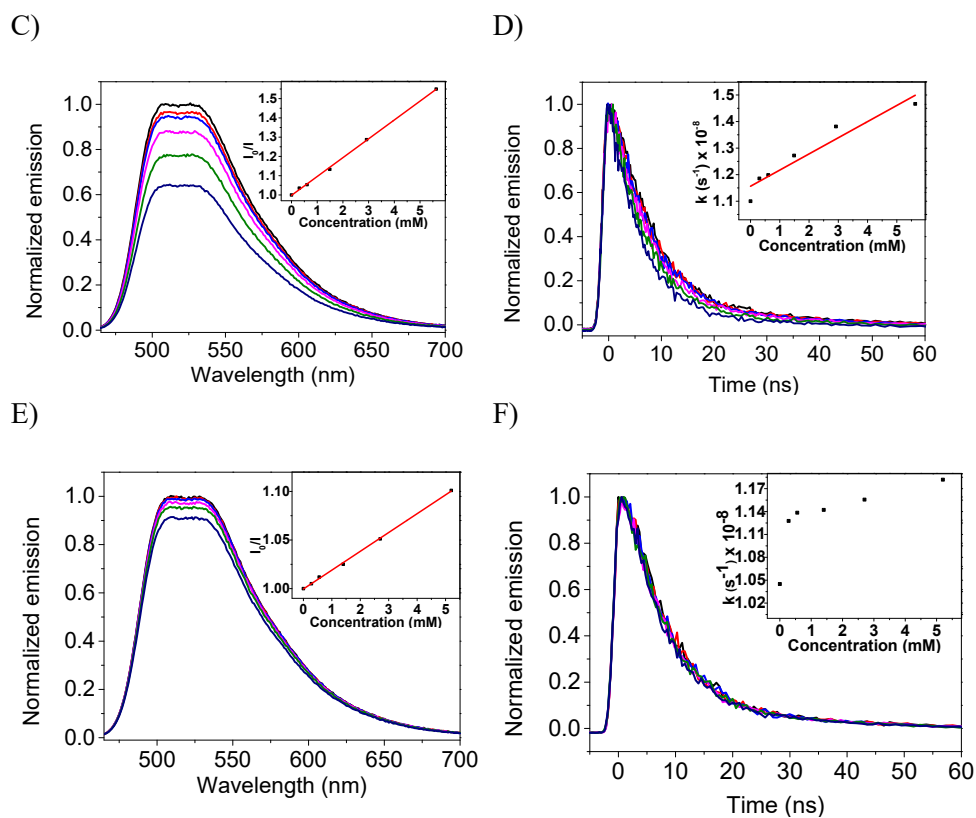


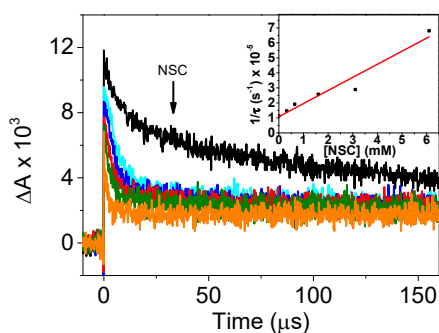
Figure 4.7. Steady-state and time-resolved fluorescence quenching experiments of $^1\text{RFTA}^*$ in acetonitrile in the presence of increasing concentrations of NSC (A, B), cotarnine (C, D) and opianic acid (E, F). Insets: corresponding Stern-Volmer analysis. All the experiments were performed in aerated CH_3CN . $\lambda_{\text{exc}}=445$ nm for steady-state and $\lambda_{\text{exc}}=460$ nm for time-resolved experiments.

Table 4.2. Quenching constants of ¹RFTA* in the presence of different contaminants, determined from steady- state (left) and time-resolved (right) experiments.

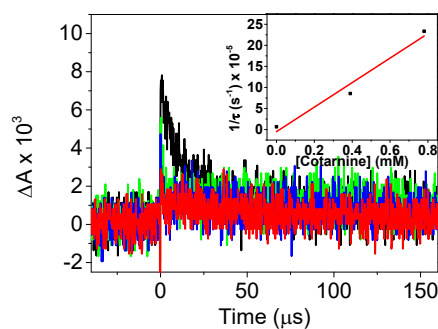
| Drugs and Photoproducts | k_{qs} ($M^{-1}s^{-1}$) from steady-state measurements | k_{qs} ($M^{-1}s^{-1}$) from time-resolved experiments |
|-------------------------|--|--|
| Noscapine (NSC) | 3.7×10^9 | - |
| Cotarnine | 1.3×10^{10} | 6.1×10^9 |
| Opianic acid | 2.6×10^9 | - |

Second, laser flash photolysis (LFP) measurements were carried out to understand the role of ³RFTA* in the degradation and the obtained results are reported in Figure 4.8. In particular, quenching of ³RFTA* by NSC was investigated at 380 nm and it gives rise to a quenching constant of $8.7 \times 10^7 M^{-1}s^{-1}$ (Figure 4.8A). In the case of cotarnine and opianic acid we changed the monitoring wavelength to 680 nm for convenience: in the case of cotarnine, the obtained quenching rate constant was $k_{qT} = 2.9 \times 10^9 M^{-1}s^{-1}$ (Figure 4.9B), while no reliable quenching could be proven for opianic acid (Figure 4.9C).

A)



B)



C)

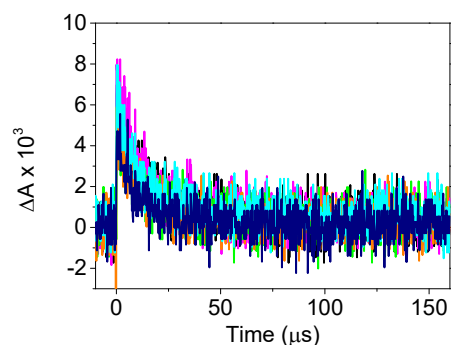


Figure 4.8. Transient absorption decays of RFTA with increasing concentrations of NSC (A), cotarnine (B) and opianic acid (C) obtained at different times after the laser pulse. Insets: Corresponding Stern-Volmer plots. Experiments were performed in deaerated acetonitrile at $\lambda_{\text{exc}} = 355$ nm.

Third, the role of $^1\text{O}_2$ was investigated by time-resolved near infrared emission. Different molecules were used as $^1\text{O}_2$ generator: RFTA ($\lambda_{\text{exc}} = 355$ nm) for NSC, and Rose Bengal ($\lambda_{\text{exc}} = 532$ nm) for cotarnine and opianic acid, to avoid the higher absorption of the quenchers at 355 nm. The obtained data are reported in Figure 4.9 and the corresponding quenching constants are $k_{q1\text{O}_2} = 7.4 \times 10^5 \text{ M}^{-1}\text{s}^{-1}$ for NSC, $4.2 \times 10^7 \text{ M}^{-1}\text{s}^{-1}$ for cotarnine and $2.6 \times 10^6 \text{ M}^{-1}\text{s}^{-1}$ for opianic acid. Once again, as in the previous cases, cotarnine is the most reactive compound.

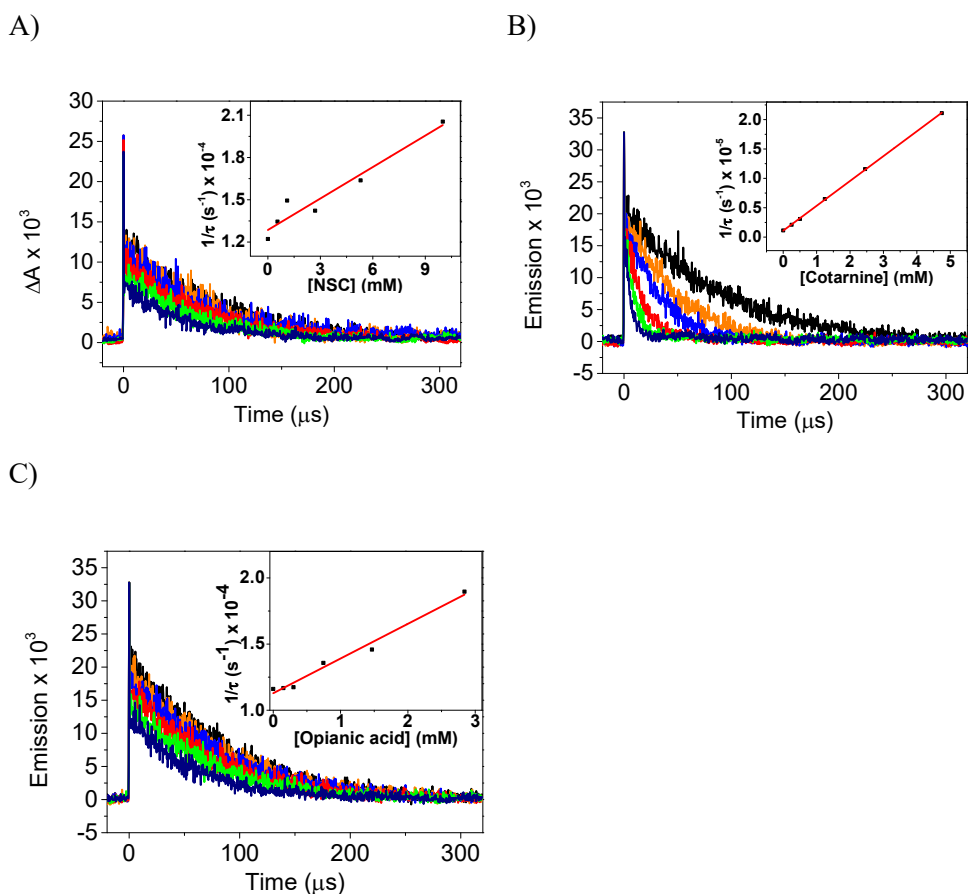


Figure 4.9. Transient emission decays of $^1\text{O}_2$ monitored at 1270 nm upon increasing concentrations of noscapine (A) cotarnine (B) and opianic acid (C). Insets: corresponding Stern-Volmer plots. The experiments were performed in aerated acetonitrile. RFTA was used as a $^1\text{O}_2$ precursor in the case of NSC ($\lambda_{\text{exc}} = 355 \text{ nm}$) and Rose Bengal was used as a precursor for cotarnine and opianic acid ($\lambda_{\text{exc}} = 532 \text{ nm}$).

4.2.3. Overall discussion

As in the previous chapter, the real contribution of the reactive and excited species has been calculated considering the obtained photophysical data and the lifetime of all the involved species at different concentrations of NSC and its metabolites. In particular, two different scenarios were considered, using two solvents: as a matter of fact, table 4.3 shows the calculated data in acetonitrile, where RFTA exhibits a high fluorescence quantum yield ($\Phi_F=0.53$), and the lifetime of the generated singlet oxygen is longer ($\tau = 81 \mu\text{s}$).

On the other hand, Table 4.4. represents an aqueous scenario, which pretends to imitate the natural aqueous systems, where RFTA has a higher intersystem crossing quantum yield ($\Phi_{ISC} = 0.74$), but lifetime of singlet oxygen is shorter ($\tau = 3.5 \mu\text{s}$).

Table 4.3. Relative contribution of the singlet and triplet excited states of RFTA and $^1\text{O}_2$ in the quenching of NSC, cotarnine and opianic acid, at the indicated concentrations in acetonitrile.

| [Q] (M) | Quencher | Quenching of $^1(\text{RFTA})^*$ (%) | $^1(\text{RFTA})^*$ intrinsic decay (%) | Quenching of $^3(\text{RFTA})^*$ (%) | $^3(\text{RFTA})^*$ intrinsic decay (%) | Quenching of $^3(\text{RFTA})^*$ by O_2 (%) | Quenching of $^1\text{O}_2$ | $^1\text{O}_2$ intrinsic decay |
|-----------|--------------|--------------------------------------|---|--------------------------------------|---|--|-----------------------------|--------------------------------|
| 10^{-3} | NSC | 2.7 | 51.6 | 0.2 | 0.1 | 45.4 | 2.6 | 42.9 |
| | Cotarnine | 4.3 | 50.7 | 5.0 | 0.1 | 39.9 | 30.9 | 9.0 |
| | Opianic acid | 1.9 | 52.0 | 0.0 | 0.1 | 46.0 | 8.1 | 37.9 |
| 10^{-5} | NSC | 0.0 | 53.0 | 0.0 | 0.1 | 46.8 | 0.0 | 46.8 |
| | Cotarnine | 0.0 | 53.0 | 0.1 | 0.1 | 46.8 | 1.5 | 45.2 |
| | Opianic acid | 0.0 | 53.0 | 0.0 | 0.1 | 46.9 | 0.1 | 46.8 |
| 10^{-8} | NSC | 0.0 | 53.0 | 0.0 | 0.1 | 46.9 | 0.0 | 46.9 |
| | Cotarnine | 0.0 | 53.0 | 0.0 | 0.1 | 46.9 | 0.0 | 46.9 |
| | Opianic acid | 0.0 | 53.0 | 0.0 | 0.1 | 46.9 | 0.0 | 46.9 |

Table 4. Relative contribution of the singlet and triplet excited states of RFTA and $^1\text{O}_2$ in the quenching of NSC, cotarnine and opianic acid, at the indicated concentrations in water.

| [Q] (M) | Quencher | Quenching of $^1(\text{RFTA})^*$ (%) | $^1(\text{RFTA})^*$ intrinsic decay (%) | Quenching of $^3(\text{RFTA})^*$ (%) | $^3(\text{RFTA})^*$ intrinsic decay (%) | Quenching of $^3(\text{RFTA})^*$ by O_2 (%) | Quenching of $^1\text{O}_2$ | $^1\text{O}_2$ intrinsic decay |
|-----------|--------------|--------------------------------------|---|--------------------------------------|---|--|-----------------------------|--------------------------------|
| 10^{-3} | NSC | 1.8 | 25.5 | 2.8 | 2.1 | 67.7 | 0.2 | 67.5 |
| | Cotarnine | 3.0 | 25.2 | 41.1 | 0.9 | 29.8 | 3.8 | 25.9 |
| | Opianic acid | 1.3 | 25.7 | 0.2 | 2.2 | 70.6 | 0.6 | 70.0 |
| 10^{-5} | NSC | 0.0 | 26.0 | 0.0 | 2.3 | 71.7 | 0.0 | 71.7 |
| | Cotarnine | 0.0 | 26.0 | 1.0 | 2.2 | 70.7 | 0.1 | 70.6 |
| | Opianic acid | 0.0 | 26.0 | 0.0 | 2.3 | 71.7 | 0.0 | 71.7 |
| 10^{-8} | NSC | 0.0 | 26.0 | 0.0 | 2.3 | 71.7 | 0.0 | 71.7 |
| | Cotarnine | 0.0 | 26.0 | 0.0 | 2.3 | 71.7 | 0.0 | 71.7 |
| | Opianic acid | 0.0 | 26.0 | 0.0 | 2.3 | 71.7 | 0.0 | 71.7 |

From the two tables, it seems clear that concentration of the quencher is a crucial parameter to determine the pathway of the degradation: at low concentrations, dynamic quenching of the reactive species is clearly negligible no matter its nature or the solvent media. On the other hand, increasing the concentration, situation is completely different in the two scenarios. In acetonitrile, in the case of NSC and opianic acid, the quenching of singlet excited state of RFTA is the predominant pathway, while in the case of cotarnine both $^1\text{RFTA}^*$ and $^3\text{RFTA}^*$ seem to be involved. Moreover, in acetonitrile the contribution of $^1\text{O}_2$ is higher, due to the longer lifetime of $^1\text{O}_2$ in the organic solvent.

On the other hand, in water triplet excited state route is predominant for NSC and cotarnine thanks to the higher intersystem crossing quantum yield of RFTA. Opianic acid is the less reactive in all the situations: these data confirm its high recalcitrant attitude shown in the experimental degradation (Figure 4.6). Consequently, the degradation of NSC works through an initial oxidation of the tricyclic nitrogenated substructure (cotarnine-like), followed by cleavage of the C-C bond between the two benzylic positions.

4.3. Conclusions

NSC was completely degraded in less than one hour, in the presence of RFTA and visible light. As in the previous chapter, analysis at UPLC-MS² was used to detect and assign the photoproducts: they were also synthesised and used as standards, to confirm the hypothesis. All these analyses gave us the opportunity to draw the oxidative pathway: NSC is degraded by the oxidative cleavage of the C-C bond between the two benzylic positions, giving rise to cotarnine and opianic acid, two organic molecules that derive also from the human metabolism of NSC. Photophysical experiments demonstrated that degradation occurs through different pathways depending on the solvent: in acetonitrile, ¹O₂ is the main involved reactive species, while in natural aqueous systems the reaction occurs through an electron transfer to the excited states of RFTA.

Once again, we have demonstrated that RFTA together with visible light was efficient for the oxidation of pharmaceutical molecules and their photoproducts.

5. Degradation of benzotriazole UV filters with acetylated riboflavin

5.1. Introduction

Another important and wide class of contaminants is the family of benzotriazole UV-stabilizers (BUVSs). They are used as additive agents to prevent yellowing and light-induced degradation of a variety of industrial products, such as personal-hygiene (body lotions, creams, shampoos, sunscreens), building materials, auto components, paints, adhesive agents, films, shoes, glasses and tires. The benzotriazole UV-stabilizers, which have a phenolic group attached to the benzotriazole structure, are known to absorb full spectrum of UV light: UV-A (320-400 nm) and UV-B (280-320 nm).[112] Considering their high spread in industrial products, BUVSs can reach water systems not only through the effluents of wastewater treatment plants (WWTPs), but they are also directly discharged *via* wash-off from human body, facilitating their entrance in the aqueous environment. Moreover, their low log K_{ow} values (around 1.23 for benzotriazole), implies a high solubility and the high bioaccumulation not only in the biota but also in human urine.[113,114] The European Chemical Agency (ECHA) file for these compounds reveals a very low potential for biodegradation (for example for UV-328 a 2-8% of biodegradation after 28 days) and a high persistency in the aqueous systems.[115] Even if toxic effects against humans for each of these compounds are not totally determined, previous studies revealed some endocrine activities and toxic effects in different types of organisms.[116,117] For these reasons, their removal from aqueous systems is necessary.

In this and in the next chapter, several benzotriazoles UV-stabilizers (BUVSs) have been selected and their degradation has been investigated in the presence of two organic photocatalysts: both acetylated riboflavin and eosin Y were tested and used for this purpose. In the current chapter, in the presence of RFTA, we decided to select three different contaminants (UV-326, UV-327 and UV-328, Figure 5.1), while in the presence of EOY (chapter 6), only UV-327 and UV-328 were investigated. In both cases, degradation trends together with the photophysical experiments allowed determining the role of the involved reactive species and postulating a plausible photodegradation mechanism.

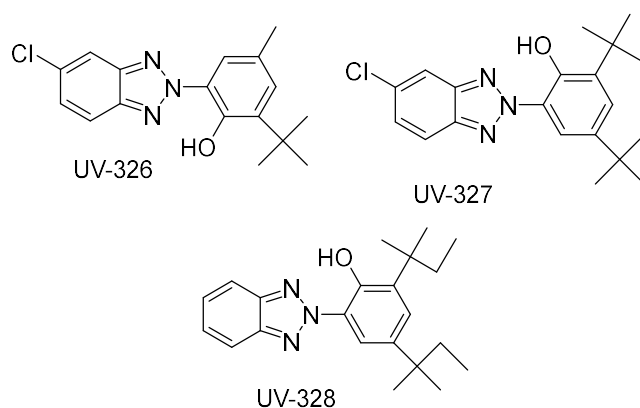


Figure 5.1. Chemical structures of selected Benzotriazole-UV stabilizers (BUVSs).

5.2. Results and discussion

The aim of this chapter is to find out the best conditions to degrade BUVSs in aqueous systems: for this purpose, different photodegradation experiments with increasing levels of complexity were designed and tested.

First, direct photolysis of separated BUVSs was carried out under blue LED light and UV-light (Figure 5.2). As expected, none of them is affected by direct UV and Visible light, in agreement with their application as solar filters.

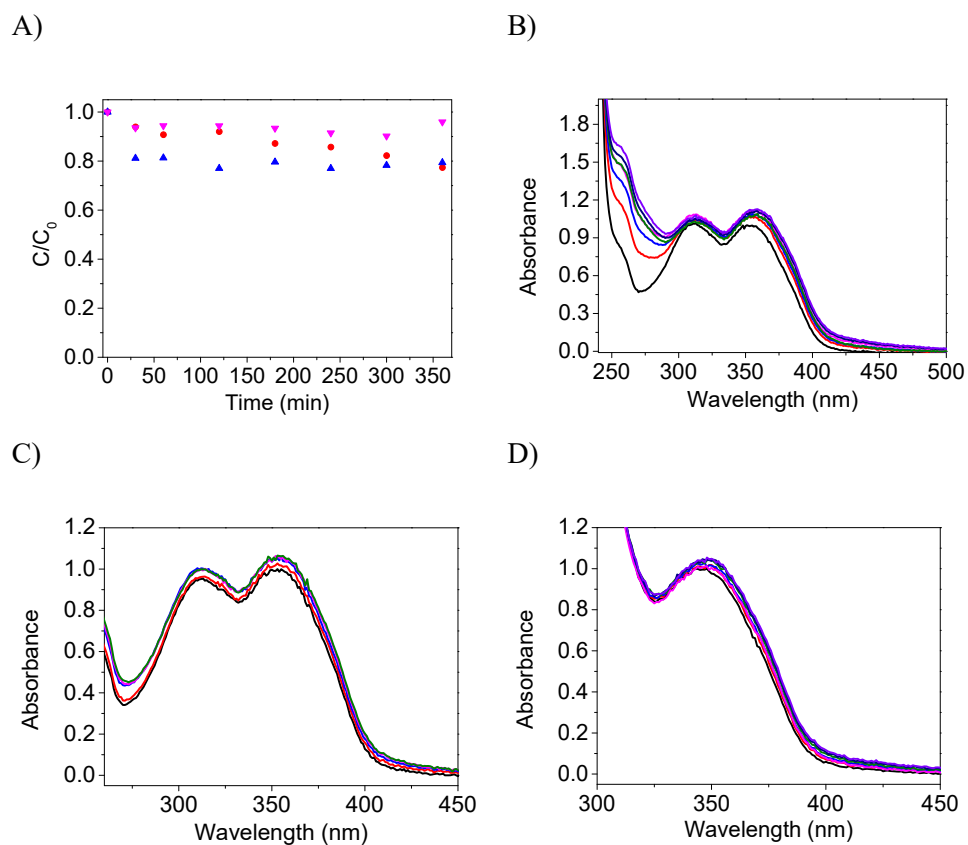


Figure 5.2. Separate photolysis of aerated aqueous solutions of UV-326 (●), UV-327 (▲) and UV-328 (▼) under blue LED light ($\lambda_{\max} = 450$ nm), monitored by HPLC (A). Photolysis of UV-326 (B), UV-327 (C) and UV-328 (D) under air, using UVA lamps ($\lambda_{\max} = 350$ nm), monitored by UV-Vis spectrophotometry up to 3h.

Secondly, an efficient electron donor was introduced in the system: 1,4-Diazabicyclo[2.2.2]octane (generally known as DABCO) was selected and solutions with each BUVS and DABCO were irradiated under UV-light (Figure 5.3). Except

from UV-326, which is slightly affected by the presence of DABCO after three hours of UV irradiation, once again BUVs are mainly unreactive.

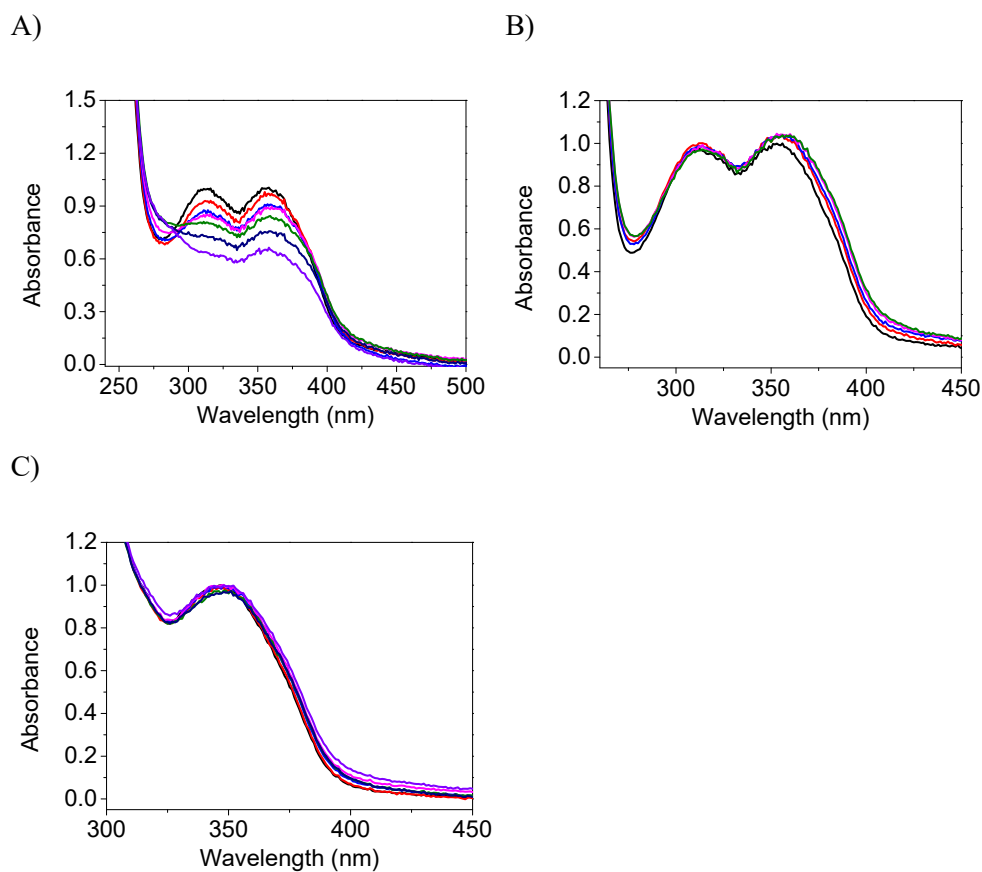


Figure 5.3. Irradiation of UV-326 (A), UV-327 (B) and UV-328 (C) under UVA lamps (λ_{\max} = 350 nm), in the presence of 10^{-2} M DABCO.

Considering the low reactivity of BUVs, RFTA was added to the system: as already explained in chapter 1.4.1 RFTA is a derivative of natural riboflavin and it is present in natural ecosystems as natural organic matter (NOM). In this case, solutions were

irradiated only under blue LED light to remove the possible absorption of solar filters, both in anaerobic and aerobic atmosphere (Figure 5.4).

Once again, UV-326 is the most reactive BUVS: under anaerobic condition, it is degraded up to 60% of the initial concentration in six hours, while UV-327 and UV-328 are negligibly affected. On the other hand, in the presence of O₂, all BUVSs are degraded up to the 40% of the initial concentration, regardless their chemical structure.

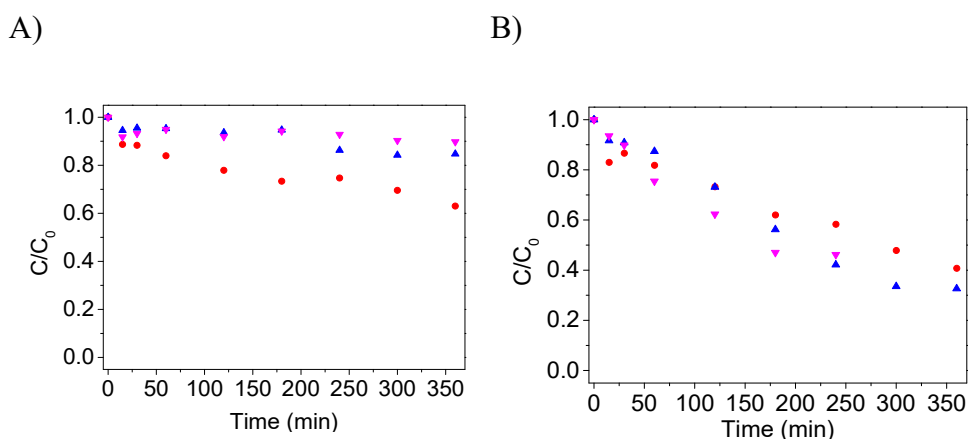


Figure 5.4. Photodegradation of UV-326 (●), UV-327 (▲) or UV-328 (▼) (10⁻⁵ M) under a blue LED (λ_{\max} = 450 nm) irradiation in the presence of RFTA (10% mol) in N₂ (A) and air (B).

Finally, a more complex scenario was recreated, with BUVSs, RFTA and DABCO simultaneously in aqueous solutions. In particular, previous studies demonstrated the ability of RFTA to generate the corresponding radical anion RFTA⁻ in the presence of an efficient electron donor (as DABCO). RFTA⁻ has reductant properties and it could be used to reduce organic contaminants in water.[50]

Obtained results are reported in Figure 5.5. DABCO was added at high concentration (1×10^{-2} M) in order to reach a complete reduction of $^1\text{RFTA}^*$. Compared to the previous photodegradation conditions, abatement of all the selected BUVSs occurs faster. In particular, in an anaerobic condition, UV-326 is completely degraded in three hours, UV-327 in six hours and 80% of UV-328 was removed in six hours.

In the presence of oxygen, photodegradation is even more efficient: UV-326 and UV-327 are completely photodegraded in two hours, while 70% of the most recalcitrant UV-328 was abated after the same irradiation time.

To sum up, the best condition to abate solar filters requires the simultaneous presence of a visible light absorbing photosensitizer (as RFTA), an efficient electron donor (as DABCO) and oxygen.

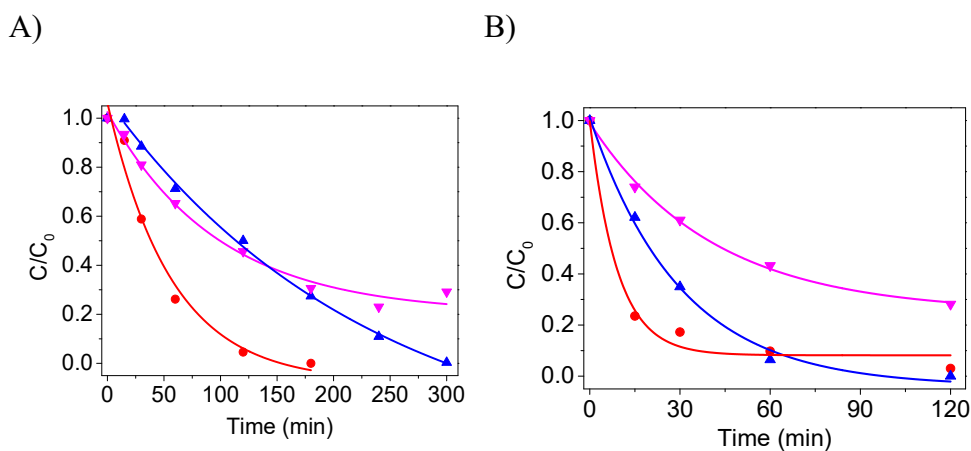
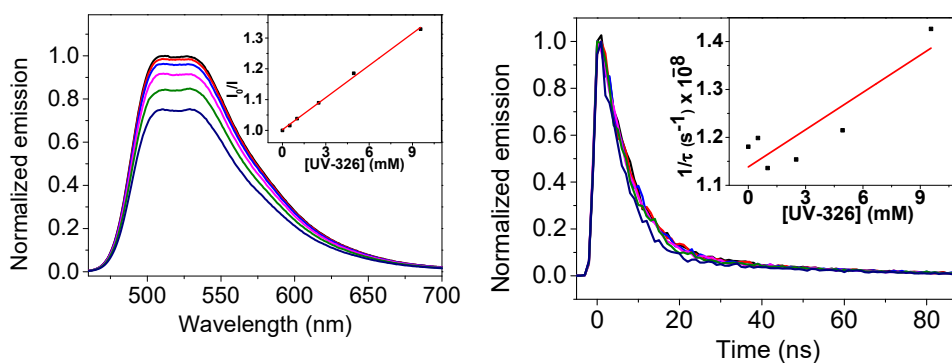


Figure 5.5. Photocatalytic degradation of aqueous mixtures of UV-326 (●), UV-327 (▲) or UV-328 (▼) (10^{-5} M) in the presence of RFTA (10% mol) and DABCO (10^{-2} M) in N₂ (A) and air (B) under blue LED irradiation ($\lambda_{\text{max}} = 450$ nm).

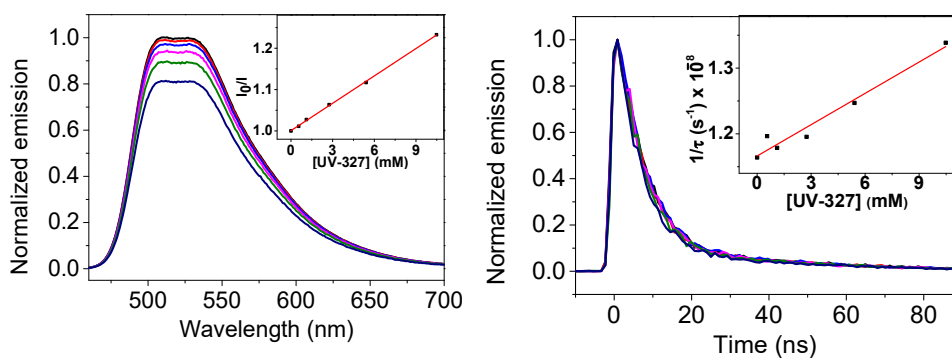
Once determined the best photodegradation conditions for the abatement of the selected BUVSs, the participation of the singlet and the triplet excited states of RFTA and the subsequently obtained reactive species was evaluated.

First, steady state and time-resolved (Figure 5.6) emission experiments were carried out in the presence of increasing concentration of the three BUVSs and DABCO. The corresponding values of the quenching constants are reported in Table 5.1.

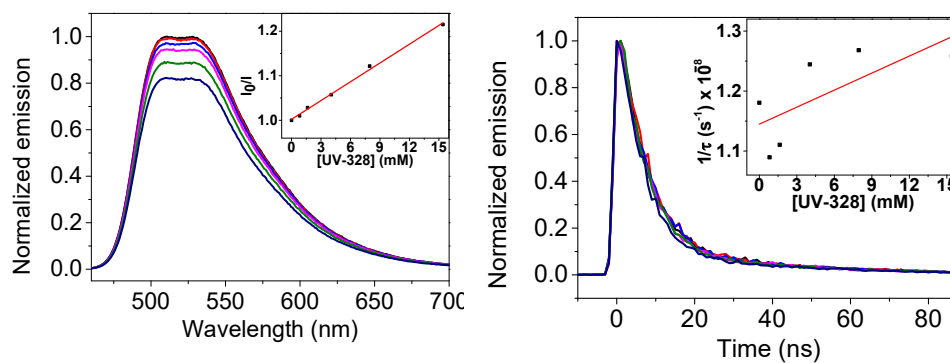
A)



B)



C)



D)

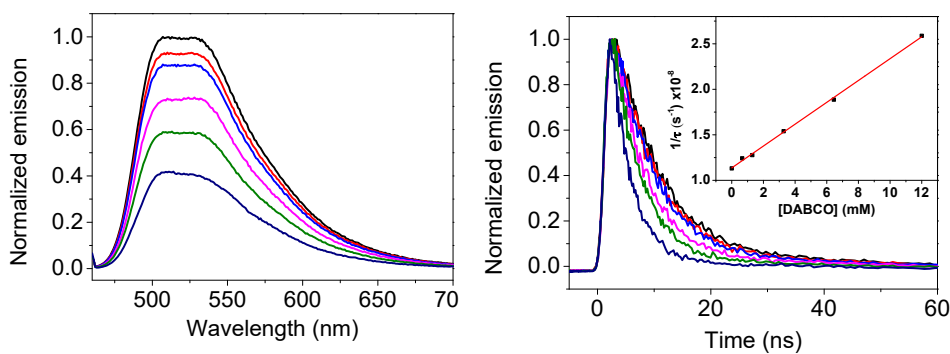


Figure 5.6. Steady-state (left) and time-resolved emission (right) quenching experiments of RFTA upon increasing concentrations of UV-326 (A); UV-327 (B) and UV-328 (C) and DABCO (D), in aerated ACN. $\lambda_{exc}=445$ nm for steady-state and $\lambda_{exc}=460$ nm for time-resolved experiments.

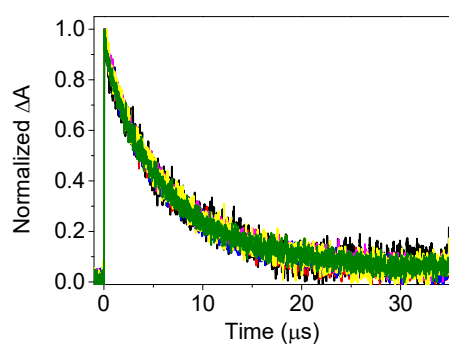
Table 5.1. Rate constant values for the reaction between each BUVs and 1 RFTA* obtained from steady-state and time-resolved quenching experiments emission

| Quencher | K_{qS} (M^{-1}) from steady-state measurements | k_{qS} ($M^{-1}s^{-1}$) from time-resolved experiments |
|----------|--|--|
| UV-326 | 34.8 | 2.6×10^9 |

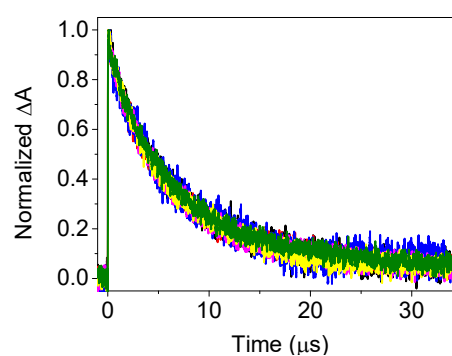
| | | |
|---------------|------|----------------------|
| UV-327 | 22.1 | 1.6×10^9 |
| UV-328 | 14.0 | 9.5×10^8 |
| DABCO | - | 1.2×10^{10} |

Next, laser flash photolysis (LFP) measurements allowed investigating the participation of the $^3\text{RFTA}^*$ in the photodegradation. Once again, increasing volumes of concentrated BUVSs were added into deaerated solutions of RFTA. As shown in Figure 5.7, no changes were noticed in the decays registered at 620 nm in the presence of high concentrations of contaminants. This indicates that direct reaction of the BUVSs with $^3\text{RFTA}^*$ is not happening.

A)



B)



C)

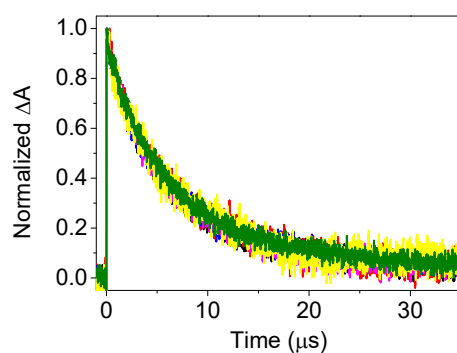


Figure 5.7. Traces of $^3\text{RFTA}^*$ recorded at 620 nm upon LFP excitation ($\lambda_{\text{exc}} = 355$ nm) of deaerated solutions of RFTA in the presence of increasing concentrations of UV-326 (A), UV-327 (B) and UV-328 (C). The experiments were performed in deaerated acetonitrile.

On the contrary, DABCO is a good quencher: not only it is able to quench efficiently the singlet excited state of RFTA, but it could also quench the small fraction of non-quenched singlets that arrives into the triplet upon intersystem crossing. As a matter of fact, LFP experiments with increasing concentration of DABCO were registered at 620 nm and the obtained data were reported in figure 5.8 A. The corresponding quenching constant value was $k_{qT} = 7.8 \times 10^9 \text{ M}^{-1}\text{s}^{-1}$. Moreover, the transient absorption spectrum, registered in the presence of 50 mM of DABCO (Figure 5.8B), revealed a new species, with a strong band at 380 nm and a less intense band between 470 nm and 650 nm: this spectrum corresponds to RFTA^- , as already assigned in previous works.[118]

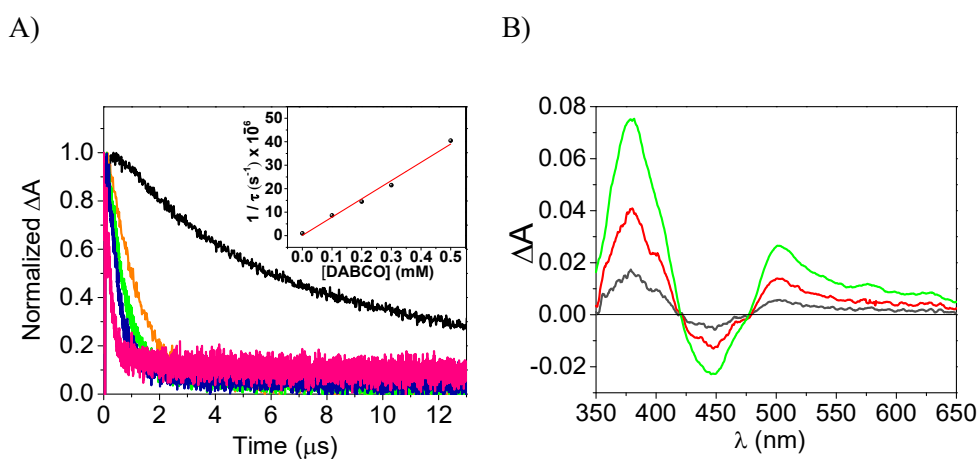


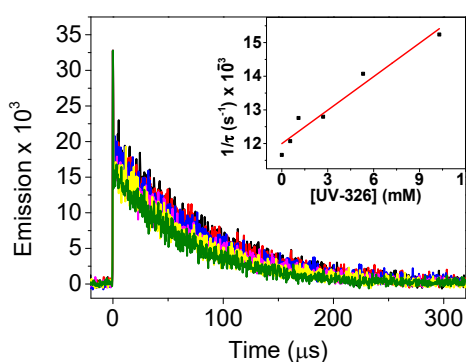
Figure 5.8. A) Quenching of $^3\text{RFTA}^*$ upon increasing concentrations of DABCO in deaerated acetonitrile, registered at 620 nm. Inset: corresponding Stern-Volmer

plot. B) Transient absorption spectra of RFTA⁻ obtained upon laser excitation of RFTA ($\lambda_{exc} = 460$ nm) in the presence of DABCO (50 mM) at 2 μ s (black line), 10 μ s (red line) and 25 μ s (green line) .

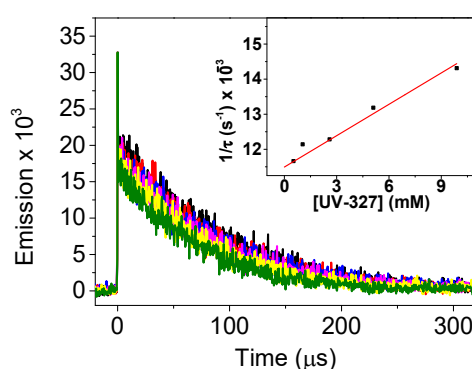
Once the interaction between the singlet and the triplet excited state of RFTA with each BUVSs and DABCO has been investigated, the interaction between the reactive intermediates and BUVSs was studied.

As already reported in the previous chapters, RFTA gives rise to singlet oxygen, which is highly reactive: in particular the reported quenching constant value of ³RFTA* by O₂ is $k_{qT} = 9.8 \times 10^8 \text{ M}^{-1}\text{s}^{-1}$. [55] Once again, aerated solutions of Rose Bengal (used as generator of ¹O₂) in acetonitrile-toluene were analysed upon LFP ($\lambda_{exc} = 532$ nm) with increasing concentrations of BUVSs. In all cases, the emission signal of ¹O₂ ($\lambda_{em} = 1270$ nm) was weekly affected by the contaminants. Stern-Volmer plots in the insets allowed the determination of the quenching constants ($k_{q1O2} = 3.3 \times 10^5 \text{ M}^{-1}\text{s}^{-1}$; $k_{q1O2} = 3.0 \times 10^5 \text{ M}^{-1}\text{s}^{-1}$ and $k_{q1O2} = 3.0 \times 10^5 \text{ M}^{-1}\text{s}^{-1}$, for UV-326, UV-327 and UV-328, respectively).

A)



B)



C)

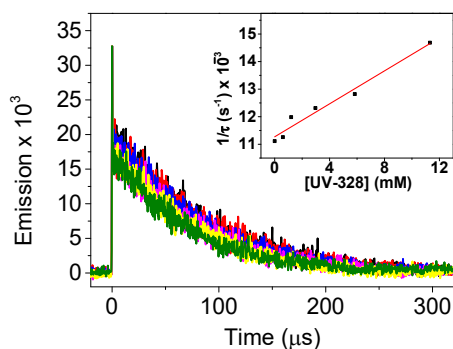


Figure 5.9. Transient emission decays of $^1\text{O}_2$ generated upon laser flash excitation ($\lambda_{\text{exc}} = 532 \text{ nm}$) of Rose Bengal ($\text{Abs} = 0.5$ at $\lambda_{\text{exc}} = 532 \text{ nm}$), and monitored at 1270 nm upon addition of increasing concentrations of UV-326 (A), UV-327 (B) and UV-328 (C). Insets: corresponding Stern-Volmer plots. The experiments were performed in aerated acetonitrile-toluene solutions.

Finally, the interaction between RFTA^- and each BUVS was evaluated through LFP, recording signals at 380 nm in the presence of increasing concentration of BUVSs. Data are represented in Figure 5.10 and from the corresponding Stern-Volmer plots, the obtained quenching rate constants values were: $k_q = 2.6 \times 10^9 \text{ M}^{-1}\text{s}^{-1}$; $k_q = 1.5 \times 10^9 \text{ M}^{-1}\text{s}^{-1}$ and $k_q = 6.9 \times 10^8 \text{ M}^{-1}\text{s}^{-1}$, for UV-326, UV-327 and UV-328, respectively.

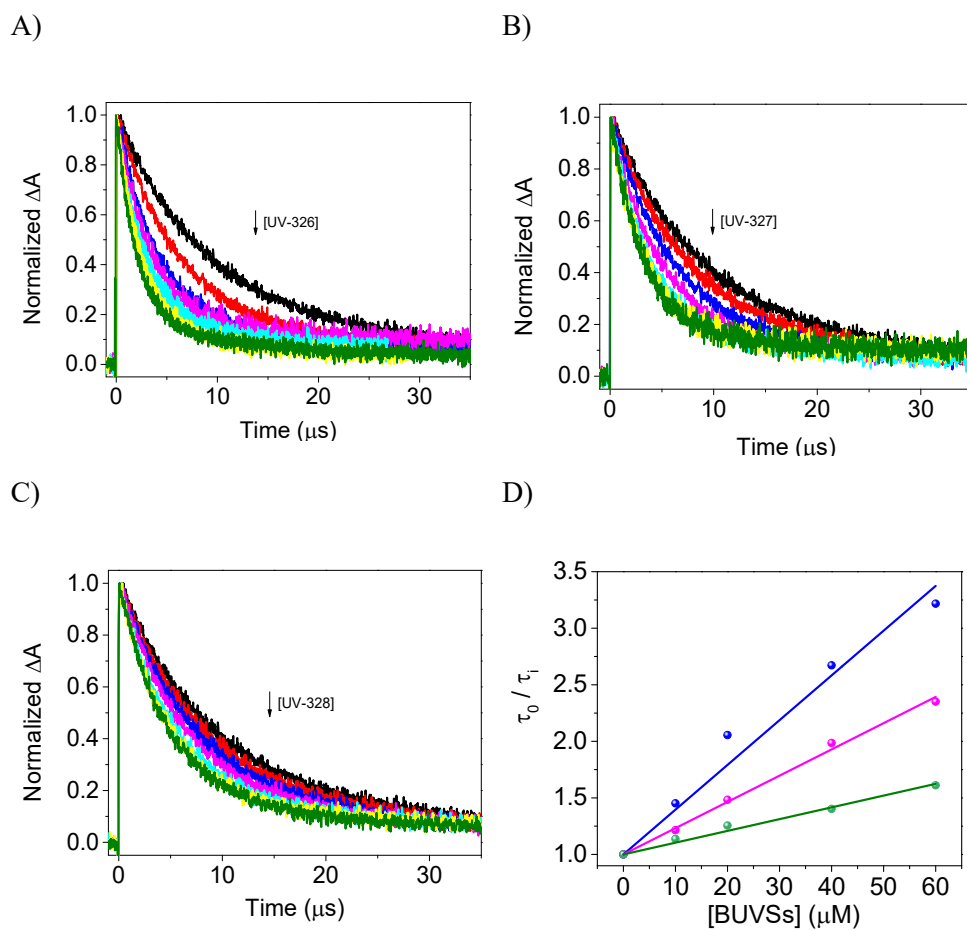


Figure 5.10. Traces of RFTA⁻ recorded at 380 nm upon LFP excitation of deaerated solutions of RFTA (Abs = 0.3 at $\lambda_{exc} = 460$ nm) in the presence of DABCO (50 mM), upon increasing concentrations of UV-326 (A), UV-327 (B) and UV-328 (C). Corresponding Stern-Volmer plots: UV-326 is in blue, UV-327 is in pink and UV-328 in green. (D).

To sum up, degradation of BUVSs was carried out under different working conditions: at the end the best one requires the simultaneous presence of RFTA as photosensitizer, visible light, oxygen, and a good electron donor as DABCO.

Photophysical measurements revealed the important role of DABCO, which efficiently quenches the singlet and the triplet excited states of RFTA, generating RFTA⁻; in absence of DABCO, O₂ quenched ³RFTA*, generating singlet oxygen ¹O₂. The direct interaction of the reactive intermediates RFTA⁻ and ¹O₂ with BUVSs was evaluated and the quenching constants were determined through the Stern-Volmer equation.

All the obtained data (quenching constants, concentrations and lifetime of the excited species) were combined and used to determine the participation of each reactive species and the contribution of each pathway, through the equations reported in chapter 1.6: all the calculated data are reported in Table 5.2.

Table 5.2. Relative contribution of the primary and secondary reactive species derived from the visible-light absorption of RFTA in the absence/presence of DABCO, in the photodegradation of the BUVSs in aerated acetonitrile solutions.

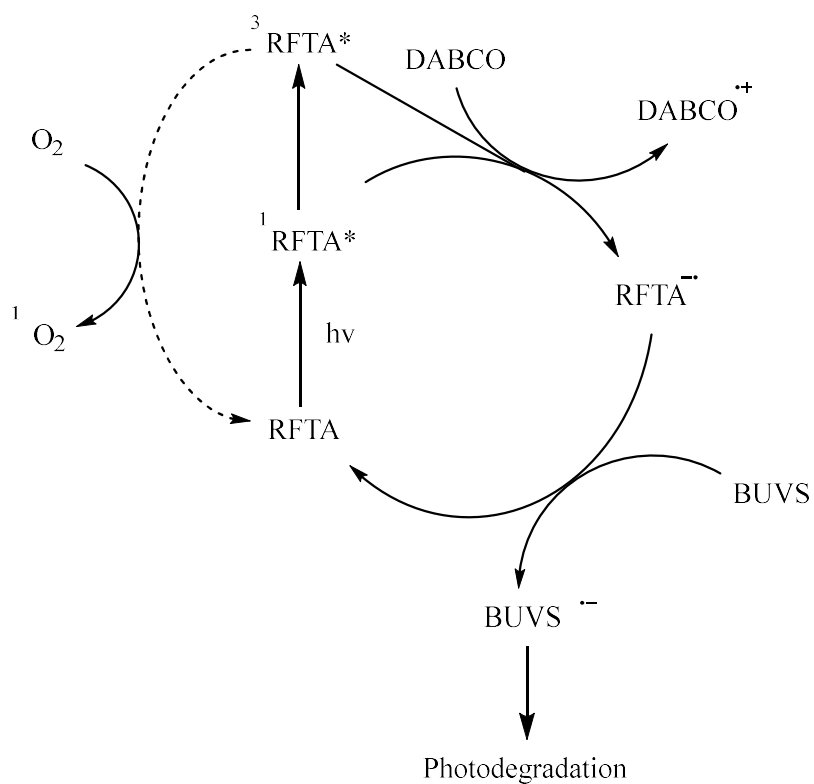
| Quenchers Processes | UV-326 (10 ⁻⁵ M) | UV-327 (10 ⁻⁵ M) | UV-328 (10 ⁻⁵ M) | DABCO (10 ⁻² M) | DABCO (10 ⁻² M) + UV-326 (10 ⁻⁵ M) | DABCO (10 ⁻² M) + UV-327 (10 ⁻⁵ M) | DABCO (10 ⁻² M) + UV-328 (10 ⁻⁵ M) |
|---|---------------------------------------|---------------------------------------|---------------------------------------|--------------------------------------|--|--|--|
| Quenching of ¹RFTA* | <0.1 | <0.1 | <0.1 | 47.0 | 47.0 | 47.0 | 47.0 |
| Fluorescence | 53.0 | 53.0 | 53.0 | 28.1 | 28.1 | 28.1 | 28.1 |

| | | | | | | | |
|---|------|------|------|------|------|------|------|
| Quenching of $^3\text{RFTA}^*$ | - | - | - | 24.1 | 24.1 | 24.1 | 24.1 |
| Quenching of $^3\text{RFTA}^*$ by O_2 | 45.7 | 45.7 | 45.7 | 0.7 | 0.7 | 0.7 | 0.7 |
| Intrinsic decay of $^1\text{O}_2$ | 45.7 | 45.7 | 45.7 | <0.1 | <0.1 | <0.1 | <0.1 |
| Quenching of $^1\text{O}_2$ | <0.1 | <0.1 | <0.1 | 0.7 | 0.7 | 0.7 | 0.7 |
| Intrinsic decay of $\text{RFTA}^{\cdot-}$ | - | - | - | - | 56.8 | 62.1 | 66.7 |
| Quenching of $\text{RFTA}^{\cdot-}$ | - | - | - | - | 14.4 | 9.1 | 4.5 |

In detail, DABCO is able to efficiently quench a high percentage of singlet and triplet excited states of RFTA, giving rise to the radical anion $\text{RFTA}^{\cdot-}$ with *ca.* 70% overall yield, regardless the BUVS or O_2 are present in the media. Even if part of this species decays without reacting, a small percentage reacts with BUVSs (14.4%, 9.1% and 4.5% for UV-326, UV-327 and UV-328, respectively) in agreement with the observed photodegradation rates. Moreover, O_2 is not able to compete with DABCO in the quenching of triplet excited state of RFTA, so it would be probably involved in the following steps of the photodegradation of BUVSs.

In the absence of DABCO, O_2 is the only element in the system, able to quench $^3\text{RFTA}^*$, forming singlet oxygen $^1\text{O}_2$. Unfortunately, neither $^1\text{O}_2$ was the reactive and excited species are able to oxidize BUVSs; consequentially photodegradation is quite inefficient after hours of irradiation.

To sum up, the presence of an electron donor as DABCO is necessary for the formation of $\text{RFTA}^{\cdot-}$, which is the only species, able to efficiently reduce BUVSs. After all the photophysical studies, the quenching constants and the calculated data of Table 5.2, an hypothetical mechanism was drawn (Scheme 5.2).



Scheme 5.2. Photodegradation of BUVSs in the presence of RFTA and DABCO and O_2 , under visible light irradiation.

5.3. Conclusions

In this chapter, we proved that RFTA could be used not only to oxidize but also to reduce CECs. As a matter of fact, in the presence of an electron donor RFTA⁻ is generated, an efficient reductant. Three different solar filters, all belonging to the benzotriazole UV- stabilizers class, were selected as CECs and efficiently removed from the system in 2 hours. Once again, photophysical experiments and quenching constants were used to determine the main degradation pathway and to draw a plausible mechanism of degradation of BUVSs.

6. Photodegradation of benzotriazole UV filters by eosin Y

Once determined the mechanism of degradation of singular BUVSs in the presence of RFTA, RFTA was substituted by eosin Y (EOY), a synthetic molecule, which is able to absorb at 530 nm, as already reported in chapter 1.4.2. In this case, a mixed solution of UV-327 and UV-328 was investigated under different working conditions. As in the previous chapter, degradation's trend and photophysical measurements are reported and a final mechanism of degradation is postulated.

Moreover, apart from DABCO, also noscapine was tested as electron donor, in order to reproduce a real environmental system, where more pollutants are contemporaneously in water. As a matter of fact, this test pretends to demonstrate that each element could react with the others according to its own chemical properties, giving rise to different electron transfer reactions. As consequence, different CECs could be degraded at the same time and under a limited light irradiation.

In parallel, experiments were repeated in natural marine water in order to evaluate a different real system.

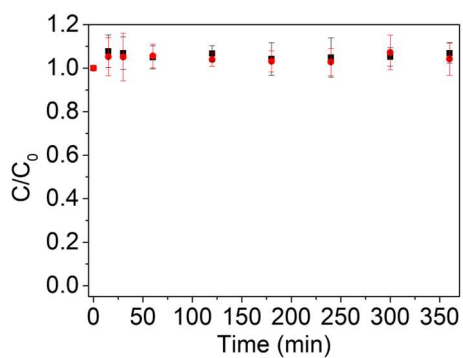
6.1. Results and discussion

6.1.1. Photodegradation of BUVSs

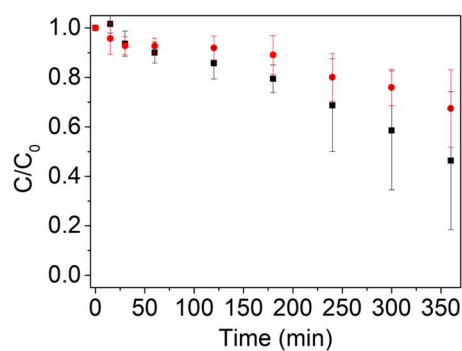
As demonstrated before, BUVSs are not affected by direct irradiation both in UV and visible light. Differently from the previous chapter, mixed solutions of BUVSs were irradiated in different conditions (both oxidative and reductive) and in aerated and deaerated atmosphere. BUVSs were irradiated under visible light first in the presence of the only photocatalyst (EOY), but unfortunately no changes were

observed (Figure 6.1A). So, a high concentration of DABCO as electron donor was added to the system: however, under nitrogen atmosphere the degradation was still very slow. As a matter of fact, only 50% of UV-327 and 30% of UV-328 were removed after six hours of irradiation (figure 6.1B). Nevertheless, in the presence of oxygen the reaction was faster: UV-327 is completely degraded after four hours, while only 10% of UV-328 is still in the system after 6 hours of irradiation (Figure 6.1C).

A)



B)



C)

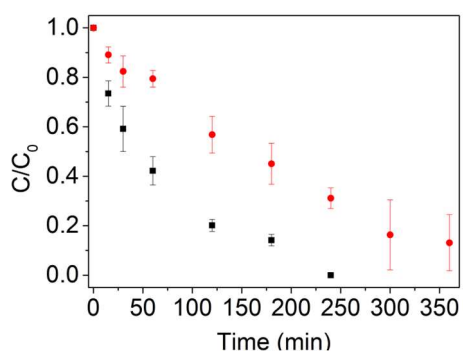


Figure 6.1. Photocatalytic degradation of aqueous mixtures of UV-327 (■) and UV-328 (●) (10^{-5} M each) in the presence of EOY (10% mol). Specific conditions: A) no DABCO, air; B) DABCO (10^{-2} M), N_2 ; C) DABCO (10^{-2} M), air.

As it can be seen in Figure 6.1, once again photodegradation of BUVSs works better in the presence of an electron donor and oxygen. However, DABCO is only an example of electron donor: in the natural environment other molecules (both natural and synthetic) could act as electron donors. Based on the previous studies of this thesis, we decided to replace DABCO with another contaminant, in order to evaluate degradation of two different contaminants at the same time in the presence of a photocatalyst and light. Considering that also EOY is considered a contaminant, this experiment tries to prove the simultaneous degradation of multiple contaminants, based on their different chemical properties.

Thus, a mixed solution of BUVSs, EOY and NSC was irradiated under LED light ($\lambda_{\max}=530$ nm) under aerated atmosphere: the obtained data in Figure 6.2 shows that degradation of both UV-327 and UV-328 is slower than the one in the presence of DABCO. Nevertheless, after six hours of irradiation only 50% of both the contaminants was degraded.

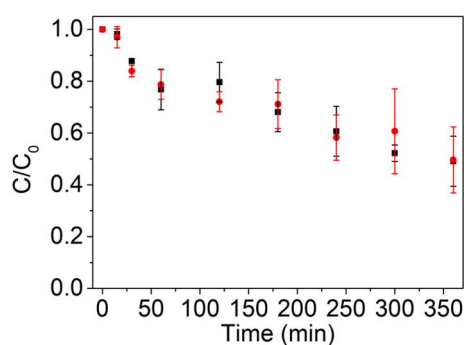


Figure 6.2. Photodegradation of UV-327 (■) and UV-328(●) in the presence of EOY and noscapine ($2 \cdot 10^{-2}$ M) as electron donor.

In parallel, another experiment was carried out substituting milli Q water with pretreated-marine water. In this case, a mix solution of BUVSs was irradiated both in the presence and in the absence of DABCO. Obtained results were compared with the one obtained in milliQ water (Figure 6.3).

In details, both in the presence and in the absence of DABCO, only 30% of both contaminants remained in the system. So, the electron donor is not determinant for the speed of the reaction: probably, the ions inside the marine water are the one affecting the speed of the photodegradation. In particular, in Figure 6.3A photodegradation is extremely faster than in milliQ water, but only because in milliQ nothing happened. On the other hand, in the presence of DABCO (Figure 6.3B), reaction is remarkably faster and efficient in milliQ water.

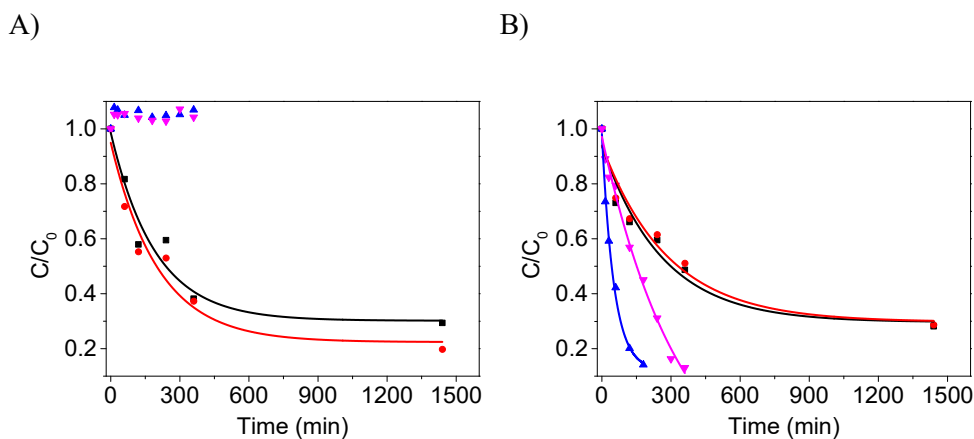


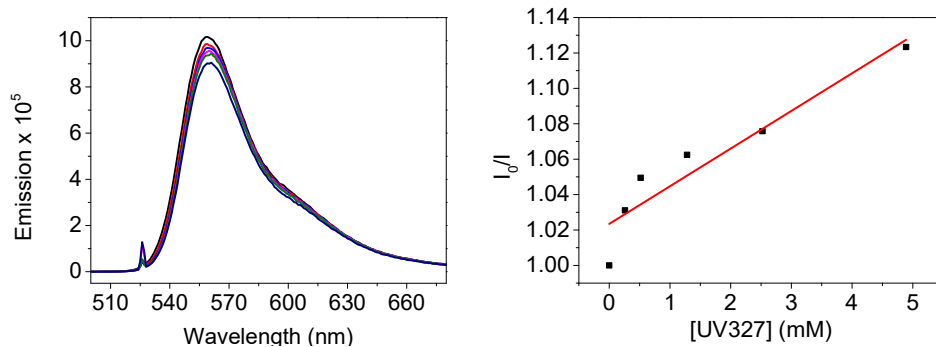
Figure 6.3. Photodegradation of UV-327 (■) and UV-328 (●) in the presence of EOY and LED light ($\lambda_{\max}=530$ nm) in marine water and of UV-327 (▲) and UV-328 (▼) in the presence of EOY and LED light ($\lambda_{\max}=530$ nm) in milliQ water in the absence (A) and in the presence of DABCO (1×10^{-2} M) (B).

6.1.2. Photochemical experiments

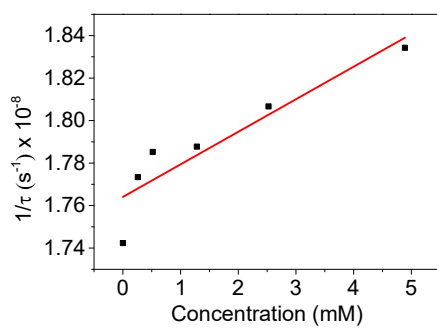
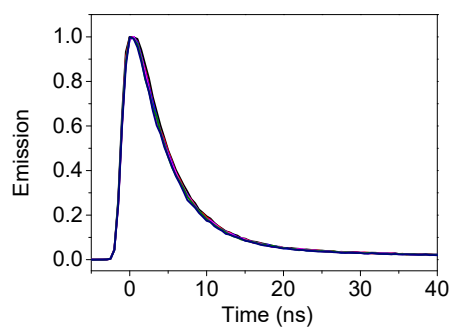
Next, photophysical measurements were carried out with the purpose of understanding the involvement of excited states of EOY in the degradation.

First, fluorescence quenching measurements were registered with increasing concentrations of BUVSs (see Figure 6.4); Stern-Volmer plots from both steady-state and time-resolved experiments and reported in Table 6.1. From the obtained data, we can conclude that singlet excited state of EOY is not affected by the addition of both UV-327 and UV-328. As a matter of fact, low rate constant values were obtained from the Stern-Volmer equation. On the other hand, the quenching of $^1\text{EOY}^*$ by DABCO is more efficient and consequently the Stern-Volmer constant values are higher (Figure 6.4 E and F and Table 6.1).

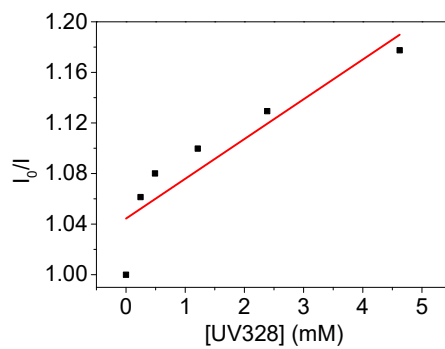
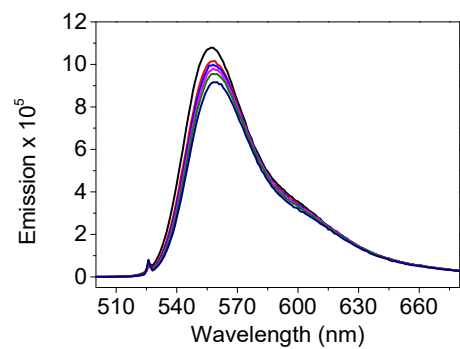
A)



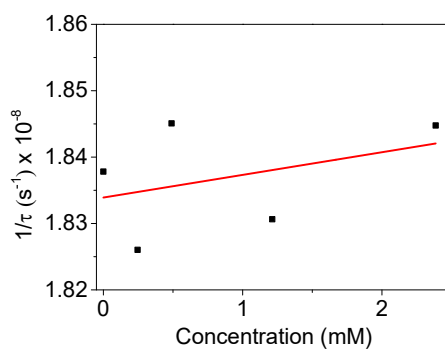
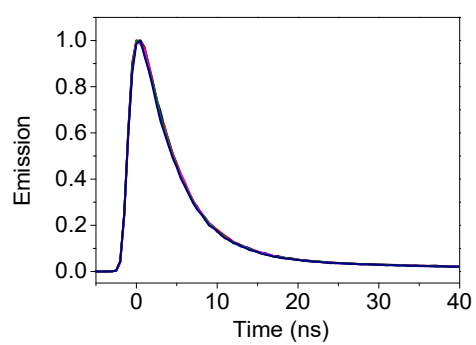
B)



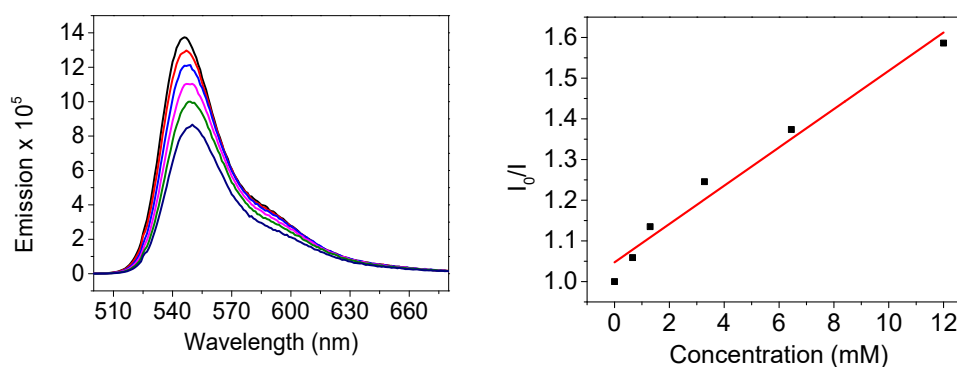
C)



D)



E)



F)

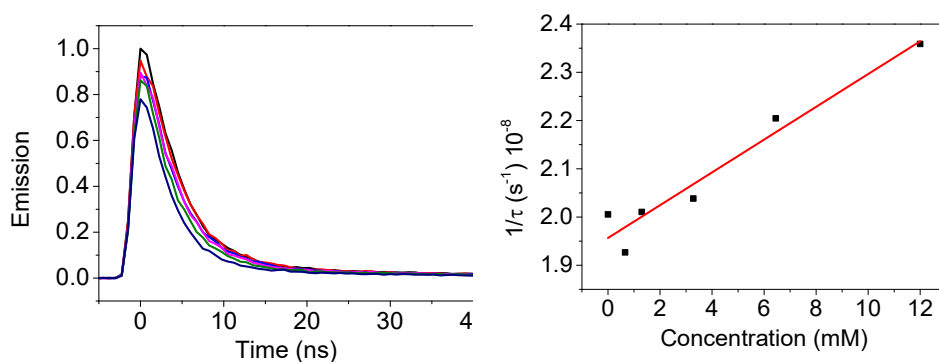


Figure 6.4. Left: Steady-state and time-resolved fluorescence experiments of EOY in the presence of increasing concentration of UV-327 (A and B), UV-328 (C and D) and DABCO (E and F). Right: corresponding Stern-Volmer plots.

Table 6.1. Stern-Volmer quenching constants of $^1\text{EOY}^*$ in the presence of increasing concentrations of BUVSs and DABCO.

| | $K_{qS} (\text{M}^{-1})$ from steady-state measurements | $k_{qS} (\text{M}^{-1}\text{s}^{-1})$ from time-resolved experiments |
|---------------|---|--|
| UV-327 | 21.27 | 1.53×10^9 |

| | | |
|---------------|-------|-------------------|
| UV-328 | 31.44 | 3.4×10^8 |
| DABCO | 46.01 | 3.4×10^9 |

Secondly, laser flash photolysis (LFP) measurements allowed investigating the contribution of the excited triplet state to the photodegradation processes.

The typical shape of ${}^3\text{EOY}^*$ in DMF is observed in Figure 6.5: the spectrum of triplet excited state of EOY is characterized by a broad absorption in the region 550–650 nm with a maximum at 580 nm. Consequently, the quenching of ${}^3\text{EOY}^*$ by the different pollutants was recorded at 580 nm.

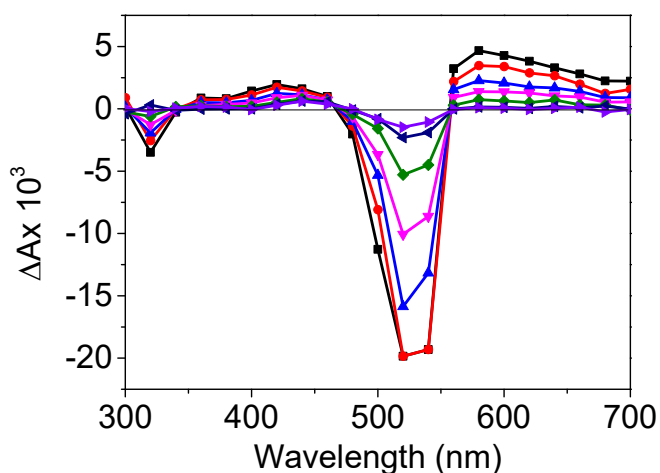
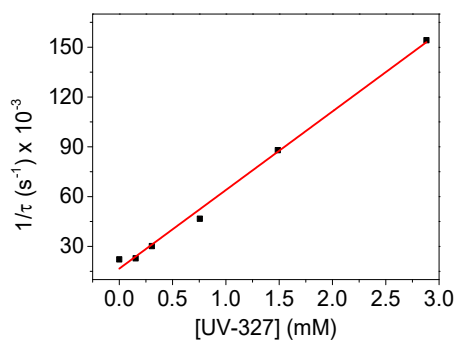
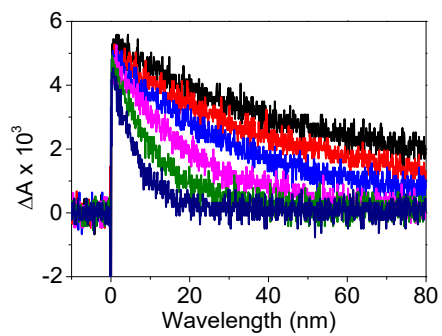


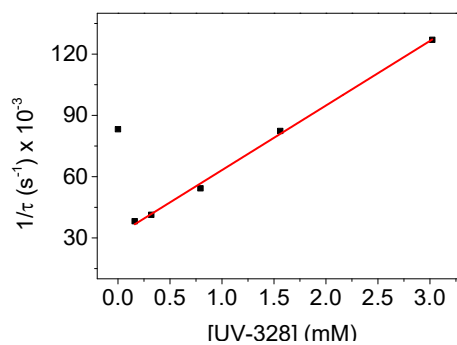
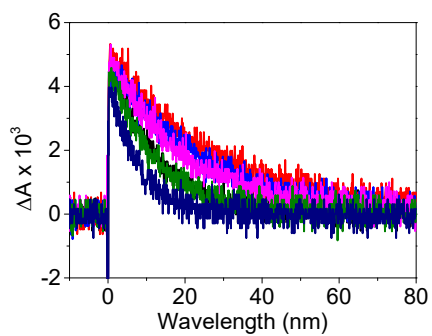
Figure 6.5. Transient absorption spectra of EOY recorded at different delay times after the 532 nm laser shot in deaerated DMF (absorbance ca. 0.3 at the excitation wavelength).

Next, LFP was carried out in the presence of increasing concentrations of BUVSs: obtained results are reported in Figure 6.6.

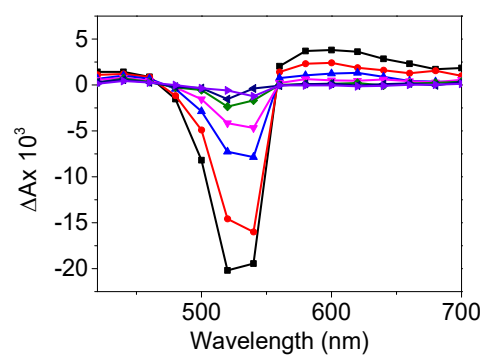
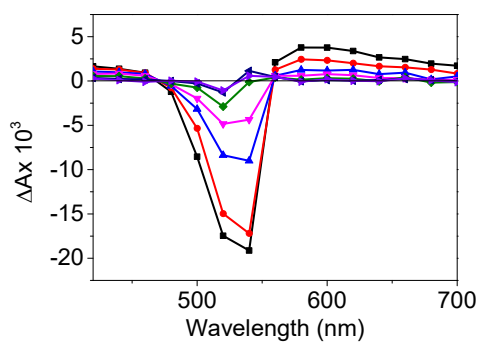
A)



B)



C)



D)

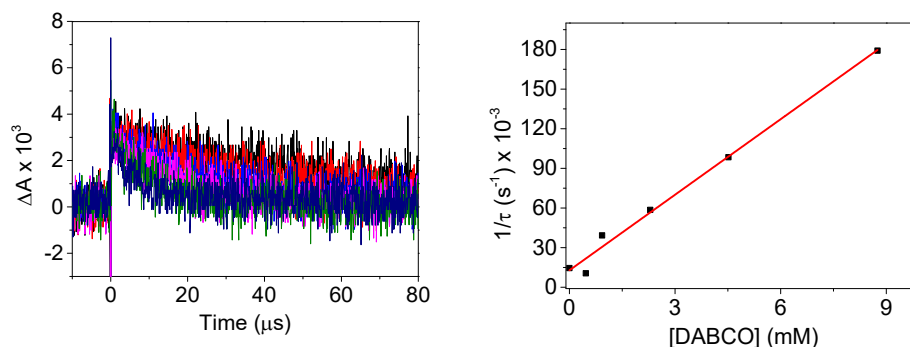


Figure 6.6. Left: Decay trace corresponding to ${}^3\text{EOY}^*$ in the presence of UV-327 (A) and UV-328 (B), recorded at 580 nm, ($\lambda_{\text{exc}} = 532$ nm). Right: Corresponding Stern-Volmer plots. The experiments were carried out in deaerated DMF (absorbance ca. 0.3 at the excitation wavelength). Corresponding Transient absorption spectra in the presence of UV-327 (on the left) and UV-328 (on the right) (C). Left: Decay trace corresponding to ${}^3\text{EOY}^*$ in the presence of DABCO (D), recorded at 580 nm, ($\lambda_{\text{exc}} = 532$ nm). Right: Corresponding Stern-Volmer plots.

Increasing concentrations of BUVSs, accelerated the decay of ${}^3\text{EOY}^*$ at 580 nm, but quenching of both contaminants seems low: therefore, rate constant k_{qT} was $4.7 \times 10^7 \text{ M}^{-1}\text{s}^{-1}$ for UV-327 and $3.2 \times 10^7 \text{ M}^{-1}\text{s}^{-1}$ in the case of UV-328. In the presence of DABCO, k_{qT} was $1.91 \times 10^7 \text{ M}^{-1}\text{s}^{-1}$. From the spectra, reported in Figure 6.6 C, no additional peaks are detected after the laser pulse.

Finally, the interaction between ${}^1\text{O}_2$ and BUVSs was already reported in the previous chapter in Figure 5.2.

6.1.3. Overall discussion

To sum up, degradation of a mixed solution of BUVSs was carried out under different conditions: once again, the presence of an electron donor (as DABCO or noscapine) and oxygen is essential to achieve a complete degradation of both UV-327 and UV-328. In particular, the change of electron donor showed a different rate of the photodegradation, according to the different electron donor capability. In general, photodegradation of both BUVSs in the presence of EOY is slower than in the presence of RFTA. Differently from the case of RFTA, no degradation is occurring without the presence of the electron donor, even if photochemical experiments reveal the direct quenching of $^3\text{EOY}^*$ by both BUVSs. As a matter of fact, triplet excited state of EOY is able to be slightly quenched by both contaminants, even if the quenching constants are quite low. However, experimental photodegradation revealed that this interaction is not enough to degrade BUVSs. Once again, an efficient electron donor (as DABCO) is necessary for the purpose. Moreover, this last experiment revealed also the possibility to photodegrade different contaminants simultaneously in real water systems, taking advantage of the different properties of the considered organic pollutants.

Moreover, preliminary test in pre-treated marine water revealed the possibility of producing the photodegradation of BUVSs in marine water without the presence of the electron donor. Probably, contained ions are responsible for the photodegradation, but more tests should be run in order to shed more light into the involved processes.

6.2. Conclusion

EOY is a synthetic organic dye, which could efficiently be used for the degradation of CECs in water under visible light. Two BUVSs, already introduced and tested in the previous chapter, were used as CECs and they were completely degraded under reductive working conditions. As a matter of fact, the presence of a sacrificial electron donor (SED) is necessary in order to generate the radical anion of EOY ($\text{EOY}^{\cdot-}$). DABCO was the most successful electron donor, but also contaminants as noscapine revealed a high efficiency. Photophysical experiments were useful to understand the interaction with the excited states of EOY and to draw a hypothetical mechanism. Last, degradation in marine water was performed to understand the degradation in a real environmental system. Therefore, more studies should be done in the future in order to understand the degradation mechanism in marine water and the reactive ions and species, involved in the reaction.

7. Experimental

7.1. Chemicals

In chapter 3, carbamazepine and atenolol were from TCI Chemicals and Sigma-Aldrich. In chapter 4, noscipine was from TCI Chemicals. Cotarnine and opianic acid were synthesized from noscipine, according to the methodology already published in literature. [119] In chapter 5 and 6, UV-326 (2-(2'-Hydroxy-3'-tert-butyl-5'-methylphenyl)-5-chloro-2H-benzotriazole, CAS 3896-11-5); UV-327 (2-(2'-Hydroxy-3',5'-di-tert-butylphenyl)-5-chloro-2H-benzotriazole, CAS 3864-99-1); UV-328 (2-(2'-Hydroxy-3',5'-di-tert-amylphenyl)-2H-benzotriazole, CAS 25973-55-1) were from TCI Chemicals. DMSO, DMF and Acetonitrile was from Scharlau. Acetylated riboflavin was synthesized from commercial Riboflavin (from TCI Chemicals).[57] Eosin Y disodium salt, CAS 17372-87-1 was from Sigma Aldrich. Water used in all the experiments was Milli-Q grade. All the reagents used in this work were of analytical grade and used without further purification.

7.2. Photodegradation experiments and analytical procedures

In chapter 3 and 4, aqueous solutions (5 mL) containing 10 mg L⁻¹ of CBZ, ATN and NSC and 1 mg L⁻¹ of RFTA underwent irradiation in stirred cylindrical closed cells (40 mm i.d. 25 mm high, made of Pyrex glass) using a 1500W Xenon lamp (Solarbox, CO. FO. MEGRA, Milan, Italy) equipped with a cutoff filter at 400 nm. The concentration of substrates over time was tracked using a Merck-Hitachi HPLC equipped with a L-4200 UV-Vis detector and a reverse-phase RP-C18 column (Lichrospher, 4 mm i.d.×12.5 mm length and 5 μm particle diameter from Merck). Elution was carried out in isocratic conditions using phosphoric acid (3 mM) and acetonitrile with a ratio 65:35 v/v for CBZ and RFTA, 40:60 v/v for ATL at 1 mL min⁻¹ flow rate, In the case of NSC, an aqueous solution of trifluoroacetic acid (TFA

0.1 %v/v)/acetonitrile (45/55, v/v) was used as eluent, flow rate 1.0 mL min⁻¹. The detection wavelength was 215 nm, 285 nm, 225 nm and 460 nm for ATN, CBZ, NSC and RFTA, respectively.

Separation and identification of the intermediate photoproducts of CBZ and ATN were carried out by a UFLC-SHIMADZU combined with QTRAP LC-MS/MS 3200 from SCIEX (Framingham, MA, USA). Electrospray ionization (ESI) was used in positive ion mode (50–600 m/z range)

The separation and identification of photoproducts of NSC were performed by a UPLC-Waters combined with a QToF spectrometer. The mobile phase was applied as a gradient composed of 0.1 % aqueous formic acid solution (component A) and 0.1 % formic acid in acetonitrile (component B). The column was equilibrated with A:B (70:30, v/v) as the mobile phase at a flow rate of 0.3 mL/min. The injection volume was 3 µL. The ESI source was operated in positive ionization mode with a capillary voltage of 1 kV. The source and desolvation temperatures were set at 120 and 400°C, respectively. The cone and desolvation gas flows were 10 and 800 L/h, respectively. Separations were accomplished by UPLC on a Zorbax Eclipse Plus C18 column (4.6 x 100 mm, 3.5 µm particle diameter). Cotarnine and opianic acid, were obtained from noscapine, according to the procedure reported in literature and used as standards in the HPLC-MS and HPLC-MS2 analysis[119].

The phototransformation products were tentatively identified based on their MS² spectra collected by enhanced product ions (EPI) mode, which was triggered by enhanced mass resolution (EMS) and enhanced resolution (ER) steps according to the information depend acquisition (IDA) mode with a threshold of 500,000 cps.

In chapters 5 and 6, mother solutions of each UV filter were prepared in DMF (1x10⁻³ M). A mother solution of eosin Y was prepared in milliQ water at 1x10⁻³M. A mother solution of DABCO (1,4-diazabicyclo[2.2.2]octane) was prepared in milliQ

water (2×10^{-1} M). For the photodegradations, aqueous mixtures of 25 mL containing the pollutants (10^{-5} M), EOY (2×10^{-6} M, 10% mol) and DABCO (10^{-2} M) when specified, were prepared and irradiated under the LEDs' light under the specified atmosphere. To monitor the progress of the photodegradations, aliquots of 0.5 mL were sampled and analyzed by HPLC-UV (Waters 600 C chromatograph equipped with a Waters 600 Pump and Controller, a Waters In-line Degasser AF, and a Waters 996 Photodiode Array Detector). A Teknokroma C18 Mediterranean Sea analytical column (25 cm \times 0.46 mm and 5 μ m particle size) was used as the stationary phase and a mixture of acetonitrile/water was used as eluent working in isocratic mode (90 % acetonitrile/10% H₂O pH 3) at a flow rate of 1.5 mL min⁻¹. The samples were analyzed at 350 nm. Calibration lines were used to determine the concentrations. Experiments were carried out in triplicate.

7.3. Toxicity tests

In order to evaluate the acute toxicity in chapter 4, the samples collected at different irradiation times were analyzed by a Microtox Model 500 Toxicity Analyzer (Milan, Italy). This bioluminescence inhibition assay monitors the changes in the natural emission of the marine bacterium *Vibrio fischeri* when challenged with toxic substances. Freeze-dried bacteria, reconstitution solution diluent (2% NaCl) and an adjustment solution (non-toxic 22% sodium chloride) were obtained from Azur (Milan, Italy). Luminescence was recorded after 5, 15, and 30 min of incubation at 15 °C. Since no substantial differences were found between the three contact times, hereafter the results related to 5 min of contact are reported. Inhibition percentage of luminescence was calculated by comparison with a toxic-free control following the established protocol using the Microtox calculation program.

7.4. Photophysical experiments

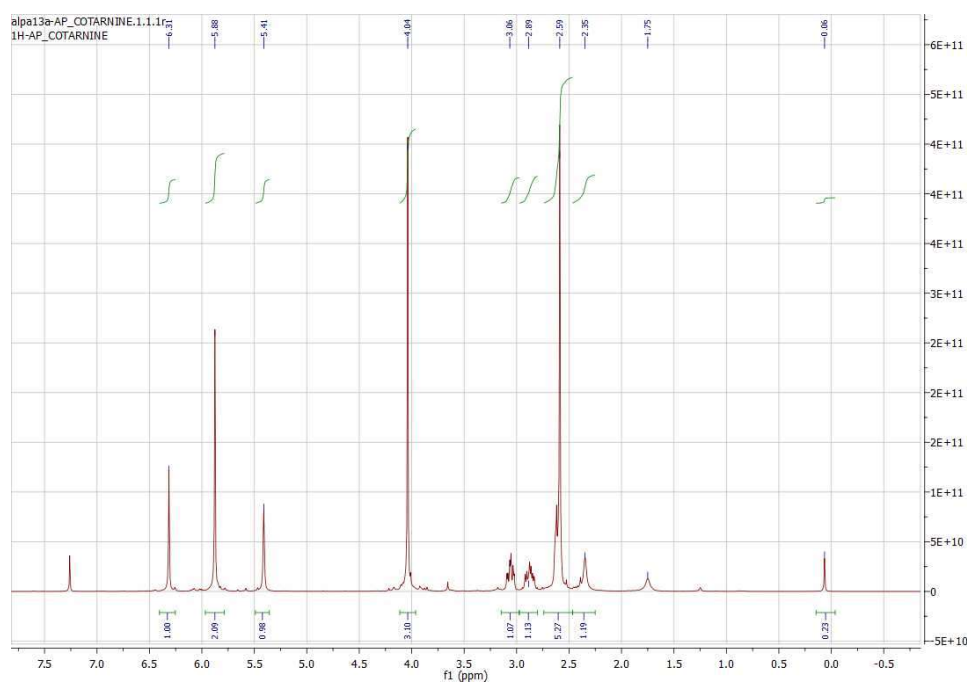
All the steady-state and time-resolved fluorescence experiments were performed using a Photon Technology International (PTI) LPS-220B, FLS1000 fluorometer (Edinburgh Instruments) and an EasyLife V (OBB) fluorometer, respectively. In particular, FLS1000 fluorimeter (Edinburgh instruments) was equipped with a 450W Xe lamp and a PMT-980 detector. Steady-state measurements were carried out exciting at $\lambda_{\text{exc}} = 460$ nm in the case of RFTA and 525 nm for EOY. Time-resolved fluorescence was measured with a diode LED ($\lambda_{\text{exc}} = 460$ nm in the case of RFTA and $\lambda_{\text{exc}} = 525$ nm in the case of EOY) as excitation source with a cut off filter (50 % transmission at 475 nm for RFTA and 550 for EOY). All the solutions were prepared in aerated acetonitrile with absorbance lower than 0.15 at 460 nm and 525 nm.

Fluorescence quantum yield (Φ_{F}) for RFTA in acetonitrile was obtained using RF in water as a standard ($\Phi_{\text{F}} = 0.26$).^[120,121] Φ_{ISC} was calculated as $1 - \Phi_{\text{F}}$.

A pulsed Nd:YAG SL404G-10 laser (Spectron Laser Systems) was employed to carry out the laser flash photolysis experiments at the excitation wavelength of 355 nm (20 mJ pulse⁻¹). The laser flash photolysis system consists of the pulsed laser, a pulsed Lo255 Oriel Xenon lamp, a 77200 Oriel monochromator, Oriel photomultiplier tube (PMT) housing, a 70705 PMT power supply, and a TDS-640A Tektronix oscilloscope. Experiments were performed using acetonitrile solution under nitrogen atmosphere with absorbance *ca.* 0.3 at the excitation wavelength. Singlet oxygen quenching experiments were performed with the same LFP equipped with a Hamamatsu NIR emission detector. The characteristic emission signal of ¹O₂ was monitored at 1270 nm upon increasing amounts of drugs in aerated acetonitrile. Quartz cuvettes of 1x1 cm were used for all the photophysical measurements that were taken at room temperature.

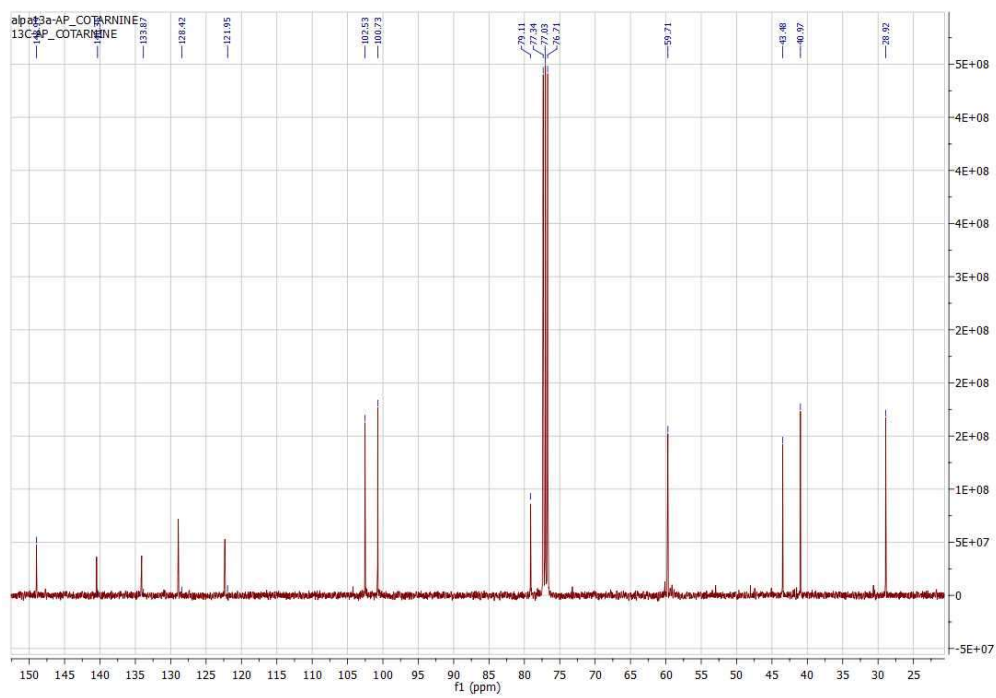
7.5. Synthesis of cotarnine and opianic acid

Cotarnine and opianic acid were synthesized from noscapine, according to the methodology already published in literature.[119] 1g of NSC was dissolved in 8 ml of HNO₃ 14%. Solution was heated at 50°C for 2 hours. After 2 h, once no more precipitate was formed, the solution was cooled to room temperature and the formed solid filtered with a sintered funnel under vacuum to obtain opianic acid. The remaining solution was neutralized slowly with 25 % KOH with continuous stirring until pH 11. The obtained precipitate (cotarnine) was filtered again with a sintered funnel under vacuum, washed with water and dried. Both cotarnine and opianic acid were characterized through NMR ¹H, ¹³C, DEPT and NOEDIF.



¹H NMR (400 MHz, CDCl₃): δ = 6.31 (s, 1H), 5.88 (s, 2H), 5.41 (d, 1H), 4.04(s, 3H), 3.06 (m, 1H), 2.89 (m, 1H), 2.59 (m, 5H), 2.35 (s, 1H) ppm.

Figure 7.1. ¹H NMR of synthesized cotarnine.



^{13}C NMR (? MHz, CDCl_3): δ = 148.9, 140.3, 133.9, 128.4, 121.9, 102.5, 100.7, 79.1, 59.7, 43.5, 40.9, 28.9 ppm.

Figure 7.2. ^{13}C NMR of synthesized cotarnine.

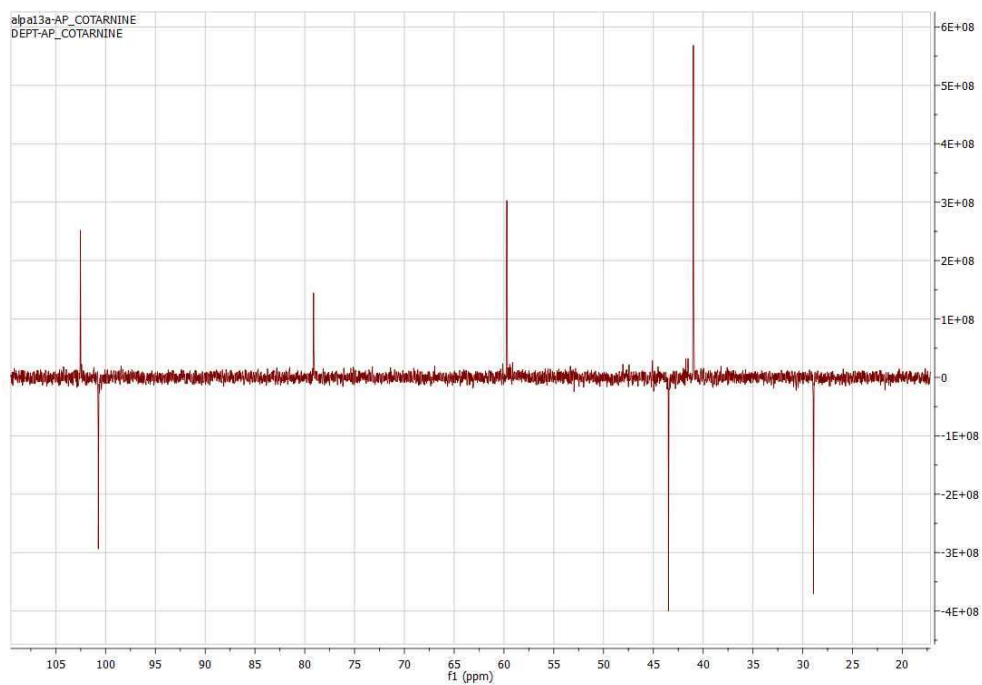


Figure 7.3. ^{13}C NMR-DEPT of synthesized cotarnine.

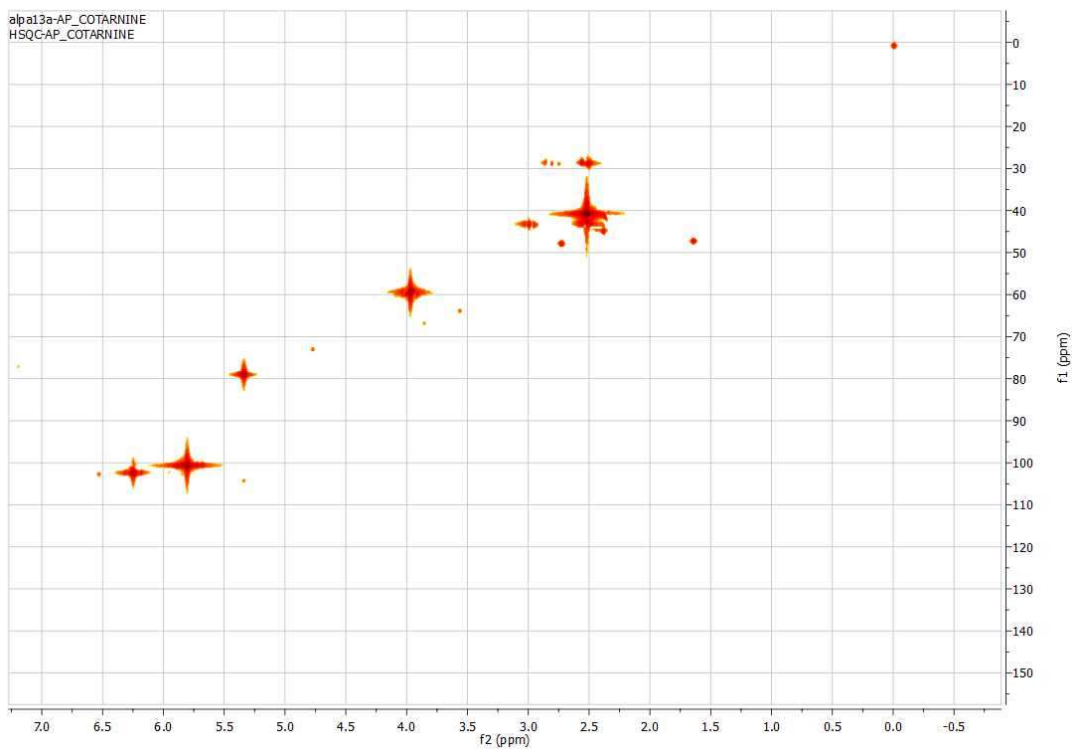
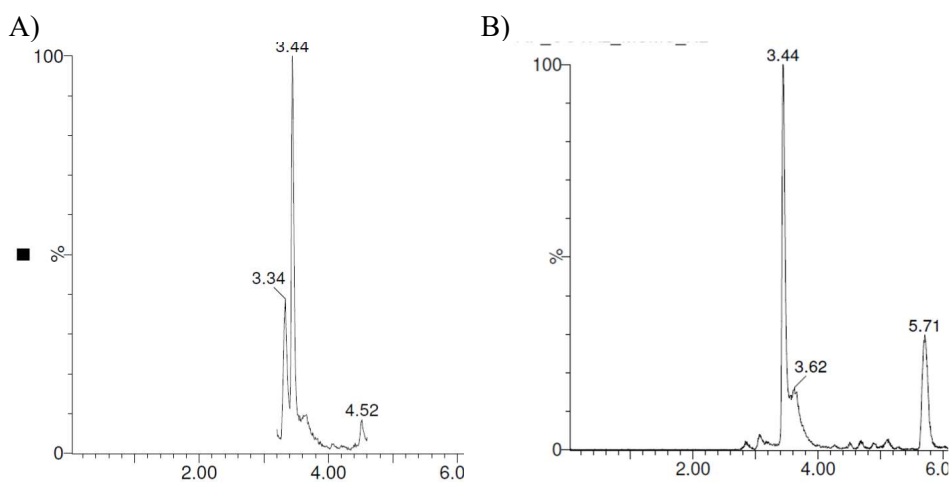


Figure 7.4. NMR-HSQC of synthesized cotarnine.



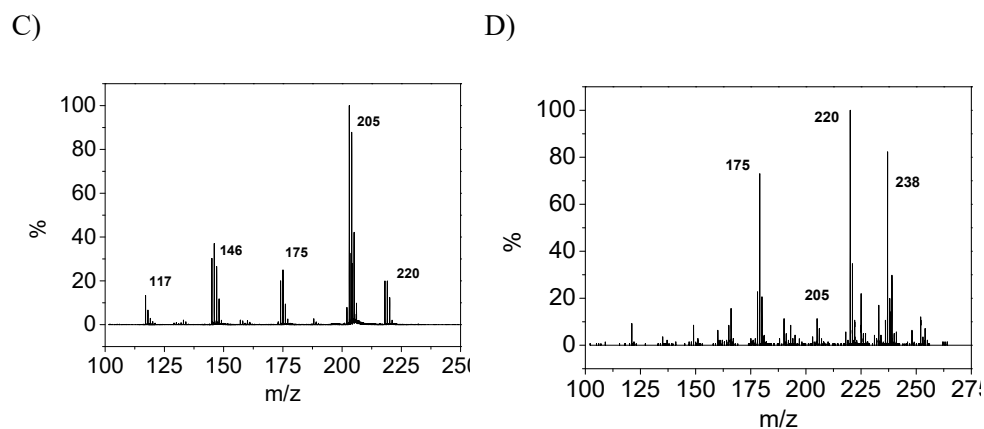


Figure 7.5. UPLC-MS analysis of the synthesized cotarnine. Selected ion monitoring (SIM) at m/z 220 (A) or m/z 238 (B). C) Mass-Mass spectrum of peak with m/z 220 in A; D) Mass-Mass spectrum of peak with m/z 238 in B.

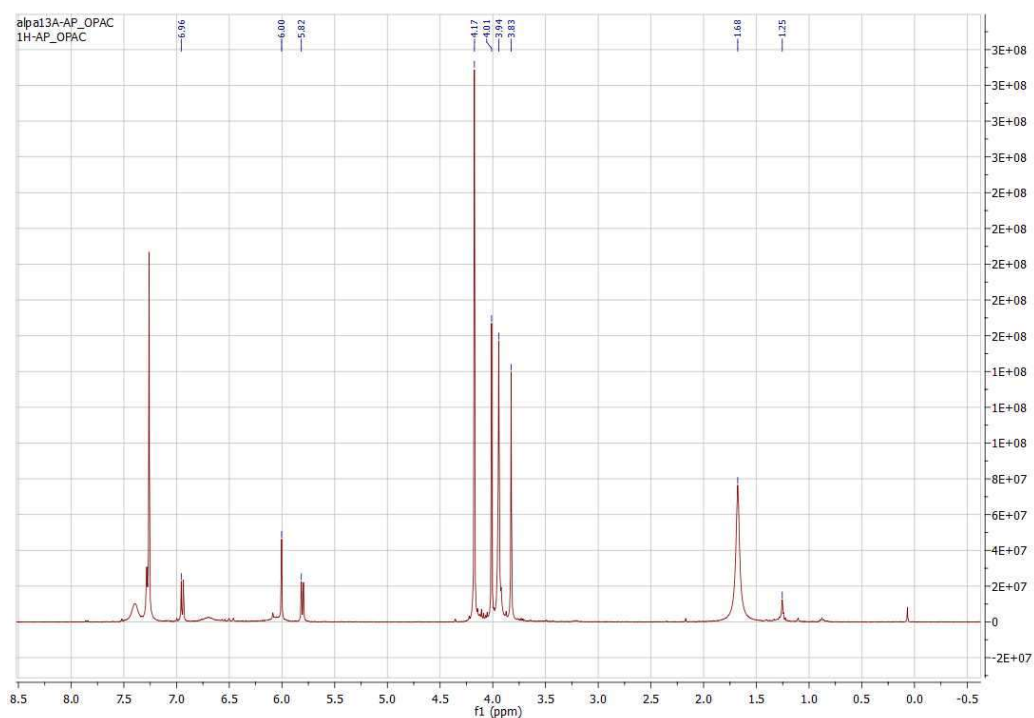


Figure 7.6. ^1H NMR of synthesized opianic acid.

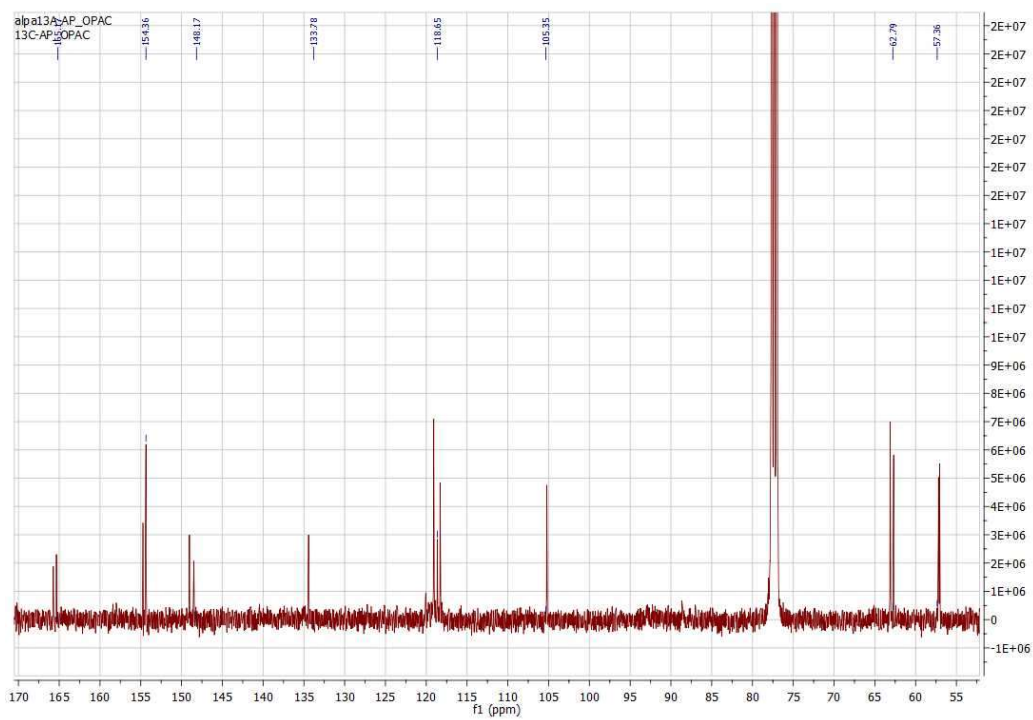


Figure 7.7. ^{13}C NMR of synthesized opianic acid.

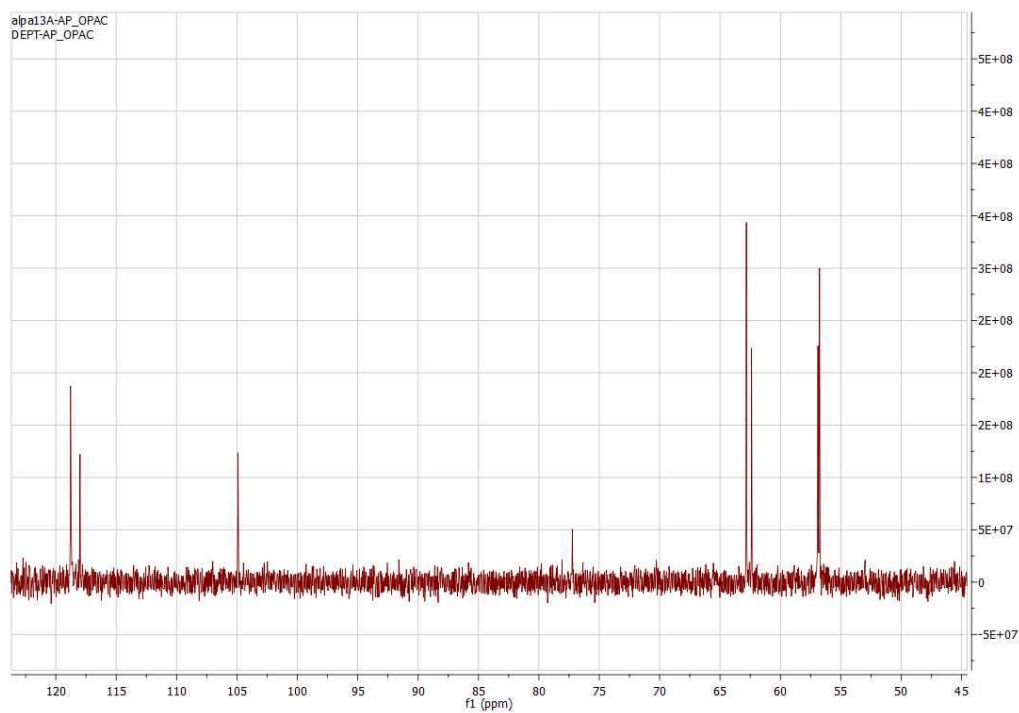


Figure 7.8. ^{13}C NMR DEPT of synthesized opianic acid.

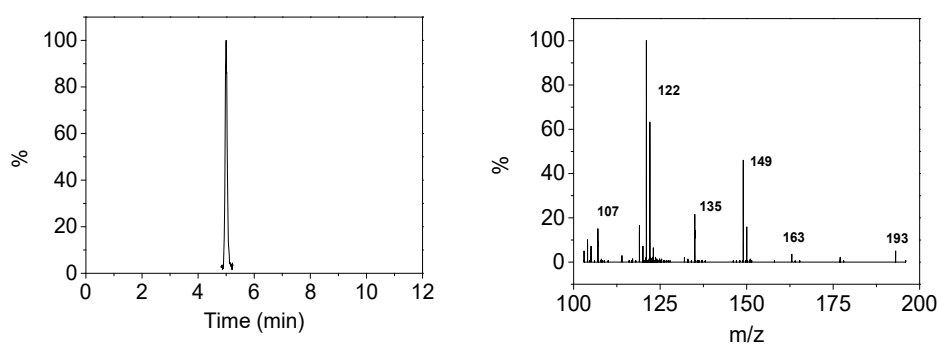


Figure 7.9. UPLC-MS analysis of the synthesized Opianic acid. Selected ion monitoring (SIM) at m/z 193 (A) and Mass-Mass spectrum of the peak at 5.7 minutes.

8. Conclusion

This PhD thesis intends the degradation of different contaminants of emerging concern (CECs) in water assisted by organic photocatalysts and visible light. In detail, acetylated riboflavin and eosin Y were efficient for the degradation of different classes of pollutants, both in oxidative and reductive conditions. Pharmaceuticals and UV-filters are the main tested CECs: in chapters 3 and 4, pharmaceuticals were easily photodegraded in oxidative conditions. These conditions required the presence of the organic photocatalyst (RFTA), visible light and air. On the other hands, BUVSs are more recalcitrant, and they need reductive conditions: these imply the presence in the system of the organic photocatalyst (RFTA or EOY), a sacrificial donor (like DABCO o NSC), visible light and air. In particular, reductive treatment of contaminants is an innovative technique to degrade organic contaminants in water.

MS and MS² analysis were useful to determine the main photodegradation products. Photophysical experiments were useful to determine the interaction between the excited species of the photocatalysts and singlet oxygen and the contaminants. Quenching constants were obtained from the experimental data and used to calculate the thermodynamic efficiency of each pathway.

Finally, degradation trends, photodegradation products, photophysical data and quenching constants were all combined in order to draw a hypothetical mechanism.

Moreover, preliminary experiments were performed in marine water in order to study a different system. Unfortunately, more studies should be performed to understand the role of all the involved species and consequently the real mechanism of degradation under that scenario.

9. References

- [1] World Health Organisation (WHO), (n.d.). <https://www.who.int/>.
- [2] P.H. Gleick, Water Use, *Annu. Rev. Environ. Resour.* 28 (2003) 275–314. <https://doi.org/10.1146/annurev.energy.28.040202.122849>.
- [3] WHO, Water for Health. Taking Charge, (n.d.). https://www.who.int/water_sanitation_health/wwdreport.pdf.
- [4] WHO, The United Nations World Water Development Report 2021, 2021.
- [5] WHO World Water Day Report, (n.d.). https://www.who.int/water_sanitation_health/takingcharge.html.
- [6] A. Fenwick, Waterborne infectious diseases - Could they be consigned to history?, *Science* (80-.). 313 (2006) 1077–1081. <https://doi.org/10.1126/science.1127184>.
- [7] P.K. Goel, *Water Pollution: Causes, Effects and Control*, New Age International, 2006.
- [8] S.E. Manahan, *Chimica dell'ambiente*, Piccin, 2000.
- [9] S. Sauvé, M. Desrosiers, A review of what is an emerging contaminant, *Chem. Cent. J.* 8 (2014) 1–7. <https://doi.org/10.1186/1752-153X-8-15>.
- [10] J.F.J.R. Pesqueira, M.F.R. Pereira, A.M.T. Silva, Environmental impact assessment of advanced urban wastewater treatment technologies for the removal of priority substances and contaminants of emerging concern: A review, *J. Clean. Prod.* 261 (2020) 121078. <https://doi.org/10.1016/j.jclepro.2020.121078>.

- [11] A.R. Ribeiro, M. Pedrosa, N.F.F. Moreira, M.F.R. Pereira, A.M.T. Silva, Environmental friendly method for urban wastewater monitoring of micropollutants defined in the Directive 2013/39/EU and Decision 2015/495/EU, *J. Chromatogr. A.* 1418 (2015) 140–149. <https://doi.org/10.1016/j.chroma.2015.09.057>.
- [12] L.G. Cortes, D. Marinov, I. Sanseverino, A.N. Cuenca, M. Niegowska, E.P. Rodriguez, T. Lettieri, Selection of substances for the 3rd Watch List under the Water Framework Directive, 2020. <https://doi.org/10.2760/194067>.
- [13] M. von Sperling, *Biological Wastewater Treatment series: Wastewater Characteristics, Treatment and Disposal.*, IWA Publis, 2007.
- [14] M. von Sperling, *Biological Wasterwater Treatment Series: Basic Principles of Wasterwater Treatment*, IWA Publishing, 2007.
- [15] EPA, *How Wastewater Treatment Works... The Basics*, (1998) 1–6.
- [16] G. V. Buxton, C.L. Greenstock, W.P. Helman, A.B. Ross, Critical Review of rate constants for reactions of hydrated electrons, hydrogen atoms and hydroxyl radicals ($\cdot\text{OH}/\cdot\text{O}^-$ in Aqueous Solution, *J. Phys. Chem. Ref. Data.* 17 (1988) 513–886. <https://doi.org/10.1063/1.555805>.
- [17] Y. Deng, R. Zhao, *Advanced Oxidation Processes (AOPs) in Wastewater Treatment*, *Curr. Pollut. Reports.* 1 (2015) 167–176. <https://doi.org/10.1007/s40726-015-0015-z>.
- [18] M. Malakootian, A. Shahesmaeili, M. Faraji, H. Amiri, S. Silva Martinez, Advanced oxidation processes for the removal of organophosphorus pesticides in aqueous matrices: A systematic review and meta-analysis, *Process Saf. Environ. Prot.* 134 (2020) 292–307. <https://doi.org/10.1016/j.psep.2019.12.004>.

- [19] D.S. Babu, V. Srivastava, P. V. Nidheesh, M.S. Kumar, Detoxification of water and wastewater by advanced oxidation processes, *Sci. Total Environ.* 696 (2019) 133961. <https://doi.org/10.1016/j.scitotenv.2019.133961>.
- [20] A. Matilainen, M. Sillanpää, Removal of natural organic matter from drinking water by advanced oxidation processes, *Chemosphere.* 80 (2010) 351–365. <https://doi.org/10.1016/j.chemosphere.2010.04.067>.
- [21] S. Parsons, *Advanced Oxidation Processes for Water and Wastewater Treatment*, IWA Publishing, 2004.
- [22] S. Giannakis, S. Rtimi, C. Pulgarin, Light-assisted advanced oxidation processes for the elimination of chemical and microbiological pollution of wastewaters in developed and developing countries, *Molecules.* 22 (2017) 1070. <https://doi.org/10.3390/molecules22071070>.
- [23] D.B. Miklos, C. Remy, M. Jekel, K.G. Linden, J.E. Drewes, U. Hübner, Evaluation of advanced oxidation processes for water and wastewater treatment – A critical review, *Water Res.* 139 (2018) 118–131. <https://doi.org/10.1016/j.watres.2018.03.042>.
- [24] T.D.P. K.S. McKenzie, A.B. Sarr, K. Mayura, R.H. Bailey, D.R. Miller, T.D. Rogers, W.P. Norred, K.A. Voss, R.D. Plattner, L.F. Kubena, Oxidative Degradation and Detoxification of Mycotoxins Using a Novel Source of Ozone, *Food Chem. Toxicol.* 35 (1997) 807–820.
- [25] S.J. Masten, S.H.R. Davies, The use of ozonization to degrade organic contaminants in wastewaters, *Environ. Sci. Technol.* 28 (1994) 180–185. <https://doi.org/10.1021/es00053a001>.
- [26] S. Gligorovski, R. Strekowski, S. Barbati, D. Vione, Environmental Implications of Hydroxyl Radicals ($\bullet\text{OH}$), *Chem. Rev.* 115 (2015) 13051–

13092. <https://doi.org/10.1021/cr500310b>.

- [27] M.N. Chong, A.K. Sharma, S. Burn, C.P. Saint, Feasibility study on the application of advanced oxidation technologies for decentralised wastewater treatment, *J. Clean. Prod.* 35 (2012) 230–238. <https://doi.org/10.1016/j.jclepro.2012.06.003>.
- [28] T. Oppenländer, *Photochemical Purification of Water and Air: Advanced Oxidation Processes (AOPs) - Principles, Reaction Mechanisms, Reactor Concepts*, Wiley-VCH, 2007.
- [29] R. Andreozzi, V. Caprio, A. Insola, R. Marotta, Advanced oxidation processes (AOP) for water purification and recovery, *Catal. Today.* 53 (1999) 51–59. [https://doi.org/10.1016/S0920-5861\(99\)00102-9](https://doi.org/10.1016/S0920-5861(99)00102-9).
- [30] M.R. Hoffmann, S.T. Martin, W. Choi, D.W. Bahnemann, Environmental Applications of Semiconductor Photocatalysis, *Chem. Rev.* 95 (1995) 69–96. <https://doi.org/10.1021/cr00033a004>.
- [31] C. von Sonntag, Advanced oxidation processes: mechanistic aspects, *Water Sci. Technol.* 58 (2008) 1015–1021. <https://doi.org/10.2166/wst.2008.467>.
- [32] I. Sciscenko, A. Arques, Z. Varga, S. Bouchonnet, O. Monfort, M. Brigante, G. Mailhot, Significant role of iron on the fate and photodegradation of enrofloxacin, *Chemosphere.* 270 (2021). <https://doi.org/10.1016/j.chemosphere.2021.129791>.
- [33] M.H. Pérez, G. Peñuela, M.I. Maldonado, O. Malato, P. Fernández-Ibáñez, I. Oller, W. Gernjak, S. Malato, Degradation of pesticides in water using solar advanced oxidation processes, *Appl. Catal. B Environ.* 64 (2006) 272–281. <https://doi.org/10.1016/j.apcatb.2005.11.013>.

- [34] I. Salmerón, K. V. Plakas, I. Sirés, I. Oller, M.I. Maldonado, A.J. Karabelas, S. Malato, Optimization of electrocatalytic H₂O₂ production at pilot plant scale for solar-assisted water treatment, *Appl. Catal. B Environ.* 242 (2019) 327–336. <https://doi.org/10.1016/j.apcatb.2018.09.045>.
- [35] T.P. Yoon, M.A. Ischay, J. Du, Visible light photocatalysis as a greener approach to photochemical synthesis, *Nat. Chem.* 2 (2010) 527–532. <https://doi.org/10.1038/nchem.687>.
- [36] D. Ravelli, M. Fagnoni, Dyes as Visible Light Photoredox Organocatalysts, *ChemCatChem.* 4 (2012) 169–171. <https://doi.org/10.1002/cctc.201100363>.
- [37] D. Ravelli, M. Fagnoni, A. Albini, Photoorganocatalysis. What for?, *Chem. Soc. Rev.* 42 (2013) 97–113. <https://doi.org/10.1039/c2cs35250h>.
- [38] D.M. Yan, J.R. Chen, W.J. Xiao, New Roles for Photoexcited Eosin Y in Photochemical Reactions, *Angew. Chemie - Int. Ed.* 58 (2019) 378–380. <https://doi.org/10.1002/anie.201811102>.
- [39] O. Cabezuelo, R. Martinez-Haya, N. Montes, F. Bosca, M.L. Marin, Heterogeneous riboflavin-based photocatalyst for pollutant oxidation through electron transfer processes, *Appl. Catal. B Environ.* 298 (2021) 120497. <https://doi.org/10.1016/j.apcatb.2021.120497>.
- [40] B.P. Vellanki, B. Batchelor, A. Abdel-Wahab, Advanced reduction processes: A new class of treatment processes, *Environ. Eng. Sci.* 30 (2013) 264–271. <https://doi.org/10.1089/ees.2012.0273>.
- [41] J. Cui, P. Gao, Y. Deng, Destruction of Per- And Polyfluoroalkyl Substances (PFAS) with Advanced Reduction Processes (ARPs): A Critical Review, *Environ. Sci. Technol.* 54 (2020) 3752–3766. <https://doi.org/10.1021/acs.est.9b05565>.

- [42] X. Liu, S. Yoon, B. Batchelor, A. Abdel-Wahab, Degradation of vinyl chloride (VC) by the sulfite/UV advanced reduction process (ARP): Effects of process variables and a kinetic model, *Sci. Total Environ.* 454–455 (2013) 578–583. <https://doi.org/10.1016/j.scitotenv.2013.03.060>.
- [43] B.P. Vellanki, B. Batchelor, Perchlorate reduction by the sulfite/ultraviolet light advanced reduction process, *J. Hazard. Mater.* 262 (2013) 348–356. <https://doi.org/10.1016/j.jhazmat.2013.08.061>.
- [44] H. Park, C.D. Vecitis, J. Cheng, W. Choi, B.T. Mader, M.R. Hoffmann, Reductive defluorination of aqueous perfluorinated alkyl surfactants: Effects of ionic headgroup and chain length, *J. Phys. Chem. A.* 113 (2009) 690–696. <https://doi.org/10.1021/jp807116q>.
- [45] N. Bensalah, R. Nicola, A. Abdel-Wahab, Nitrate removal from water using UV-M/S2O4²⁻ advanced reduction process, *Int. J. Environ. Sci. Technol.* 11 (2014) 1733–1742. <https://doi.org/10.1007/s13762-013-0375-0>.
- [46] V.S.V. Botlaguduru, B. Batchelor, A. Abdel-Wahab, Application of UV-sulfite advanced reduction process to bromate removal, *J. Water Process Eng.* 5 (2015) 76–82. <https://doi.org/10.1016/j.jwpe.2015.01.001>.
- [47] S. Khan, M. Sayed, M. Sohail, L.A. Shah, M.A. Raja, Chapter 6 - Advanced Oxidation and Reduction Processes, Elsevier Inc., 2018. <https://doi.org/10.1016/B978-0-12-814790-0.00006-5>.
- [48] R.G. Bacher A., Eberhard S, Fischer M., Kis K., Biosynthesis of Vitamin B2 (riboflavin), *Annu. Rev. Nutr.* 20 (2000) 153–167. <https://doi.org/10.1146/annurev.nutr.20.1.153>.
- [49] H.J. Powers, Riboflavin (vitamin B-2) and health, *Am. J. Clin. Nutr.* 77 (2003) 1352–1360. <https://doi.org/https://doi.org/10.1093/ajcn/77.6.1352>.

- [50] R. Martinez-Haya, M.A. Miranda, M.L. Marin, Metal-Free Photocatalytic Reductive Dehalogenation Using Visible-Light: A Time-Resolved Mechanistic Study, *European J. Org. Chem.* 2017 (2017) 2164–2169. <https://doi.org/10.1002/ejoc.201601494>.
- [51] C. Gambetta, W.A. Massad, A. V. Nesci, N.A. García, Vitamin B2-sensitized degradation of the multifunctional drug Evernyl, in the presence of visible light-microbiological implications, *Pure Appl. Chem.* 87 (2015) 997–1010. <https://doi.org/10.1515/pac-2015-0407>.
- [52] G. Morales, A. Pajares, J. Natera, J.P. Escalada, W. Massad, N.A. García, The riboflavin-photosensitized degradation of the uv-absorbing azo dye-metabolites Benzidine and o-Tolidine. Kinetic and mechanistic aspects, *J. Photochem. Photobiol. A Chem.* 344 (2017) 49–55. <https://doi.org/10.1016/j.jphotochem.2017.04.035>.
- [53] E. Reynoso, M.B. Spesia, N.A. García, M.A. Biasutti, S. Criado, Riboflavin-sensitized photooxidation of Ceftriaxone and Cefotaxime. Kinetic study and effect on *Staphylococcus aureus*, *J. Photochem. Photobiol. B Biol.* 142 (2015) 35–42. <https://doi.org/10.1016/j.jphotobiol.2014.11.004>.
- [54] R. Huang, E. Choe, D.B. Min, Kinetics for singlet oxygen formation by riboflavin photosensitization and the reaction between riboflavin and singlet oxygen, *J. Food Sci.* 69 (2004). <https://doi.org/10.1111/j.1365-2621.2004.tb09924.x>.
- [55] D.R. Cardoso, S.H. Libardi, L.H. Skibsted, Riboflavin as a photosensitizer. Effects on human health and food quality, *Food Funct.* 3 (2012) 487–502. <https://doi.org/10.1039/c2fo10246c>.
- [56] R. Martinez-Haya, M.A. Miranda, M.L. Marin, Type I vs Type II

- photodegradation of pollutants, *Catal. Today.* 313 (2018) 161–166. <https://doi.org/10.1016/j.cattod.2017.10.034>.
- [57] D.U. McCormick, Flavin Derivatives via Bromination of the 8-Methyl Substituent (1), *J. Heterocycl. Chem.* 7 (1970) 447–450. <https://doi.org/10.1002/jhet.5570070240C>.
- [58] A. Alvarez-Martin, S. Trashin, M. Cuykx, A. Covaci, K. De Wael, K. Janssens, Photodegradation mechanisms and kinetics of Eosin-Y in oxic and anoxic conditions, *Dye. Pigment.* 145 (2017) 376–384. <https://doi.org/10.1016/j.dyepig.2017.06.031>.
- [59] C.J. Cooksey, Quirks of dye nomenclature. 10. Eosin Y and its close relatives, *Biotech. Histochem.* 93 (2018) 211–219. <https://doi.org/10.1080/10520295.2017.1413207>.
- [60] M.E. Selsted, H.W. Becker, Eosin Y: A reversible stain for detecting electrophoretically resolved protein, *Anal. Biochem.* 155 (1986) 270–274. [https://doi.org/10.1016/0003-2697\(86\)90436-7](https://doi.org/10.1016/0003-2697(86)90436-7).
- [61] A. Penzkofer, A. Beidoun, S. Speiser, Singlet excited-state absorption of eosin Y, *Chem. Phys.* 170 (1993) 139–148. [https://doi.org/10.1016/0301-0104\(93\)80099-U](https://doi.org/10.1016/0301-0104(93)80099-U).
- [62] A. Penzkofer, A. Beidoun, M. Daiber, Intersystem-crossing and excited-state absorption in eosin Y solutions determined by picosecond double pulse transient absorption measurements, *J. Lumin.* 51 (1992) 297–314. [https://doi.org/10.1016/0022-2313\(92\)90059-I](https://doi.org/10.1016/0022-2313(92)90059-I).
- [63] D.P. Haria, B. König, Synthetic applications of eosin Y in photoredox catalysis, *Chem. Commun.* 50 (2014) 6688–6699. <https://doi.org/10.1039/c4cc00751d>.

- [64] V. Srivastava, P.P. Singh, Eosin y catalysed photoredox synthesis: A review, *RSC Adv.* 7 (2017) 31377–31392. <https://doi.org/10.1039/c7ra05444k>.
- [65] R. Martínez-Haya, A.A. Heredia, W.D. Castro-Godoy, L.C. Schmidt, M.L. Marin, J.E. Argüello, Mechanistic Insight into the Light-Triggered CuAAC Reaction: Does Any of the Photocatalyst Go?, *J. Org. Chem.* 86 (2021) 5832–5844. <https://doi.org/10.1021/acs.joc.1c00272>.
- [66] Y. Liu, Y. Chen, Y. Shi, D. Wan, J. Chen, S. Xiao, Adsorption of toxic dye Eosin Y from aqueous solution by clay/carbon composite derived from spent bleaching earth, *Water Environ. Res.* 93 (2021) 159–169. <https://doi.org/10.1002/wer.1376>.
- [67] F. Kooli, S. Rakass, Y. Liu, M. Abboudi, H.O. Hassani, S.M. Ibrahim, F. Al Wadaani, R. Al-Faze, Eosin removal by cetyl trimethylammonium-cloisites: Influence of the surfactant solution type and regeneration properties, *Molecules.* 24 (2019). <https://doi.org/10.3390/molecules24163015>.
- [68] A. Jabłoński, Über den Mechanismus der Photolumineszenz von Farbstoffphosphoren, *Zeitschrift Für Phys.* 94 (1935) 38–46. <https://doi.org/10.1007/BF01330795>.
- [69] D. Dzebo, Photon Upconversion through Triplet-Triplet Annihilation Towards Higher Efficiency and Solid State Applications, 2016. <https://doi.org/http://sci-hub.tw/10.13140/RG.2.2.34379.18722>.
- [70] J.. Scaiano, N.J. Turro, V. Ramamurthy, Modern molecular photochemistry of organic molecules, Wiley Online Library, 2012.
- [71] D. Rehm, A. Weller, Kinetik und Mechanismus der Elektronenübertragung bei der Fluoreszenzlöschung in Acetonitril, *Berichte Der Bunsengesellschaft.* 73 (1969) 834–839. <https://doi.org/10.1002/bbpc.19690730818>.

- [72] S.P. Pitre, C.D. McTiernan, J.C. Scaiano, Understanding the Kinetics and Spectroscopy of Photoredox Catalysis and Transition-Metal-Free Alternatives, *Acc. Chem. Res.* 49 (2016) 1320–1330. <https://doi.org/10.1021/acs.accounts.6b00012>.
- [73] T. Rasheed, M. Bilal, A.A. Hassan, F. Nabeel, R.N. Bharagava, L.F. Romanholo Ferreira, H.N. Tran, H.M.N. Iqbal, Environmental threatening concern and efficient removal of pharmaceutically active compounds using metal-organic frameworks as adsorbents, *Environ. Res.* 185 (2020) 109436. <https://doi.org/10.1016/j.envres.2020.109436>.
- [74] C.G. Daughton, T.A. Ternes, Pharmaceuticals and personal care products in the environment: Agents of subtle change?, *Environ. Health Perspect.* 107 (1999) 907–938. <https://doi.org/10.1289/ehp.99107s6907>.
- [75] B. Pan, P. Ning, B. Xing, Part V - Sorption of pharmaceuticals and personal care products, *Environ. Sci. Pollut. Res.* 16 (2009) 106–116. <https://doi.org/10.1007/s11356-008-0052-x>.
- [76] C.R. Ohoro, A.O. Adeniji, A.I. Okoh, O.O. Okoh, Distribution and chemical analysis of pharmaceuticals and personal care products (PPCPs) in the environmental systems: A review, *Int. J. Environ. Res. Public Health.* 16 (2019) 3026. <https://doi.org/10.3390/ijerph16173026>.
- [77] D.R. Baker, B. Kasprzyk-Hordern, Critical evaluation of methodology commonly used in sample collection, storage and preparation for the analysis of pharmaceuticals and illicit drugs in surface water and wastewater by solid phase extraction and liquid chromatography-mass spectrometry, *J. Chromatogr. A.* 1218 (2011) 8036–8059. <https://doi.org/10.1016/j.chroma.2011.09.012>.

- [78] F. Pomati, S. Castiglioni, E. Zuccato, R. Fanelli, D. Vigetti, C. Rossetti, D. Calamari, Effects of a complex mixture of therapeutic drugs at environmental levels on human embryonic cells, *Environ. Sci. Technol.* 40 (2006) 2442–2447. <https://doi.org/10.1021/es051715a>.
- [79] Y. Tian, X. Xia, J. Wang, L. Zhu, J. Wang, F. Zhang, Z. Ahmad, Chronic Toxicological Effects of Carbamazepine on *Daphnia magna* Straus: Effects on Reproduction Traits, Body Length, and Intrinsic Growth, *Bull. Environ. Contam. Toxicol.* 103 (2019) 723–728. <https://doi.org/10.1007/s00128-019-02715-w>.
- [80] R. Andreatti, R. Marotta, G. Pinto, A. Pollio, Carbamazepine in water: Persistence in the environment, ozonation treatment and preliminary assessment on algal toxicity, *Water Res.* 36 (2002) 2869–2877. [https://doi.org/10.1016/S0043-1354\(01\)00500-0](https://doi.org/10.1016/S0043-1354(01)00500-0).
- [81] S. Batra, R. Bhushan, Bioassay, determination and separation of enantiomers of atenolol by direct and indirect approaches using liquid chromatography: A review, *Biomed. Chromatogr.* 32 (2018) 1–21. <https://doi.org/10.1002/bmc.4090>.
- [82] A.A. Godoy, F. Kummrow, P.A.Z. Pamplin, Occurrence, ecotoxicological effects and risk assessment of antihypertensive pharmaceutical residues in the aquatic environment - A review, *Chemosphere.* 138 (2015) 281–291. <https://doi.org/10.1016/j.chemosphere.2015.06.024>.
- [83] H. Cui, H.M. Hwang, S. Cook, K. Zeng, Effect of photosensitizer riboflavin on the fate of 2,4,6-trinitrotoluene in a freshwater environment, *Chemosphere.* 44 (2001) 621–625. [https://doi.org/10.1016/S0045-6535\(00\)00333-7](https://doi.org/10.1016/S0045-6535(00)00333-7).

- [84] J.S. Stanojević, J.B. Zvezdanović, D.Z. Marković, Riboflavin degradation in the presence of quercetin in methanol under continuous UV-B irradiation: The ESI-MS-UHPLC analysis, *Monatshefte Fur Chemie*. 146 (2015) 1787–1794. <https://doi.org/10.1007/s00706-015-1561-1>.
- [85] I. Ahmad, T. Mirza, Z. Anwar, S. Ahmed, M.A. Sheraz, M.A. Ejaz, S.H. Kazi, Photodegradation of formylmethylflavin by side-chain and isoalloxazine ring cleavage in alkaline solution: A kinetic study, *J. Photochem. Photobiol. A Chem.* 374 (2019) 106–114. <https://doi.org/10.1016/j.jphotochem.2019.01.028>.
- [86] S. Castiglioni, R. Bagnati, D. Calamari, R. Fanelli, E. Zuccato, A multiresidue analytical method using solid-phase extraction and high-pressure liquid chromatography tandem mass spectrometry to measure pharmaceuticals of different therapeutic classes in urban wastewaters, *J. Chromatogr. A*. 1092 (2005) 206–215. <https://doi.org/10.1016/j.chroma.2005.07.012>.
- [87] R. Andreozzi, R. Marotta, N. Paxéus, Pharmaceuticals in STP effluents and their solar photodegradation in aquatic environment, *Chemosphere*. 50 (2003) 1319–1330. [https://doi.org/10.1016/S0045-6535\(02\)00769-5](https://doi.org/10.1016/S0045-6535(02)00769-5).
- [88] P. Calza, C. Medana, E. Padovano, V. Giancotti, C. Baiocchi, Identification of the unknown transformation products derived from clarithromycin and carbamazepine using liquid chromatography/high-resolution mass spectrometry, *Rapid Commun. Mass Spectrom.* 26 (2012) 1687–1704. <https://doi.org/10.1002/rcm.6279>.
- [89] C. Martínez, M. Canle L, M.I. Fernández, J.A. Santaballa, J. Faria, Kinetics and mechanism of aqueous degradation of carbamazepine by heterogeneous

photocatalysis using nanocrystalline TiO₂, ZnO and multi-walled carbon nanotubes-anatase composites, *Appl. Catal. B Environ.* 102 (2011) 563–571. <https://doi.org/10.1016/j.apcatb.2010.12.039>.

- [90] S. Chiron, C. Minero, D. Vione, Photodegradation processes of the antiepileptic drug carbamazepine, relevant to estuarine waters, *Environ. Sci. Technol.* 40 (2006) 5977–5983. <https://doi.org/10.1021/es060502y>.
- [91] C.B. C. Medana, P. Calza, F. Carbone, E. Pelizzetti, H. Hidaka, Characterization of atenolol transformation products on light-activated TiO₂ surface by high-performance liquid chromatography/high-resolution mass spectrometry, *Rapid Commun. Mass Spectrom.* 22 (2008) 301–313. <https://doi.org/10.1002/rcm.3370>.
- [92] J. Radjenović, C. Sirtori, M. Petrović, D. Barceló, S. Malato, Solar photocatalytic degradation of persistent pharmaceuticals at pilot-scale: Kinetics and characterization of major intermediate products, *Appl. Catal. B Environ.* 89 (2009) 255–264. <https://doi.org/10.1016/j.apcatb.2009.02.013>.
- [93] Y. Ji, L. Zhou, C. Ferronato, X. Yang, A. Salvador, C. Zeng, J.M. Chovelon, Photocatalytic degradation of atenolol in aqueous titanium dioxide suspensions: Kinetics, intermediates and degradation pathways, *J. Photochem. Photobiol. A Chem.* 254 (2013) 35–44. <https://doi.org/10.1016/j.jphotochem.2013.01.003>.
- [94] S. Klemenc, Noscapine as an adulterant in illicit heroin samples, *Forensic Sci. Int.* 108 (2000) 45–49. [https://doi.org/10.1016/S0379-0738\(99\)00201-7](https://doi.org/10.1016/S0379-0738(99)00201-7).
- [95] A. C. G. Rida, Padmashree; LiVecche, Dillon; Ogden, Angela; Zhou, Jun; Ritu, The Noscapine Chronicle: A Pharmaco-Historic Biography of the Opiate Alkaloid Family and its Clinical Applications, *Physiol. Behav.* 35

(2015) 1072–1096. <https://doi.org/10.1002/med.21357>.The.

- [96] M.A. Altinoz, G. Topcu, A. Hacimuftuoglu, A. Ozpinar, A. Ozpinar, E. Hacker, İ. Elmaci, Noscapine, a Non-addictive Opioid and Microtubule-Inhibitor in Potential Treatment of Glioblastoma, *Neurochem. Res.* 44 (2019) 1796–1806. <https://doi.org/10.1007/s11064-019-02837-x>.
- [97] H.A. Bickerman, A.L. Barach, The experimental production of cough in human subjects induced by citric acid aerosols; preliminary studies on the evaluation of antitussive agents., *Am. J. Med. Sci.* 228 (1954) 156–163. <https://doi.org/10.1097/00000441-195408000-00005>.
- [98] D.W. Empey, L.A. Laitinen, G.A. Young, C.E. Bye, D.T.D. Hughes, Comparison of the antitussive effects of codeine phosphate 20 mg, dextromethorphan 30 mg and noscapine 30 mg using citric acid-induced cough in normal subjects, *Eur. J. Clin. Pharmacol.* 16 (1979) 393–397. <https://doi.org/10.1007/BF00568199>.
- [99] R.A. Padmashree C. G. Rida, Dillon LiVecche, Angela Ogden, Jun Zhou, The Noscapine Chronicle: A Pharmaco-Historic Biography of the Opiate Alkaloid Family and its Clinical Applications, *Med Res Rev.* 35 (2015) 1072–1096. <https://doi.org/10.1002/med.21357>.
- [100] M.A. Altinoz, G. Topcu, A. Hacimuftuoglu, A. Ozpinar, A. Ozpinar, E. Hacker, İ. Elmaci, Noscapine, a Non-addictive Opioid and Microtubule-Inhibitor in Potential Treatment of Glioblastoma, *Neurochem. Res.* 44 (2019) 1796–1806. <https://doi.org/10.1007/s11064-019-02837-x>.
- [101] B. Sung, K.S. Ahn, B.B. Aggarwal, Noscapine, a benzyloquinoline alkaloid, sensitizes leukemic cells to chemotherapeutic agents and cytokines by modulating the NF-κB signaling pathway, *Cancer Res.* 70 (2010) 3259–

3268. <https://doi.org/10.1158/0008-5472.CAN-09-4230>.

- [102] Y. Ke, K. Ye, H.E. Grossniklaus, D.R. Archer, H.C. Joshi, J.A. Kapp, Noscapine inhibits tumor growth with little toxicity to normal tissues or inhibition of immune responses, *Cancer Immunol. Immunother.* 49 (2000) 217–225. <https://doi.org/10.1007/s002620000109>.
- [103] P.E. Ghaly, C.D.M. Churchill, R.M. Abou El-Magd, Z. Hájková, P. Dráber, F.G. West, J.A. Tuszynski, Synthesis and biological evaluation of structurally simplified noscapine analogues as microtubule binding agents, *Can. J. Chem.* 95 (2017) 649–655. <https://doi.org/10.1139/cjc-2016-0649>.
- [104] N. Kumar, D. Sood, P.J. van der Spek, H.S. Sharma, R. Chandra, Molecular Binding Mechanism and Pharmacology Comparative Analysis of Noscapine for Repurposing against SARS-CoV-2 Protease, *J. Proteome Res.* 19 (2020) 4678–4689. <https://doi.org/10.1021/acs.jproteome.0c00367>.
- [105] N. Kumar, A. Awasthi, A. Kumari, D. Sood, P. Jain, T. Singh, N. Sharma, A. Grover, R. Chandra, Antitussive noscapine and antiviral drug conjugates as arsenal against COVID-19: a comprehensive chemoinformatics analysis, *J. Biomol. Struct. Dyn.* (2020) 1–16. <https://doi.org/10.1080/07391102.2020.1808072>.
- [106] National Institute of Technology and Evaluation, Japan CHEMicals Collaborative Knowledge database (J-CHECK), (n.d.). https://www.nite.go.jp/chem/jcheck/List6Action?category=211&request_locale=en.
- [107] S.A. Ebrahimi, Noscapine, a possible drug candidate for attenuation of cytokine release associated with SARS-CoV-2, *Drug Dev. Res.* 81 (2020) 765–767. <https://doi.org/10.1002/ddr.21676>.

- [108] C.A. Winter, L. Flataker, Toxicity studies on noscapine, *Toxicol. Appl. Pharmacol.* 3 (1961) 96–106. [https://doi.org/10.1016/0041-008X\(61\)90013-8](https://doi.org/10.1016/0041-008X(61)90013-8).
- [109] C. Tiveron, B. Hartley-asp, C.J. Johansson, F. Pacchierotti, Noscapine does not show aneugenic activity in mouse oocytes, *Mutagenesis.* 8 (1993) 311–315. <https://doi.org/10.1093/mutage/8.4.311>.
- [110] A. DeBono, B. Capuano, P.J. Scammells, Progress Toward the Development of Noscapine and Derivatives as Anticancer Agents, *J. Med. Chem.* 58 (2015) 5699–5727. <https://doi.org/10.1021/jm501180v>.
- [111] N. Tsunoda, H. Yoshimura, Metabolic fate of noscapine. II. Isolation and identification of novel metabolites produced by c - c bond cleavage, *Xenobiotica.* 9 (1979) 181–187. <https://doi.org/10.3109/00498257909038719>.
- [112] H. Nakata, S. Murata, J. Filatreau, Occurrence and Concentrations of Benzotriazole UV Stabilizers in Marine Organisms and Sediments from the Ariake Sea, Japan", *Environ. Sci. Technol.* 43 (2009) 7999. <https://doi.org/10.1021/es902653t>.
- [113] A.G. Asimakopoulos, L. Wang, N.S. Thomaidis, K. Kannan, Benzotriazoles and benzothiazoles in human urine from several countries: A perspective on occurrence, biotransformation, and human exposure, *Environ. Int.* 59 (2013) 274–281. <https://doi.org/10.1016/j.envint.2013.06.007>.
- [114] D.S. Hart, L.C. Davis, L.E. Erickson, T.M. Callender, Sorption and partitioning parameters of benzotriazole compounds, *Microchem. J.* 77 (2004) 9–17. <https://doi.org/10.1016/j.microc.2003.08.005>.
- [115] ECHA, Substance Name : 2- (2H-Benzotriazol-2- EC Number : 247-384-8

CAS Number : 25973-55-1 Member State Committee, 1 (2014) 247–384.

- [116] K. Fent, G. Chew, J. Li, E. Gomez, Benzotriazole UV-stabilizers and benzotriazole: Antiandrogenic activity in vitro and activation of aryl hydrocarbon receptor pathway in zebrafish eleuthero-embryos, *Sci. Total Environ.* 482–483 (2014) 125–136. <https://doi.org/10.1016/j.scitotenv.2014.02.109>.
- [117] Z.Q. Shi, Y.S. Liu, Q. Xiong, W.W. Cai, G.G. Ying, Occurrence, toxicity and transformation of six typical benzotriazoles in the environment: A review, *Sci. Total Environ.* 661 (2019) 407–421. <https://doi.org/10.1016/j.scitotenv.2019.01.138>.
- [118] R. Martinez-Haya, J. Gomis, A. Arques, M.L. Marin, A.M. Amat, M.A. Miranda, Time-resolved kinetic assessment of the role of singlet and triplet excited states in the photocatalytic treatment of pollutants at different concentrations, *Appl. Catal. B Environ.* 203 (2017) 381–388. <https://doi.org/10.1016/j.apcatb.2016.10.042>.
- [119] S.K. Choudhury, P. Rout, B.B. Parida, J.C. Florent, L. Johannes, G. Phaomei, E. Bertounesque, L. Rout, Metal-Free Activation of C(sp³)–H Bond, and a Practical and Rapid Synthesis of Privileged 1-Substituted 1,2,3,4-Tetrahydroisoquinolines, *European J. Org. Chem.* 2017 (2017) 5275–5292. <https://doi.org/10.1002/ejoc.201700471>.
- [120] P.F. Heelis, The photophysical and photochemical properties of flavins (isoalloxazines), *Chem. Soc. Rev.* 11 (1982) 15–39. <https://doi.org/10.1039/CS9821100015>.
- [121] G. Weber, F.W.J. Teale, Determination of the absolute quantum yield of fluorescent solutions, *Trans. Faraday Soc.* 53 (1957) 646–655.

<https://doi.org/10.1039/tf9575300646>.